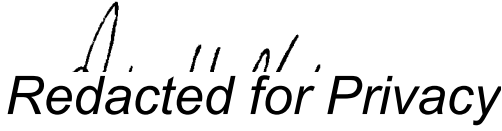


AN ABSTRACT OF THE THESIS OF

Colin Daniel Poellot for the degree of Master of Science in Geology, presented on June 5, 2000. Title: Ice Surface Reconstruction and Energy Balance Modeling of Alpine Glaciers

Abstract approved:  *Redacted for Privacy*
Peter U. Clark

Glacial deposits on San Francisco Mountain, Arizona, were mapped in order to provide constraints on ice extents in separate valleys for late Pleistocene glacial events. Qualitative and semi-quantitative relative dating methods were employed in order to correlate moraines between drainages and to provide a basis for distinguishing between separate glacial events within drainages. Morphologic and surficial weathering characteristics that were measured include degree of moraine dissection, moraine crestal width, moraine inner and outer slope angle, surface boulder frequency, percentage of weathered surface boulders, percentage of pitted surface boulders, maximum pit depth, and percentage of split boulders. Results of the relative dating study support past studies that differentiate 3 separate drift sequences on the mountain. Five separate glacier surfaces were reconstructed from the mapped moraine crests, four for the most recent glaciation, and one for the intermediate glacial event. ELAs from the reconstructed glaciers range from 3140 to 3400 meters.

In addition, a numerical model was developed that uses an energy balance approach to calculate annual ablation over a glacier surface. The energy balance

approach used in the model was designed to allow the model to test sensitivity of former glaciers to changes in temperature or precipitation. Required model inputs include a two-dimensional elevation map of the glacier surface and surrounding topography, as well as climate records that include daily values of air temperature, wind speed, precipitation, atmospheric vapor pressure, incoming shortwave radiation, and incoming longwave radiation. Model outputs include the net specific balance and equilibrium line altitude of the glacier. Model simulations of mass balance are compared with observed data from the 1990 ablation season at Haut Glacier d'Arolla, Valais, Switzerland. Calculated ablation values closely match observed values, thereby supporting the validity of the model. A preliminary model run was also accomplished for the 5 Pleistocene glaciers reconstructed on San Francisco Mountain, Arizona, using output from a regional climate model as input. The model delivers a glacier that is nearly in mass balance for one of the reconstructions.

ICE SURFACE RECONSTRUCTION AND ENERGY BALANCE MODELING OF ALPINE GLACIERS

by

Colin Daniel Poellot

A Thesis Submitted

To

Oregon State University

In Partial Fulfillment of
the requirements for the
degree of

Master of Science

Presented June 5, 2000
Commencement June 2001

Master of Science thesis of Colin Daniel Poellot presented on June 5, 2000.

APPROVED:

Redacted for Privacy

Major Professor, representing Geology

Redacted for Privacy

Chair of Department of Geosciences

Redacted for Privacy

Dean of the Graduate School

I understand that my thesis will become part of the permanent collection of Oregon State University Libraries. My signature below authorizes release of my thesis to any reader upon request.

Redacted for Privacy

Colin Daniel Poellot, Author

TABLE OF CONTENTS

CHAPTER 1: INTRODUCTION	1
CHAPTER 2: GLACIAL DEPOSITS OF SAN FRANCISCO MOUNTAIN, ARIZONA	3
ABSTRACT	4
INTRODUCTION	5
Geology	6
Climate and Vegetation	9
Previous Work	10
METHODS	10
DESCRIPTION OF DRIFT UNITS	12
Stage III Drift Unit	13
Stage II Drift Unit	17
Stage I Drift Unit	19
Holocene Events	20
DISCUSSION OF RELATIVE AGE DATA	21
Morphologic parameters	22
Weathering Characteristics	23
RECONSTRUCTION OF GLACIER SURFACES	26
CONCLUSIONS	30
REFERENCES	30
CHAPTER 3: DEVELOPMENT AND TESTING OF A NUMERICAL MASS BALANCE MODEL FOR ALPINE GLACIERS	33
LIST OF VARIABLES USED IN EQUATIONS	34
ABSTRACT	37
INTRODUCTION	38

TABLE OF CONTENTS (CONTINUED)

MODEL DESCRIPTION	41
Input and Output Files	42
Solar and Terrain Subroutines	46
Net Balance Subroutine	52
APPLICATION OF MODEL TO A MODERN GLACIER	60
Model Results	63
Model Accuracy	66
APPLICATION OF MODEL TO FORMER GLACIERS	73
Model Inputs	73
Model Results	76
CONCLUSIONS	82
REFERENCES	83
CHAPTER 4: SUMMARY	88
BIBLIOGRAPHY	90
APPENDIX	96
NET BALANCE PROGRAM CODE	97
MAIN PROGRAM BLOCK	97
PARAMETERS SUBROUTINE	111
SOLAR SUBROUTINE	114
TERRAIN SUBROUTINE	116
HORIZON SUBROUTINE	118
ENERGY BALANCE SUBROUTINE	123

LIST OF FIGURES

Figure	Page
2.1 Location of San Francisco Mountain and White Mountains, Arizona	7
2.2 Major topographic features of San Francisco Mountain. Topography is from U.S.G.S. 7.5' Digital Elevation Models of Humphreys Peak, Sunset Crater West, and White Horse Hills quadrangles. UTM projection based on 1927 North American Datum	8
2.3 Glacial deposits on San Francisco Mountain with moraine crests and relative dating collection sites.	15
2.4 A reconstruction of the most extensive Stage II Inner Basin glacier. The ELA is shown with a dashed contour line.	27
2.5 Reconstruction of four Stage I glaciers. Equilibrium line altitudes are shown as dashed contour lines and labeled.	28
3.1 General flowchart of program.	43
3.2 Schematic of horizon angle calculation. Open circles represent DEM grid points. The closed circle represents the origin of a single horizon angle search along shown azimuth. Diamonds represent points in the DEM where elevations are interpolated from surrounding grid nodes to determine the maximum angle to the horizon, as shown in the side view.	50
3.3 Contour map of glacier and terrain DEM for Haut Glacier d'Arolla. Shaded area indicates the surface of the glacier as represented in the model. Elevation is accurate to within 1 meter for the glacier surface, and to within 10 meters for the surrounding terrain (Sharp, pers. comm., 1998).	62
3.4 Net specific balance of Haut Glacier d'Arolla for 1990 ablation season. Elevation contours are shown in gray. Net balance values are in meters water equivalent.	65
3.5 Observed versus modeled cumulative ablation for Haut Glacier d'Arolla. Cumulative ablation shown in meters water equivalent.	67
3.6 Daily modeled and observed ablation values for Haut Glacier d'Arolla. Ablation values are in meters water equivalent.	69

LIST OF FIGURES (CONTINUED)

Figure	Page
3.7 Scatter plots of measured versus modeled ablation for stake locations shown in Figure 3.3	70
3.8 Scatter plots of measured versus modeled ablation for stake locations 3 and 4 with the data from July 15-20 removed.	71
3.9 a: Scatter plot of measured versus modeled ablation data combined from all stake locations. b: Scatter plot of measured versus modeled ablation values for all stake locations excluding the data from July 15-20 at stake locations 3 and 4.	72
3.10 Reconstructed glaciers on San Francisco Mountain, Arizona from the youngest moraine set on the mountain.	74
3.11 Reconstructed glacier for the second oldest moraine set on San Francisco Mountain, Arizona.	75
3.12 Comparison of LGM model run results with original reconstructed elevation contours and ELAs for the youngest reconstructed glaciers on San Francisco Mountain.	80
3.13 Comparison of LGM model run results with original reconstructed elevation contours and ELA for the second youngest reconstructed glacier on San Francisco Mountain.	81

LIST OF TABLES

Table		Page
2.1	Semi-quantitative relative dating measurements of drift units.	16
2.2	Magnitude of change in relative dating parameters between drift units.	22
3.1	List of user defined parameters required as program input.	44
3.2	Parameters used in model run on Haut Glacier d'Arolla.	63
3.3	Average daily values of energy balance equation components for Haut Glacier d'Arolla.	66
3.4	Individual model calculated components of longwave radiation for Haut Glacier d'Arolla.	66
3.5	Input parameters for San Francisco Mountain reconstructed glaciers.	77
3.6	Results of model runs on the San Francisco Mountain former glaciers.	78

ICE SURFACE RECONSTRUCTION AND ENERGY BALANCE MODELING OF ALPINE GLACIERS

CHAPTER 1

INTRODUCTION

Alpine glaciers have long been recognized as being closely linked with local, regional, and global climate, both in their rapid response time to climate change, and in their capacity to influence local climate (Meier, 1965; Walters and Meier, 1989; McClung and Armstrong, 1993; Paterson, 1994). The complex feedback processes between glacier and climate are ultimately recorded in the deposits resulting from glacial advances and retreats. The geologic record of alpine glacier advances can thus provide an important source of paleoclimate information in a region. This thesis is composed of two manuscripts that address the reconstruction and mass balance modeling of former ice surfaces to enable sensitivity testing of specific climate forcing mechanisms (i.e. temperature and precipitation) on former glaciers.

The first paper describes the mapping of glacial deposits of San Francisco Mountain, Arizona, to provide constraints on former ice limits during the Pleistocene. Relative dating data were collected from moraine crests in order to determine the extent of ice advance during separate glaciations. Mapped moraine crest elevations were used to reconstruct four digital elevation models of former glacier surfaces for the youngest glaciation, and one glacier surface from the second oldest glaciation. It is assumed from the results of the study that the most recent glaciation on the mountain

represents the last glacial maximum, although it is possible that the youngest moraines are from a younger cooling event, and the middle moraine set represents the last glacial maximum.

The second paper describes the development and testing of a surface energy balance model that is designed to be driven by climate data generated by a high-resolution regional climate model. The model calculates specific net balance over a two dimensional (2-D) glacier surface by summing precipitation and ablation over a specified time period. Modeled 2-D net balance over the surface of the glacier can be used to determine the equilibrium line altitude of the glacier.

The model was tested with field data collected during the 1990 ablation season at Haut Glacier d'Arolla, Valais, Switzerland (Arnold et al., 1996). All necessary inputs except incoming longwave radiation were provided, and daily ablation values at four separate points were used for testing of model output. Although testing with more complete modern data over longer timespans would be ideal, the model should provide sufficient accuracy to be used for sensitivity testing on former glaciers. The tested model was then applied to the reconstructed glaciers from the first paper. The model delivers a glacier that is nearly in mass balance for the reconstruction of the second oldest reconstructed glacier on the mountain.

CHAPTER 2

GLACIAL DEPOSITS OF SAN FRANCISCO MOUNTAIN, ARIZONA

Colin D. Poellot

ABSTRACT

Glacial deposits on San Francisco Mountain, Arizona, were mapped in order to provide constraints on ice extents in separate valleys for late Pleistocene glacial events. Qualitative and semi-quantitative relative dating methods were employed in order to correlate moraines between drainages and to provide a basis for distinguishing between separate glacial events within drainages. Morphologic and surficial weathering characteristics that were measured include degree of moraine dissection, moraine crestal width, moraine inner and outer slope angle, surface boulder frequency, percentage of weathered surface boulders, percentage of pitted surface boulders, maximum pit depth, and percentage of split boulders. Results of the relative dating study support past studies that differentiate three separate drift sequences on the mountain. Five separate glacier surfaces were reconstructed from the mapped moraine crests, four for the most recent glaciation, and one for the intermediate glacial event. ELAs from the reconstructed glaciers range from 3140 to 3400 meters.

INTRODUCTION

As mid latitude alpine glaciers respond rapidly (decade to century scale) to climate change, interpreting the paleoclimatic signal of glacial advances and retreats is important in determining spatial and temporal paleoclimatic variations on a regional scale. The traditional method of interpreting late Pleistocene climatic conditions from glacial deposits involves reconstructing the equilibrium line altitude (ELA) of a network of former glaciers, then calculating temperature lapse rates and precipitation increases necessary to sustain glaciers at those altitudes by evaluating the paleo-ELAs against modern ELAs (Porter, 1964; Mathews, 1967; Meierding, 1982; Leonard, 1984). However, while it is possible to infer general paleoclimate conditions from the geologic record of glacial deposits using this method, it is not possible to deduce specific climate forcing mechanisms or changes. Paleoclimate reconstructions in the western U.S. resulting from such studies have led to differing or conflicting results (Zielinski and McCoy, 1987; Leonard, 1989; Locke, 1990; Bevis, 1995). Results of a high resolution regional climate modeling experiment suggest that the time series of glacier fluctuations in the Rocky Mountains may have been phase shifted with respect to glacier fluctuations in the Sierra Nevada and Cascade ranges as the glaciers in the different regions responded differently to changes in temperature and precipitation (Hostetler and Clark, 1997).

The glacial deposits of San Francisco Mountain, Arizona, were mapped as part of a project designed to evaluate the impact of specific climate forcing mechanisms on a regional network of late Pleistocene alpine glaciers in the western United States. Relative dating data were collected from moraine crests in order to determine the

extent of ice advance during separate glaciations. Mapped moraine crest elevations were used to reconstruct ice surface extents for the youngest glaciation in four separate valleys, and ice extents in one valley for the second oldest glaciation. It is assumed from the results of the study that the most recent glaciation on the mountain represents the last glacial maximum, although it is possible that the middle moraine set represents the last glacial maximum, and the youngest moraines are from a younger cooling event. The field-based glacier reconstructions from this study will be used to evaluate independent reconstructions derived from regional climate modeling experiments that drive an energy-balance model of glacier mass balance.

Geology

San Francisco Mountain, commonly referred to as the San Francisco Peaks, is a composite volcanic cone located near the southern boundary of the Colorado Plateau at 35° 20'N and 111° 40'W (Figure 2.1). San Francisco Mountain is one of two alpine areas in Arizona that were glaciated during the late Pleistocene, the other being the White Mountains in southeastern Arizona (Merrill and Péwé, 1972). Rising over 1500 meters above the surrounding basaltic plateau, the mountain is an agglomeration of silicic lava flows, domes and intrusions. The volcano has been breached and eroded, producing four major peaks and many lesser peaks. The summit of the mountain, Humphreys Peak, rises to 3850 meters and is the highest point in Arizona. The peaks surround a northeast trending valley that is divided into two sections: the Inner Basin, which lies above 2900 meters, and the Interior Valley (Figure 2.2). The

Inner Basin and Interior Valley harbored the majority of ice during the Pleistocene glaciations, but glaciers were also present in four drainages on the north and west flanks of the cone (Figure 2.2).

The main cone of the volcano was built up by a sequence of andesite, dacite, and latite flows that were erupted between 1.8 and 0.4 Ma (Péwé and Updike, 1976). The Inner Basin and Interior Valley were formed prior to eruption of Sugarloaf Mountain, a rhyodacite dome that blocks the mouth of the Interior Valley (Figure 2.2). Sugarloaf Mountain has a K-Ar age of 218 ± 21 ka (Sheridan and Updike, 1975; Richmond, 1987).

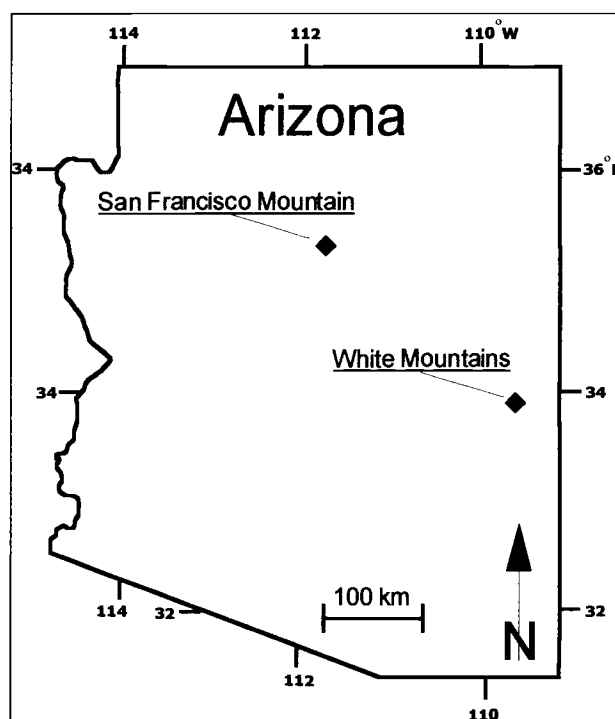


Figure 2.1: Location of San Francisco Mountain and White Mountains, Arizona.

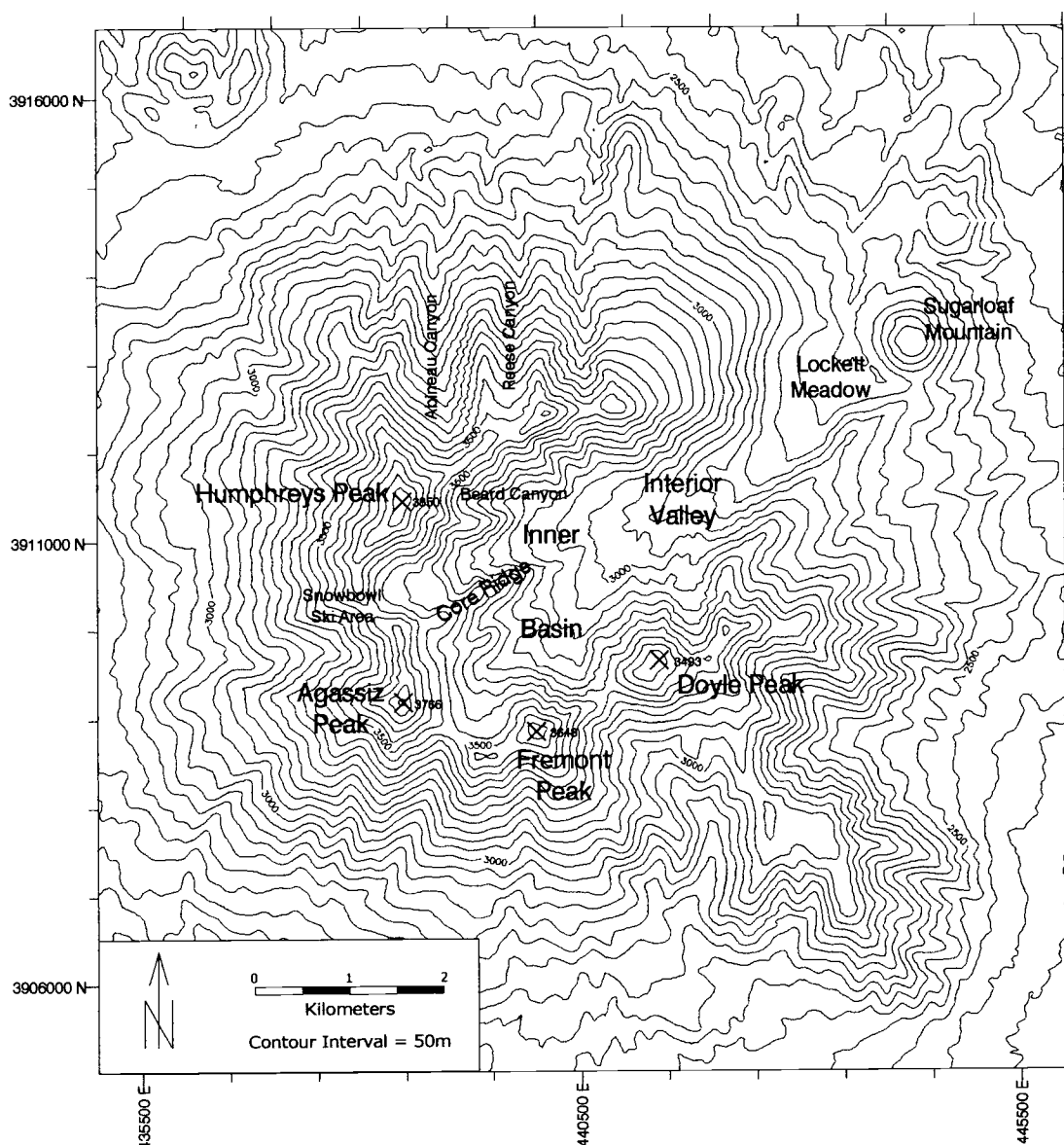


Figure 2.2: Major topographic features of San Francisco Mountain. Topography is from U.S.G.S. 7.5' Digital Elevation Models of Humphreys Peak, Sunset Crater West, and White Horse Hills quadrangles. UTM projection based on 1927 North American Datum.

Unconsolidated surficial deposits on the slopes of the volcano may be separated into recent alluvial and colluvial deposits, late Pleistocene glacial deposits, and deposits of the Quaternary Sinagua Formation. The Sinagua Formation is made up of six members that include pyroclastic flows, debris-flow fans, and alluvial fans. These deposits are poorly sorted, and poorly stratified or unstratified. They are often composed of a wide range of lithologies and contain boulders up to 5 meters in diameter (Péwé and Updike, 1976).

Climate and Vegetation

San Francisco Mountain receives 75-88 cm of precipitation annually, more than twice that of the surrounding plateau (Péwé and Updike, 1976). The majority of precipitation is presently delivered in the summer months by moist tropical air that moves inland from the Gulf of California and Gulf of Mexico (Mitchell, 1976). The volume of precipitation is sufficient that the entire mountain is forested. Pearson (1931) divided the vegetation of the mountain into four distinct zones based on forest type. The Franciscan Zone lies above 3500 meters, and is composed of alpine tundra and vegetation. Between 3500 and 3050 meters is the Agassiz Zone, which is dominated by Engleman spruce and Bristlecone pine. The Datil Zone, between 3050 and 2600 meters, contains Douglas fir, aspen, and limber pine. Below 2600 meters, the Coloradan Zone is a mix of Ponderosa pine, yellow pine, fir, aspen, juniper, and oak (Pearson, 1931). The timberline on the mountain generally lies between 3050 and 4200 meters.

Previous Work

The first recognition of Pleistocene glaciation on San Francisco Mountain is attributed to Atwood (1905) who described deposits of the youngest glaciation. Sharp (1942) described deposits from three separate glacial events and correlated the deposits to the Illinoian, Iowan-Wisconsin, and Late Wisconsin based on moraine morphology, position, degree of dissection, and surface boulder frequency. A more extensive study by Péwé and Updike (1976) supported Sharp's evaluation of three glacial stages, and included revised ages for some moraines based on more extensive relative dating and geologic investigation. Péwé and Updike qualitatively compared moraine preservation, soil development, general weathering characteristics, and stratigraphic position to assign ages of Illinoian, Early Wisconsin, and Late Wisconsin to the three glacial events.

METHODS

As the deposits of the Sinagua Formation on the lower slopes of the volcano often resemble glacial till, as do relict, soil covered talus cones on the upper slopes, glacial deposits were identified based on a combination of stratigraphy, landform morphology, and position relative to glaciated drainages. I identified drainages that appeared to have been glaciated by looking for signs of cirque development at the heads of valleys and morainal deposits downvalley. Due to the rapid rate of weathering of exposed volcanic materials, direct evidence of glacial erosion in the form of polish or striations are noticeably absent from both the till and the bedrock

around the cirques, although glacial polish was found in one cirque above the Inner Basin. Trimlines on valley walls were also hard to identify due to the rapid weathering and erosion of exposed bedrock. Moraines were first differentiated in their respective drainages by noting the elevation and distance downvalley from the cirque headwall, as any glaciation in a given drainage is assumed to obliterate any record of older, less extensive events (Gibbons et al., 1984).

In order to correlate moraines between drainages and to differentiate different glacial events in the stratigraphic record, I employed a set of relative dating techniques following Burke and Birkeland (1979). The principle of morphologic relative dating is based on the fact that weathering and soil formation are time dependent. Thus the ages of landforms that are formed at different times, but exist in similar climatic and vegetative environments, may be differentiated by examining the degree to which weathering has affected the morphology and soil development of each landform. As time limitations precluded collection of subsurface weathering and soil data, I limited my data set to moraine morphology and surficial weathering characteristics.

Morphologic data collected included moraine crestal widths, inner and outer slope angles, and surface boulder frequencies. The following weathering data were collected from boulders on the moraine crests: percentage of weathered surface boulders; percentage of pitted boulders; mean pit depths on pitted boulders; and percentage of boulders that have been split. These data were collected following the guidelines established by Burke and Birkeland (1979), with the following exception. Burke and Birkeland (1979) recorded the maximum pit depth out of a random 50 boulders on the moraine crest, and reported the average pit depth for the first 25

boulders encountered that contained pits. As I never encountered a deposit with 25 boulders that were pitted, and on one moraine only found one boulder out of 50 that was pitted, I only reported the maximum pit depth for each deposit.

I attempted to measure morphologic parameters where the moraines appeared to have been least modified by external erosional forces (stream undercutting, road building, etc.) in order to minimize error induced by local factors. I took surface weathering data on moraine crests with slopes of 3 degrees or less to minimize the possibility that boulders on the surface had been recently exhumed or emplaced from above, and I tried to sample the portion of the moraine crest that had the greatest amount of surface boulders present. As the moraines are located at a variety of elevations in different vegetation zones, I could not limit my sampling to moraines within one particular zone; however, I attempted to select collection sites that had similar vegetation densities and exposure wherever possible. As weathering rates may be different for different lithologies, I limited my study of weathering characteristics to the two most predominant lithologies, a pyroxene andesite and a hypersthene dacite that had similar weathering characteristics.

DESCRIPTION OF DRIFT UNITS

I initially separated drift units by stratigraphic position in the respective drainages. Where more than two sets of moraines were present in close proximity, moraines were grouped according to a qualitative assessment of moraine morphology and the degree to which moraines had been dissected by erosional forces. According

to these initial criteria, three separate drift units, Stage I to III, are described, with Stage I being the most recent deposits, and Stage III the oldest.

Stage III Drift Unit

The most extensive and oldest existing glacial deposits on San Francisco Mountain are found around Lockett Meadow at the mouth of the Interior Valley. Stage III till deposits extend to an altitude of 2560 meters, just over 7 kilometers from the cirque headwalls at the head of the Inner Basin (Figure 2.3). Ice of this glaciation flowed down the Interior Valley over Lockett Meadow, and abutted against Sugarloaf Mountain, removing part of a tuff ring that was deposited from the Sugarloaf Mountain eruption (Péwé and Updike, 1976). Stage III deposits are poorly preserved, and have been highly dissected and modified by erosion, especially on the northern side of Lockett Meadow, where drainage from the Inner Basin and Interior valley has incised at least 70 meters through both glacial and volcanoclastic deposits and into the underlying bedrock.

Most of the side and base of Sugarloaf Mountain are covered with talus from the rhyolite dome, but some glacial till is preserved on the western and southern sides of the dome. Ice flowed around Sugarloaf Mountain to the south, leaving nested terminal moraines just east of Lockett Meadow. Part of the tuff ring is preserved on the northwest flank of Sugarloaf Mountain, and lies unconformably against unstratified glacial deposits on the western side of the dome, so the maximum extent of ice probably did not reach north of Lockett Meadow. The top of the tuff ring

grades into a well-developed terrace on the west flank of Sugarloaf Mountain at 2646 meters elevation (50m above Lockett Meadow). Péwé and Updike (1976) described this terrace as a meltwater channel that may mark the highest extent of ice during the Stage III glaciation. This hypothesis is supported by the existence of a bedrock terrace on the ridge north of Lockett Meadow that roughly matches the elevation of the terrace on Sugarloaf Mountain and is littered with erratics.

The most prominent glacial feature around Lockett Meadow is the long high ridge on the southern side of the valley that slopes down to Sugarloaf Mountain. This ridge was interpreted by Sharp (1942) as being a lateral moraine of Iowan-Wisconsin age. Péwé and Updike (1976) refer to the ridge as an andesite flow with a thin veneer of Illinoian till plastered on the northern slope. I investigated roadcuts and shallow pits around the summit of the ridge, and found till on both the northern and southern slopes, with no bedrock outcrops within 30 meters of the ridge crest on the southern side (Figure 2.3). I therefore similarly interpret the crest of the ridge as a Stage III lateral moraine (e.g. Sharp, 1942).

Due to the lack of preservation of Stage III moraines, I was only able to collect a complete set of relative dating data from one location on the lateral moraine near Sugarloaf Mountain (Table 2.1). The moraine crests are very broad and undulatory. The largest boulders reach 3 meters in diameter, and are mainly composed of pyroxene andesite and hypersthene dacite, although in the subsurface all the lithologies present on the mountain are represented. The frequency of surface boulders greater than 50 cm is very low, and many of the subsurface clasts have

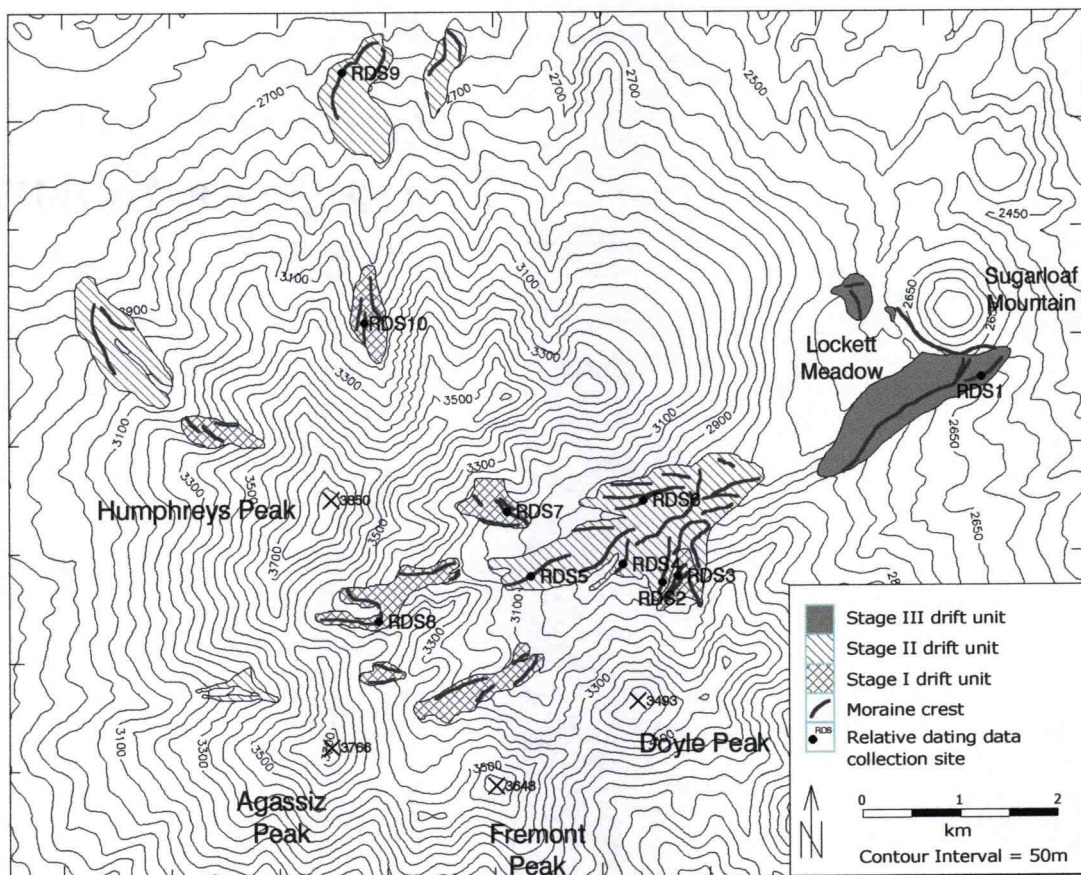


Figure 2.3: Glacial deposits on San Francisco Mountain with moraine crests and relative dating data collection sites.

Table 2.1: Semi-quantitative relative dating measurements of drift units.

Drift Unit	RDS No.†	CW (m)	SA (I/O)	SBF	SPD ‡ (cm)	%W	%P	MPD (cm)	%S
III	1	33	13/18	36	66.5	83.33	46.67	10	56.67
II	2	18.9	24/31	50		76.67	33.33	4.5	13.33
	4	16.5	22/25	36		66.67	23.33	3	13.33
	5	13.7	35/17	40		76.67	23.33	3.4	33.33
	6	12.8	25/35	97		73.33	30	4	43.33
	9	13.5	26/19	39		90	16.67	4.2	53.33
	Mean:	15.08	26.4/25.4	52.4		76.67	25.33	3.82	31.33
	<i>Std. Dev.</i>	<i>2.56</i>	<i>5.03/7.67</i>	<i>25.48</i>	32	<i>8.5</i>	<i>6.5</i>	<i>0.61</i>	<i>17.89</i>
I	3	10.9	30/30	89		46.67	26.67	2.3	30
	7	10.1	28/26	41		76.67	13.33	2.5	10
	8	10.5	20/20	50		66.67	3.33	1.7	3.33
	10	10.7	30/30	53		56.67	16.67	2.3	13.33
	Mean	10.55	27/26.5	58.25		61.67	15	2.2	14.17
	<i>Std. Dev.</i>	<i>3.98</i>	<i>4.76/4.73</i>	<i>27.05</i>	18	<i>30.12</i>	<i>10.35</i>	<i>0.85</i>	<i>11.46</i>

Explanation of abbreviations: **RDS No.** - Relative Dating Site Number; **CW** - Crestal Width; **SA (I/O)** - Slope Angle (Inner/Outer); **SBF** - Surface Boulder Frequency; **SPD** - Average Soil Profile Depth; **%W** - Percentage of Weathered Boulders; **%P** - Percentage of Pitted Boulders; **MPD** -Maximum Pit Depth; **%S** - Percentage of Split Boulders.

† Relative Dating Sites are shown in Figure 2.3.

‡ Soil Profile Depths from Péwé and Updike (1976).

undergone a high degree of disintegration due to weathering. Péwé and Updike (1976) described soil profiles (A and B horizons) in the Stage III till to be between 44 and 89 cm thick. The Stage III deposits lie within the Datil and Coloradan vegetation zones; the lower deposits are forested mainly by Ponderosa pine, while the upper slopes of the right lateral moraine are forested with aspen. No recognizable deposits are preserved on the steep walls of the Interior Valley, although where talus accumulation is limited erratics may be found above the younger deposits.

Stage II Drift Unit

The deposits of the middle drift unit are best preserved in the Interior Valley and Inner Basin, where lateral, medial and terminal moraines suggest that ice from at least five cirques coalesced. Four cirques on the northern and western flanks of San Francisco Mountain also contain deposits interpreted to be Stage II drift.

There are two main sets of moraines in the Interior Valley that I interpreted to be of the Stage II unit based on morphologic and weathering characteristics. The lower moraine set extends to 2745 meters elevation, 4.5 km from the cirque headwalls (Figure 2.3). A younger set extends 3.2 km from the cirque headwalls (Figure 2.3). Both sets of moraines have been cut through by stream erosion. Lateral moraines in the Inner Basin and in a cirque east of Doyle Peak extend up to approximately 3000 meters, and are as high as 60 meters above the valley floor. A large medial moraine protrudes from a long ridge that divides the Inner Basin and separates the cirques of Humphreys Peak from those on Agassiz Peak. A smaller ridge divides two cirques on Agassiz Peak and was overridden by ice during the Stage III, and probably the Stage II events, as indicated by erratics on a saddle of its crest. All of the Stage II moraines in the Interior Valley and Inner Basin lie within the Datil vegetation zone and are forested mainly by thick groves of aspen, although spruce may be locally present.

The four drainages outside the Interior Valley that were glaciated during the Stage II events are Abineau and Reese Canyons on the north flank of San Francisco Mountain, and Philomena Canyon and the Snowbowl on the west flank. The moraines in the Snowbowl have been mechanically altered during creation of the Snowbowl ski area so I have relied on maps and observations made by P  w   and

Updike (1976) for my data in this drainage. Stage II moraines in Abineau Canyon and Reese Canyon extend about 3.6 km from the headwalls and terminate around 2600 meters elevation (Figure 2.3). These moraines are morphologically similar to the Stage II moraines in the Interior Valley, but they lie in the Coloradan vegetation zone, so the surface weathering characteristics of the surface boulders may not correlate closely with those at higher elevations. The moraines in Philomena canyon reach a minimum elevation of 2830 meters and terminate 3.2 km from the headwall (Figure 2.3). The Stage II moraines are the only moraines preserved in the Snowbowl, where they were found at 3170 meters elevation, ~ 1 km from the headwall (Péwé and Updike, 1976). Primary vegetation on the Philomena and Snowbowl moraines consists of thick stands of Engleman spruce with scattered dense aspen groves on the lower slopes.

I sampled relative dating characteristics on 5 Stage II moraines (Figure 2.3, Table 2.1). The Stage II moraines have much steeper slopes and narrower crests than the Stage III moraines, but the crests are still undulatory and have undergone significant dissection in places (up to 20 meters). Boulders in the till are up to 5 meters in diameter, and the percentages of pitted and split boulders in general are much lower than in the Stage III till. Subsurface observations made in roadcuts indicate that little disintegration or grussification has occurred on subsurface clasts. Péwé and Updike (1976) report soil horizons on the younger Stage II moraines to be around 32 cm thick.

Stage I Drift Unit

The youngest and least extensive glacial deposits on San Francisco Mountain are the Stage I moraines. Ice during the Stage I glaciation was present in 5 cirques surrounding the Inner Basin, and in Abineau and Philomena Canyons on the north and west faces of Humphreys Peak. Glaciers during this event were contained in their cirques and did not coalesce in the Inner Basin. In most of the cirques around the Inner Basin there are two sets of Stage I moraines preserved. The maximum extent of the moraines ranges from 1.1 to 1.6 km from the cirque headwalls, at elevations ranging from 3050 meters in Beard Canyon to 3350 meters at Snowslide Spring. The highly variable elevations may be a factor of local shading and microclimate effects. Crests of Stage I lateral moraines are up to 20 meters above their respective valleys, and some extend up into the cirques, although many have been partially or completely buried by talus, protalus ramparts, or younger rock glaciers.

Stage I moraines are better preserved and fresher in appearance than either the Stage II or III moraines. These moraines range from the Agassiz zone to the Franciscan zone, and are heavily forested below 3500 meters by Engelman spruce and are relatively barren above 3500 meters.

I sampled relative dating characteristics on four Stage I moraines (Figure 2.3, Table 2.1). Outer slope angles and crestal widths had to be estimated at two of the sites as the moraines were plastered against either the valley walls or against an outer Stage I moraine. These moraines contain lithologies that are unique to their respective cirques, so the size and frequency of boulders greater than 50 cm reflects the different source lithologies. Cirques that contain more resistant andesites and

dacites have larger and more frequent boulder accumulations compared to those with more latite and rhyolite as source material for boulders. As the surface boulders on the lower, older moraines are predominantly andesite, only Stage I moraines with andesitic boulders were selected for relative dating measurements. On these moraines, boulders up to 5 meters diameter were found. Slope crests were sharp and straight, with only localized dissection related to the steep slopes surrounding the moraines. The surface boulders showed barely any pitting or splitting compared to the older moraines. Péwé and Updike (1976) report soil horizons on Stage I moraines ranging from 14-22 cm.

Holocene Events

Both Sharp (1942) and Péwé and Updike (1976) described post-Stage I periglacial processes that they attributed to the Holocene. In a cirque on the east face of Agassiz Peak, two rock glaciers exist, one of which has buried till of the Stage I glaciation. The boulders in the rock glaciers show little sign of weathering, and there is little vegetation growing among the rocks. The older of the two rock glaciers has trees beginning to grow through its fringes, and the boulders have more lichens than those of the younger rock glacier. Another rock glacier exists in the well developed cirque on the southeast face of Humphreys Peak. The boulders in this rock glacier are also barely weathered, unvegetated, encroach upon Stage I moraines, and are relatively free of lichens. In addition to the rock glaciers, protalus ramparts that are younger than the Stage I moraines are present in several of the Inner Basin cirques and in

Abineau Canyon. Relative dating data were not collected on any of these younger deposits, but based on the lack of vegetation and lichens on the boulders it is assumed that they are of Holocene age.

DISCUSSION OF RELATIVE AGE DATA

If there is a difference in the age of drift units that is resolvable out of a relative dating study, then some of the relative dating parameters measured should show a consistent variation from one deposit to another. If none of the parameters show such a consistent relationship, than the deposits are either too similar in age to resolve differences through relative dating methods, the deposits being measured are affected by different rates of weathering (i.e. different climates or vegetation zones), or the deposits have been affected by some process that obscures their age by altering their morphology or weathering characteristics.

The rate at which relative dating parameters develop decreases exponentially with time (Colman and Pierce, 1986). Thus the magnitude of variation in RD characteristics between different drift units cannot be viewed as a linear indicator of age separation. With respect to resolving different first-order glacial events in the Sierra Nevada range, Burke and Birkeland (1979) suggest that the average values of weathering parameters vary by a factor of two between moraines. However, young drift units that differ by a factor of two will have a smaller age difference than older units that differ by a factor of two. Without knowing the rate of change of weathering over time at a given location it is impossible to know the absolute

difference in age of separate drift units. The relative dating characteristics measured in this study were thus used solely to separate stratigraphic drift sequences. Table 2.2 shows the magnitude of change between the mean values of relative dating parameters between the respective moraine sets.

Table 2.2: Magnitude of change in relative dating parameters between drift units.

Drift Unit	CW (m)	SA (I/O)	SBF	SPD †	%W	%P	MPD	%S
I/II	1.43	1.02/1.04	1.11	1.78	1.24	1.69	1.74	2.21
I/III	3.13	2.08/1.47	1.62	3.70	1.35	3.11	4.54	3.99
II/III	2.19	2.03/1.41	1.46	2.08	1.09	1.84	2.62	1.81

Explanation of abbreviations: **CW** - Crestal Width; **SA (I/O)** - Slope Angle (Inner/Outer); **SBF** - Surface Boulder Frequency; **SPD** - Average Soil Profile Depth; **%W** - Percentage of Weathered Boulders; **%P** - Percentage of Pitted Boulders; **MPD** -Maximum Pit Depth; **%S** - Percentage of Split Boulders.

† Soil Profile information from Péwé and Updike (1976).

Morphologic parameters

Of the morphologic parameters (crestal width, slope angle, and surface boulder frequency), the crestal widths seem to show the most consistent relationship between moraines in different positions. The Stage I and II moraines are separated by a factor of 1.43, while the Stage III moraine crest is 2.19 times the average Stage II and 3.19 times the average Stage I crestal widths. Slope angles show no significant change between Stages I and II.

I suggest that the slope angles in this study are controlled more by initial moraine height-to-width ratios and by local erosional factors than by steady-state weathering forces. The Stage I moraines were very low to begin with, and although they have consistently narrower crests than Stage II moraines, they may obtain stable slopes faster due to their reduced height. The Stage I moraines measured were also supported on their outer slopes either by other moraines or by valley walls, while the Stage II moraines are located away from the valley walls, and are exposed to a greater amount of erosion.

As noted above, the surface boulder frequency depends largely on the quantity of resistant boulders emplaced in a moraine. The source areas for three of the Stage I moraines sampled contain outcrops of dacite and rhyolite that tend to be eroded as small clasts that break down quickly. Because the Stage II moraines have a larger source area of the more resistant andesite and dacite rocks that make up the bulk of surface boulders, it is not unreasonable that they would have a higher percentage of surface boulders greater than 50 cm diameter per unit area.

Weathering Characteristics

The weathering characteristics of the surface boulders on San Francisco Mountain also vary widely in their magnitude of difference between moraine sets. All of the lithologies sampled for the weathering characteristics were pyroxene andesite and hypersthene dacite that exhibit similar weathering characteristics, so the magnitude of change between relative dating sites should be largely reflective of their

age separations assuming the lack of external influences. The percentage of weathered boulders shows a general increase from Stage I to III, but the largest magnitude of change is still less than 1.5. The surfaces of the exposed volcanic rocks weather quickly, as evidenced by the high percentage of Stage I boulders weathered, and the scarcity of glacial polish or striations found on boulders and bedrock surfaces.

The average percentage of pitted boulders, the maximum pit depth, and the percentage of split boulders all show significant variances between the respective moraine sets. The presence and depth of pits is much easier to quantify than just distinguishing between fresh and weathered surfaces. It seems to be a much more useful criteria in this case for determining relative age. The small amount of soil information available (Pewe and Updike, 1976) also suggests that each drift unit represents a separate glacial event.

There are some inconsistencies between individual units (Table 2.1) which may result from external influences. The forested areas on San Francisco Mountain are highly prone to forest fires. Forest fires have been shown to equalize weathering characteristics between boulders of different ages by inducing spalling (Burke and Birkeland, 1979). Other factors that could influence surface weathering characteristics include differential vegetation densities and regrowth following forest fires, differential weathering in the different vegetation zones, or differential weathering due to exposure to microclimatic effects (stronger winds on different slopes, more precipitation or runoff in a particular drainage, greater exposure to sunlight, etc.). For example, my relative dating site 9 has morphologic characteristics typical of a Stage II moraine, but weathering characteristics that are similar to site 1 (Stage III moraine)

with the exception of pit depth. Site 9 is located in the Coloradan vegetation zone and is characterized by Ponderosa pine forest, as is site 1, while the rest of the Stage II sites are in the Datil zone and are forested with dense stands of aspen. In this case, the vegetation similarities between sites 1 and 9 may be influencing the weathering characteristics.

The most useful relative dating characteristics on San Francisco Mountain appear to be the crestal width, soil profile depth, percentage of pitted and split boulders, and mean pit depth. These characteristics all show variations of more than a factor of two between stages I and III, and stages II and III. The difference between stages I and II vary from 1.5 for crestal width to 2.2 for percentage of split boulders, but considering the rapid weathering characteristics of the volcanic rocks, I conclude that the three separate drift units do represent separate glacial events, as has been suggested by Sharp (1942) and by Péwé and Updike (1976).

The fact that the Stage III deposits lie unconformably over and against the tuff ring of Sugarloaf Mountain means that the maximum age of the Stage III glaciation is ~218 ka. The description of the moraine morphology, stratigraphy, and relative dating characteristics is consistent with other studies of alpine glaciation across the Colorado Plateau and Great Basin that have found threefold sequences of glaciation (Richmond, 1986; Bevis, 1995). From these constraints and the relative dating relationships, it may be reasonable to assign the Stage III glaciation to oxygen-isotope stage 6, the Stage II glaciation to oxygen-isotope stage 4, and the Stage I glaciation to oxygen-isotope Stage 2. However, in light of the rapid weathering characteristics of the volcanic material on the surface of the moraines, and the lack of

more detailed sub-surface weathering and soil catena data, I would not rule out the possibility that the uppermost Stage I moraines may represent a post-glacial cooling event, with the Stage II moraines reflecting the last glacial maximum.

RECONSTRUCTION OF GLACIER SURFACES

The reconstruction of a former ice surface of a valley glacier is possible using valley geometry and constraints on the extent and thickness of the former glacier from the geologic record (Nye, 1952; Matthews, 1967). I used the position of terminal moraines to constrain the extents of glacier advances. Lateral moraine crest elevations were then used to establish the former ice surface profile downvalley. Due to the lack of trimlines and polished surfaces, the ice surface elevation of the accumulation zone had to be extrapolated from the change in elevation of existing lateral moraines. One valley glacier was reconstructed from the oldest set of Stage II moraines in the Inner Basin (Figure 2.4), and four cirque glaciers were reconstructed from Stage I moraines (Figure 2.5).

The basal shear stress of each initial reconstruction was calculated using the general formula for valley glaciers established by Nye (1952):

$$\tau = \rho ghC \sin(\alpha)$$

where τ is shear stress in bar, ρ is ice density, g is gravitational acceleration, h is ice thickness, α is the slope of the valley floor, and C is a shape factor. The shape factor allows for the effect of drag on the glacier by the valley walls, and is determined by

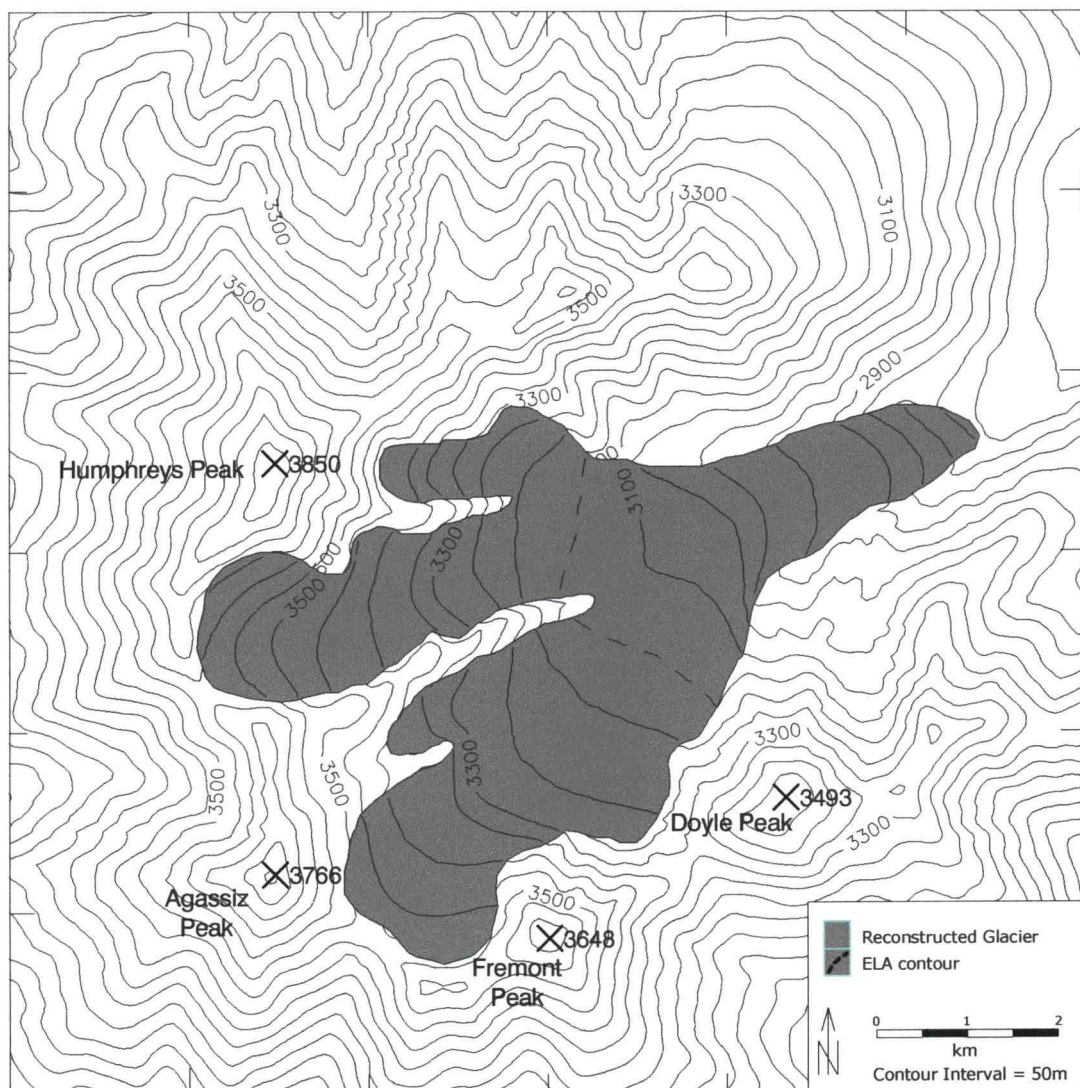


Figure 2.4: A reconstruction of the most extensive Stage II Inner Basin glacier. The ELA is shown with a dashed contour line.

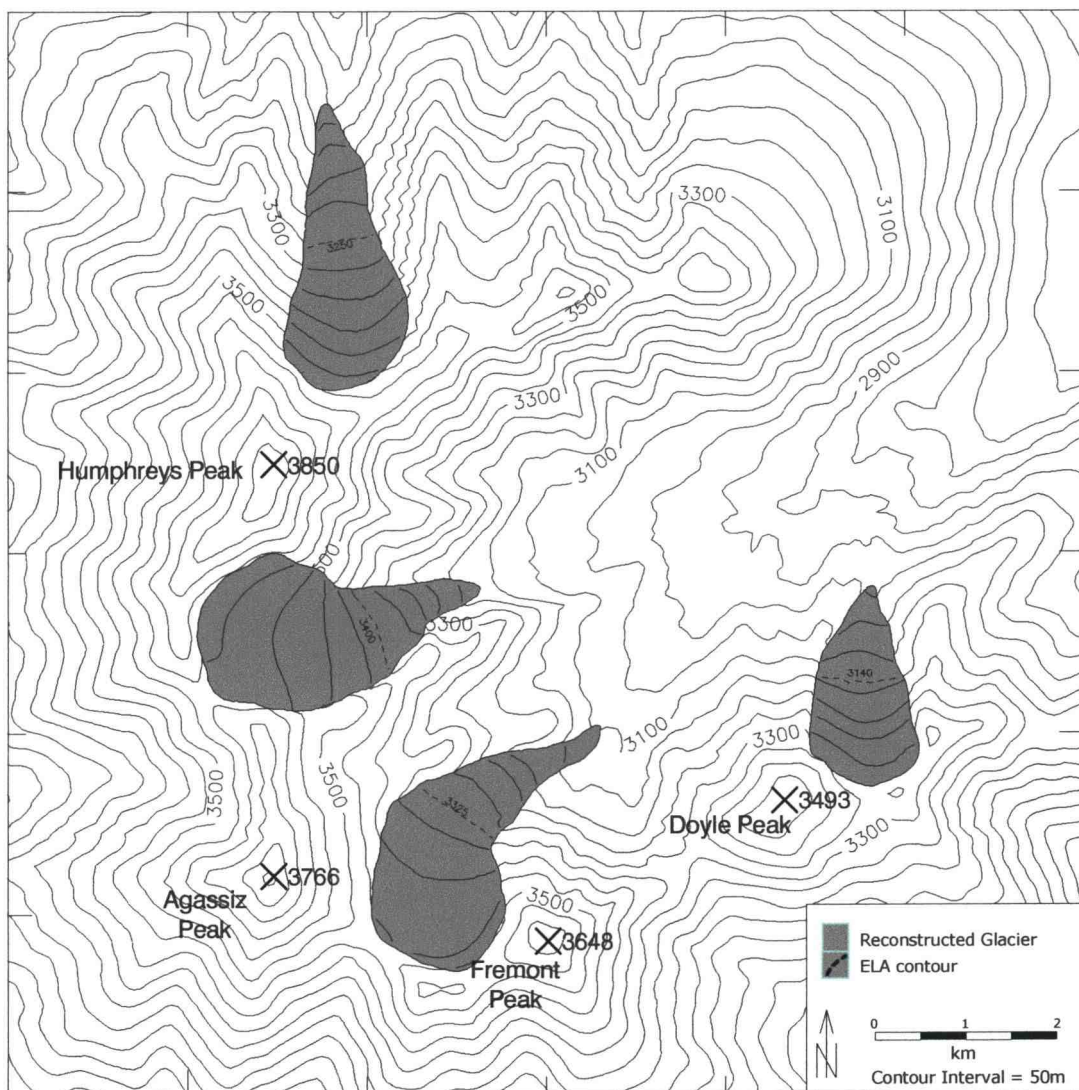


Figure 2.5: Reconstruction of four Stage I glaciers. Equilibrium line altitudes are shown as dashed contour lines and labeled.

dividing the cross sectional area of the glacier by the perimeter of the valley cross section that is in contact with the ice (Nye, 1952). The ice surface elevation that was extrapolated in the accumulation zone was then further adjusted to bring the basal shear stress of the approximated profile to values between 0.5 and 1.5 bars as established by general observation of valley glacier basal shear stresses in the literature (Nye, 1952, Matthews, 1967, Porter et al., 1983, Paterson, 1994).

A boundary for each reconstructed glacier was established following calculation of former ice thickness, and the surface area of the glacier was calculated to obtain an equilibrium line altitude (ELA) of each glacier. I used the accumulation area ratio (AAR) method of calculating ELA, with an AAR of 0.65 following Meierding (1982). As glacier flow is generally extending in the accumulation zone, and compressing in the ablation zone, contour lines were drawn according to elevation with respect to the ELA (concave up glacier above the ELA, and concave down glacier below the ELA) as observed on modern glaciers (Matthews, 1967; Paterson, 1994). The final glacier surface digital elevation model was obtained by digitizing the ice surface elevations along the glacier boundary and contour lines, and applying a kriging interpolation algorithm to produce a regular grid of elevations using SURFER 6 ® mapping software (Golden Software, 1995).

The ELA for the reconstructed Stage II glacier is about 3150m (Figure 2.4). The reconstructed Stage I moraines show ELAs ranging from ~3140m for a sheltered north facing cirque to 3400m for an east facing cirque (Figure 2.5). These roughly match the regional paleo-ELA reported for late-Wisconsin glaciers in Porter et al. (1982) as being between 3000 and 3300 meters.

CONCLUSIONS

Glacial moraines were mapped on San Francisco Mountain, Arizona, and semi-quantitative relative dating data were collected from ten moraines in order to separate glacial events within individual drainages, and to correlate events between drainages. The results of the weathering data corroborate earlier studies that suggest a threefold sequence of glaciation on the mountain. The youngest moraines were most likely deposited around the last glacial maximum. The other two drift units may reflect the presence of glaciers during oxygen-isotope stages 4 and 6, respectively. Glaciers from the two most recent glacial events were reconstructed to show possible ice extents for the last glacial maximum. Paleo-ELAs ranging from 3100 to 3400 meters agree with regional reconstructions.

REFERENCES

- Atwood, W.W., 1905, Glaciation of San Francisco Mountain, Arizona: *Journal of Geology*, v. 8, pp. 276-279.
- Bevis, K.A., 1995, Reconstruction of late Pleistocene paleoclimatic characteristics in the Great Basin and adjacent areas: Unpublished Doctoral Thesis, Oregon State University, 270 pp.
- Burke, R.M., and Birkeland, P.W., 1979, Reevaluation of multiparameter relative dating techniques and their application to the glacial sequence along the eastern escarpment of the Sierra Nevada, California: *Quaternary Research*, v. 11, pp. 21-51.
- Colman, S.M., and Pierce, K.L., 1986, Glacial sequence near McCall, Idaho: Weathering rinds, soil development, morphology, and other relative-age criteria: *Quaternary Research*, v. 25, pp. 25-42.

- Gibbons, A.B., Megeath, J.D., and Pierce, K.L., 1984, Possibility of moraine survival in a succession of glacial advances: *Geology*, v. 12, pp. 327-330.
- Golden Software, 1995, Surfer v. 6.01 Surface Mapping System: Golden Software Inc., Golden, Colorado.
- Hostetler, S.W., and Clark, P.U., 1997, Climatic controls of western U.S. glaciers at the last glacial maximum: *Quaternary Science Reviews*, v. 16, pp. 505-511.
- Leonard, E.M., 1984, Late Pleistocene equilibrium-line altitudes and modern snow accumulation patterns, San Juan Mountains, Colorado, United States.: *Arctic and Alpine Research*, v. 16, pp. 65-76.
- Leonard, E.M., 1989, Climatic change in the Colorado Rocky Mountains: Estimates based on modern climate at late Pleistocene equilibrium lines, *Arctic and Alpine Research*, v. 21, pp. 245-255.
- Locke, W.W., 1990, Late Pleistocene glaciers and climate of western Montana, U.S.A., *Arctic and Alpine Research*, v. 22, pp. 1-13.
- Mathews, W.H., 1967, Profiles of late Pleistocene glaciers in New Zealand: *New Zealand Journal of Geology and Geophysics*, v. 10, pp. 146-163.
- Meierding, T.C., 1982, Late Pleistocene glacial equilibrium-line altitudes in the Colorado Front Range: A comparison of methods: *Quaternary Research*, v. 18, pp. 289-310.
- Merrill, R.E., and Péwé, T.L., 1972, Late Quaternary glacial chronology of the White Mountains, east-central Arizona: *Journal of Geology*, v. 80, pp. 493-501.
- Mitchell, V.L., 1976, The regionalization of climate in the western United States: *Journal of Applied Meteorology*, v. 15, pp. 920-927.
- Nye, J.F., 1952, A comparison between the theoretical and the measured long profile of the Unteraar glacier: *Journal of Glaciology*, v. 2, pp. 103-107.
- Paterson, W.S.B., 1994, *The Physics of Glaciers: Third Edition*: Pergamon Press, New York, 250 pp.
- Pearson, G.A., 1931, Forest types in the southwest as determined by climate and soil: U.S. Department of Agriculture Technical Bulletin, v. 247, p. 144.
- Péwé, Troy L., and Updike, Randall C., 1976, San Francisco Peaks, A guidebook to the geology, Second Edition: Museum of Northern Arizona, Flagstaff, Arizona, 80 pp.

- Porter, S.C., 1964, Composite Pleistocene snow line of Olympic Mountains and Cascade Range, Washington: Geological Society of America Bulletin, v. 75, pp. 477-481.
- Porter, S.C., Pierce, K.L., and Hamilton, T.D., 1983, Late Wisconsin mountain glaciation in the western United States: *in* Porter, S.C., ed., Late Quaternary environments of the United States, Volume 1, The late Pleistocene: Minneapolis, University of Minnesota Press, pp. 71-114.
- Richmond, G.M., 1987, Stratigraphy and correlation of glacial deposits of the Rocky Mountains, the Colorado Plateau, and the ranges of the Great Basin: Quaternary Science Reviews, v. 5, pp. 99-127.
- Sharp, R.P., 1942, Multiple Pleistocene glaciation on San Francisco Mountain, Arizona: Journal of Geology, v. 42, pp. 481-503.
- Sheridan, M.G., and Updike, R.G., 1975, Sugarloaf Mountain tephra - Pleistocene rhyolitic deposit of base-surge origin in northern Arizona: Geological Society of America Bulletin, v. 86, pp. 571-581.
- Zielinski, G.A., and McCoy, W.D., 1987, Paleoclimatic implications of the relationship between modern snowpack and late Pleistocene equilibrium-line altitudes in the mountains of the Great Basin, western U.S.A., Arctic and Alpine Research, v. 19, pp. 127-134.

CHAPTER 3

DEVELOPMENT AND TESTING OF A NUMERICAL MASS BALANCE MODEL FOR ALPINE GLACIERS

Colin D. Poellot

LIST OF VARIABLES USED IN EQUATIONS

Variable	Description	Units
$\bar{\beta}$	mean horizon angle for DEM grid cell	radians
α	surface albedo	dimensionless
ε	emissivity of terrain	dimensionless
σ	Stephan Boltzman constant	$\text{Wm}^{-2}\text{K}^{-1}$
α	surface albedo of glacier	dimensionless
ρ_a	density of dry air	kgm^{-3}
α_b	base albedo	dimensionless
α_{basin}	basin albedo	dimensionless
α_{ns}	albedo of new snow	dimensionless
α_{os}	albedo of old snow	dimensionless
α_s	albedo of snow	dimensionless
Δt	timestep	varies
ΔX	DEM column spacing	meters
ΔY	DEM row spacing	meters
A	aspect of glacier surface	radians
\hat{A}	solar azimuth	radians
a1-a4	variables for initializing base albedo	dimensionless
a5	aging factor for α_s	dimensionless
a6,a7	snow weathering variables	dimensionless
A_i	surface area of DEM cell	m^2
A_n	Total Surface Area	m^2
B	variable used to calculate EOT	dimensionless
B_i	net surface mass balance of DEM cell	m.w.e.
B_n	average net surface mass balance	m.w.e.
c_p	specific heat of air	$\text{Jkg}^{-1}\text{K}^{-1}$
D	solar declination	radians
d	snow depth	meters
DifSW	diffuse shortwave radiation	Wm^{-2}
DirSW	direct shortwave radiation	Wm^{-2}
E	elevation of DEM grid cell	meters
e_a	atmospheric vapor pressure	Pa
EB	surface energy balance	m.w.e.
ELA	equilibrium line altitude	meters
EOT	equation of time	dimensionless

LIST OF VARIABLES USED IN EQUATIONS (CONTINUED)

Variable	Description	Units
e_s	saturation vapor pressure at the surface	Pa
G	net incoming shortwave radiation	Wm^{-2}
\hat{h}	solar altitude above the horizon	radians
HA	hour angle of sun	radians
H_l	turbulent flux of latent heat	Wm^{-2}
H_s	turbulent flux of sensible heat	Wm^{-2f}
I	clear sky direct and diffuse radiation	Wm^{-2}
K_h	transfer coefficient	dimensionless
lat	latitude	radians
L_f	latent heat of ice	Jkg^{-1}
lon	longitude	radians
LSoT	local solar time	minutes
LSTM	local standard time meridian	radians
LT	local time	minutes
L_v	latent heat of vaporization	Jkg^{-1}
LW_{in}	incoming longwave radiation	Wm^{-2}
LW_{lapse}	lapse rate for LW_{in}	Wm^{-2}
LW_n	net longwave radiation	Wm^{-2}
LW_{out}	outgoing longwave radiation	Wm^{-2}
M_s	cumulative ablation over melt season	m.w.e.
N	day number of year	
P	atmospheric pressure	Pa
P_0	atmospheric pressure at sea level	Pa
S	slope of glacier surface	radians
Sn	snow accumulation	m.w.e.
snowd	snow depth	meters
spack1,2	parameters for linear regression of snow depth	dimensionless
t	time period	varies
T_A	air temperature	K
t_c	current day number	
T_s	surface temperature	K
t_s	day number of last snow accumulation	
u	wind speed	ms^{-1}
$V_{f(sky)}$	sky view factor	dimensionless

LIST OF VARIABLES USED IN EQUATIONS (CONTINUED)

Variable	Description	Units
$V_{f(\text{terrain})}$	terrain view factor	dimensionless
x	DEM column number	dimensionless
y	DEM row number	dimensionless
β	horizon angle for DEM grid cell	radians

ABSTRACT

We develop a model that uses an energy balance approach to calculate annual ablation over a glacier surface. Required model input includes a two-dimensional elevation map of the glacier surface and surrounding topography, as well as climate records that include daily values of air temperature, wind speed, precipitation, atmospheric vapor pressure, incoming shortwave radiation, and incoming longwave radiation. Model outputs include the net specific balance and equilibrium line altitude of the glacier. Model simulations of mass balance are compared with observed data from the 1990 ablation season at Haut Glacier d'Arolla, Valais, Switzerland. Calculated ablation values closely match observed values, thereby supporting the validity of the model. A preliminary model run was also accomplished for 5 Pleistocene glaciers reconstructed on San Francisco Mountain, Arizona, using output from a regional climate model as input. The model delivers a glacier that is nearly in mass balance for one of the reconstructions. The energy balance approach used in the model was designed to allow the model to test sensitivity of former glaciers to changes in temperature or precipitation.

INTRODUCTION

Alpine glaciers have long been recognized as being closely linked with local, regional, and global climate, both in their rapid response time to climate change, and in their capacity to influence local climate (Meier, 1965; Walters and Meier, 1989; McClung and Armstrong, 1993; Paterson, 1994). The complex feedback processes between glacier and climate are ultimately recorded in the deposits resulting from glacial advances and retreats. The geologic record of alpine glacier advances can thus provide an important source of paleoclimate information in a region. For example, the chronology of alpine glaciers in the western U.S. during the last glaciation suggests that glacier advances and retreats were linked to rapid climate fluctuations recorded by marine sediment records in the North Atlantic (Porter et al., 1983; Phillips et al., 1993; Clark and Bartlein, 1995). The ability to accurately test the sensitivity of former glaciers to specific climate variables is desirable in that it would allow testing of hypotheses concerning the patterns of regional paleoclimate change.

The traditional method of interpreting late Pleistocene climatic conditions from glacial deposits involves reconstructing the equilibrium line altitude (ELA) of a network of former glaciers, then calculating temperature lapse rates and precipitation increases necessary to sustain glaciers at those altitudes by evaluating the paleo-ELAs against modern ELAs (Porter, 1964; Mathews, 1967; Meierding, 1982; Leonard, 1984). However, while it is possible to infer general paleoclimate conditions using this method, it is not possible to deduce specific climate forcing mechanisms or changes, and paleoclimate reconstructions in the western U.S. resulting from such studies have often led to differing or conflicting results (Zielinski and McCoy, 1987; Leonard, 1989;

Locke, 1990; Bevis, 1995). One approach that has been developed recently is an empirical method for computing mass balance from precipitation and temperature fields simulated by a regional climate model (Hostetler and Clark, 1997). This approach does allow for isolation and sensitivity testing of the relative contributions of precipitation and temperature that controlled the spatial patterns of alpine glaciers at the LGM. Although the calculation of net balance in this model (Hostetler and Clark, 1997) is based indirectly on energy balance principles, it does not account for the complete description of these balances, nor does it resolve important local conditions (e.g. topographic shading) that may significantly affect mass balance.

This paper describes the structure and testing of a surface energy balance model that is designed to be driven by climate data generated by a high-resolution regional climate model. The goal was to develop a mass balance model for alpine glaciers and ice caps that would enable sensitivity testing of specific climate forcing mechanisms (i.e. temperature and precipitation) on former glaciers. The model calculates specific net balance over a two dimensional (2-D) glacier surface by summing precipitation and ablation over a specified time period. Modeled 2-D net balance over the surface of the glacier can be used to determine the equilibrium line altitude of the glacier.

The advantage of using an energy balance approach is that it will allow perturbation of specific variables to gauge the result on glacier balance and resulting equilibrium line altitudes for former alpine glaciers. The model could also be used to calculate changes in surface melt as a proxy for meltwater input to paleo lakes (McCoy and Williams, 1985). Moreover, calculated net balance and ELAs could be used to

determine the activity index of former glaciers as an indicator of glacial erosion rates (Andrews, 1972). In addition to being used as a tool in paleoclimate research, the model could be used on modern glaciers in conjunction with climate models to test hypothesis regarding climate change, including glacier response to increasing levels of CO₂ in the atmosphere (Gregory and Oerlemans, 1998).

The model was tested with field data collected during the 1990 ablation season at Haut Glacier d'Arolla, Valais, Switzerland (Arnold et al., 1996). All necessary inputs except incoming longwave radiation were provided, and daily ablation values at four separate points were used for testing of model output. As with similar energy balance models (Oerlemans, 1992; Zuo and Oerlemans, 1996; Arnold et al., 1996) the parameterization of the albedo provides the largest uncertainty in model output. Although testing with more complete modern data over longer timespans would be ideal, the model should provide sufficient accuracy to be used for sensitivity testing on former glaciers.

The model was also applied to reconstructed Pleistocene glaciers on San Francisco Mountain, Arizona, using output from a regional climate model as input. Two 4-year records of climate data were supplied: one from the present as a control run, and one from the last glacial maximum (LGM). The climate data were applied to four glaciers from the most recent glaciation, and to one glacier from the second most recent glaciation.

MODEL DESCRIPTION

The model is an executable file designed to run on standard PC architecture. The model calculates the net balance of a glacier for a prescribed time period by summing the net accumulation and net ablation over the glacier surface. The glacier surface is represented in a two dimensional digital elevation model (DEM) in order to account for elevation changes and terrain variables. The use of the DEM allows the model to take into account surface slope and aspect, as well as the effects of shading and reflection of solar radiation from the surrounding terrain at each grid node. The model timestep is variable, allowing the use of hourly or daily climate data. In all energy balance equations, the surface of the glacier is fixed at the melting point (273.15°K), and melting occurs whenever the energy balance is positive. This assumption is common to many surface energy balance models applied to mid to low-latitude glaciers, where most melting occurs in summer months when the mean air temperature is above freezing and the energy balance is positive (Olyphant, 1986; Oerlemans, 1992; Arnold et al., 1996; Zuo and Oerlemans, 1996).

The average net surface mass balance B_n of a glacier subdivided into k grid cells is calculated:

$$B_n = \frac{1}{A_n} \sum_{i=1}^k B_i A_i \quad (3.1)$$

where A_n is the total glacier area (m^2), B_i is the individual net balance of a DEM cell, and A_i is the area of a DEM cell. The units of B_n are meters water equivalent (m.w.e.).

The B_i is calculated as:

$$B_i = \sum^t [S_n + \min(0, -EB)] \Delta t \quad (3.2)$$

$$EB = \{(1 - \alpha)G + LW_n + H_s + H_l\} / L_f \quad (3.3)$$

where t is the time period and Δt is the timestep, S_n is accumulation of snow (m.w.e.), EB is the energy balance at the glacier surface (m.w.e.), α is the surface albedo, G is total incoming solar radiation at the surface, including direct, diffuse, and reflected radiation, LW_n is net (i.e. $LW_{in} + LW_{out}$) longwave radiation, H_s and H_l represent the turbulent fluxes of sensible and latent heat between the surface and the atmosphere, and L_f is the latent heat of fusion of ice. Positive values represent energy gain at the surface

Input and Output Files

A basic flowchart illustrating the structure of the code is shown in Figure 3.1. The complete code is provided in the Appendix. An initial model run for a glacier requires four input files: 1) an ASCII file containing the climate data for each timestep; 2) a DEM of the glacier surface; 3) a DEM of the entire glacier basin; and 4) a file that contains glacier specific parameters including geographic data, albedo equation variables, and other user-defined options (Table 3.1). Subsequent model runs use lookup files generated by the first run as input in place of the basin DEM.

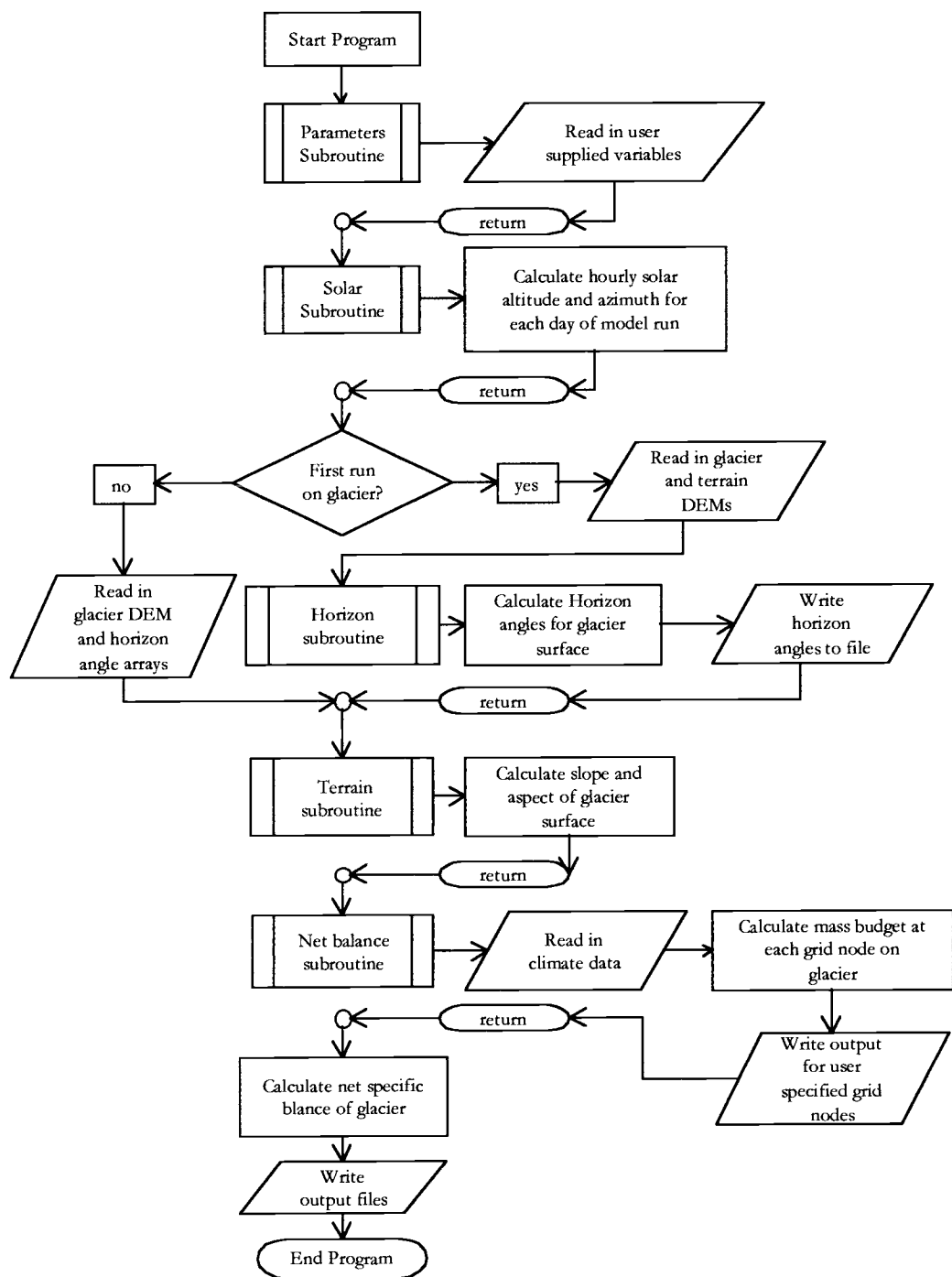


Figure 3.1: General flowchart of program.

Table 3.1: List of user defined parameters required as program input

Variable	Units	Description
belev	meters	base elevation of climate data
zone	dimensionless	time zone based on Greenwich Universal Time (e.g. pacific time zone = -8)
lat	decimal degrees	glacier latitude
lon	decimal degrees	glacier longitude
ELA	meters	initial equilibrium line altitude of glacier
a1 – a4	dimensionless	variables used to calculate initial background albedo
a5-a7	dimensionless	variables used to albedo calculation
spack1, spack2	dimensionless	variables used to initialize snowpack at the beginning of the model run
pre_laps	degrees/meter	precipitation lapse rate for adjustment to input climate data and/or sensitivity testing
tmstp	dimensionless	number of timesteps per day to perform energy balance calculations
numstk	dimensionless	number of points on the glacier the program will write daily climate and mass budget data files for.
stkloc	row #, column #	x,y coordinates of grid nodes for output files
status	“old” or “new”	“new” if the model run is the first for the glacier “old” if horizon angles do not need to be re calculated for subsequent model runs on a glacier.
Tdep	degrees (positive or negative)	temperature depression: number of degrees to adjust the temperature that is input from the climate data file (for sensitivity tests)

Climate Data Input

Climate variables required by the model are air temperature ($^{\circ}\text{C}$), wind speed (m s^{-1}), atmospheric vapor pressure (Pa) at 2 meters above the surface, incoming global shortwave radiation ($\text{J m}^{-2} \text{ timestep}^{-1}$) as received by a horizontal surface, incoming longwave radiation ($\text{J m}^{-2} \text{ timestep}^{-1}$), and precipitation in meters water

equivalent (m.w.e.). Air temperature, wind speed and vapor pressure are all average values per timestep, while radiation and precipitation are in cumulative amounts per timestep. The model is designed to work with climate data from a single climate station or climate model node.

Elevation Data Input

The elevation data required to represent the glacier surface and surrounding topography are initially input into the model via two DEMs. The DEM that is used in the energy balance subroutine contains only elevation values for the surface of the glacier. The second DEM contains elevation data for the entire glacier basin, and it must cover a wide enough geographic area to include any ridges or peaks that may obstruct the direct rays of the sun from striking the glacier during the day. The basin DEM is only required for the first model run on any given glacier. Once the horizon angle lookup tables have been calculated for a given glacier, they are used as input for subsequent runs, thereby reducing computation time.

Output Files

The program generates a variety of output files for analysis. An ELA for the glacier is calculated over the course of the model run by comparing the net balance at equal elevation intervals on the glacier DEM. The ELA, the net specific balance for the surface of the glacier over the model run, and the net components of the energy balance equation used to calculate ablation (equation 3.3) are written to a summary

file. The summary file also contains all the input parameters and geographic information about the glacier to insure knowledge of parameters for a given run, and so that the run may be duplicated. Every model run generates a file of the spatial distribution of net specific balance over the glacier surface. This net balance file is in the same format as the DEMs, so contour maps of the net balance can be produced. The program also writes the daily means of climate variables, solar radiation receipts, energy balance components, accumulation, and ablation amounts for points on the glacier surface that are user specified in the 'Parameters' input file. The first run on any glacier produces two horizon angle files that are used as inputs for subsequent runs on the glacier. The program can also produce DEM files containing the slope and aspect of each grid cell, as well as files that contain tables of solar elevation and aspect for each day of the climate record. Glacier specific variables and output file options are input through the 'Parameters' file. Table 3.1 lists all the required variables and gives a brief description of each. The variables used to calculate albedo and initial snowpack conditions are discussed below in the Net Balance section.

Solar and Terrain Subroutines

Solar Coordinates

To adjust incoming shortwave radiation to the glacier slope and aspect, the angle of the incident solar beam must be known. The program calculates solar elevation above the horizon and solar azimuth on an hourly timestep for each day of the climate record. Variables required include the glacier latitude and longitude, the

local time zone, and the start day and length of the climate record. Most published equations for determining solar coordinates use the Julian calendar for determining local standard time and solar declination (Walraven, 1978; Meeus, 1998). While these equations give results that are accurate to 0.001 degrees or better, they are not valid for paleoclimate research predating 4712 B.C. (Meeus, 1998). My model uses a more general set of equations to calculate the EOT and solar declination based on Grobneck (1999) and Carlson (1995). Given the assumptions involved in reconstructing former glacier surfaces, the precision of these equations is sufficient for adjusting incoming solar radiation. The equations are (Grobneck, 1999):

the equation of time (EOT):

$$\text{EOT} = 9.87 * \sin(2B) - 7.53 * \cos(B) - 1.5 * \sin(B) \quad (3.4)$$

$$B = 360 * (N - 81) / 365 \quad (3.5)$$

where N is the day number of the year (Jan. 1=day 1);

the solar declination (D):

$$D = 23.45 * [\sin 360 / 365 * (284 + N)] \quad (3.6)$$

the local solar time (LSOT) in minutes:

$$\text{LSoT} = (\text{LT} + 4 * (\text{lon} - \text{LSTM}) + \text{EOT}) / 60 \quad (3.7)$$

where LT is the local time in minutes, lon is local longitude, and LSTM is the local standard time meridian measured in degrees away from Greenwich (east is positive, west is negative);

and the hour angle of the sun (HA):

$$\text{HA} = (\text{LSoT} - 12.) * -15 \quad (3.8)$$

Once the hour angle and declination are calculated, the solar altitude (\hat{h}) and azimuth (\hat{A}) are calculated as:

$$\hat{h} = \arcsin[\sin(\text{lat}) * \sin(\text{DEC}) + \cos(\text{lat}) * \cos(\text{DEC}) * \cos(\text{HA})] \quad (3.9)$$

$$\hat{A} = \arccos\left\{\frac{\sin(\hat{h}) * \sin(\text{lat}) - \sin(\text{DEC})}{\cos(\hat{h}) * \cos(\text{lat})}\right\} \quad (3.10)$$

All angles are converted to radians in the program.

Terrain Adjustments

Slope and aspect for the glacier surface at each grid cell are calculated from the elevations of the surrounding grid nodes using the following equations (Williams et al., 1972):

$$S = \arctan \left\{ \left[(E_{(x,y+1)} - E_{(x,y-1)}) / 2(\Delta Y) \right]^2 + \left[(E_{(x+1,y)} - E_{(x-1,y)}) / 2(\Delta X) \right]^2 \right\}^{\frac{1}{2}} \quad (3.11)$$

$$A = \arctan \left\{ \left[(E_{(x-1,y)} - E_{(x+1,y)}) / 2(\Delta X) \right] / \left[(E_{(x,y-1)} - E_{(x,y+1)}) / 2(\Delta Y) \right] \right\} \quad (3.12)$$

where S is the positive slope angle from horizontal, with values ranging from 0 to $\pi/2$, A is the slope aspect which ranges from $-\pi$ to π , where a value of 0 corresponds to slopes facing due south, positive values to slopes facing east of south, and negative values to slopes facing west of south, x corresponds to column numbers in the DEM array, y corresponds to row numbers, E is the elevation of the grid node at location (x, y) , and ΔX and ΔY represent the grid spacing in the DEM array (Figure 3.2). Slope and aspect for grid nodes on the glacier boundary are calculated by interpolating elevations between the glacier boundary and the nearest grid nodes on the interior of the glacier.

The model computes shading of the glacier surface by the surrounding terrain at each timestep, following the method introduced by Dozier and Outcalt (1979) in which a lookup table of horizon angles is computed for each point on the glacier surface. The horizon angle is the largest angle between the grid node in question and all other points in the DEM along a specific azimuth (Figure 3.2). The algorithm used in the program starts at a grid node, and moves towards the edge of the DEM along

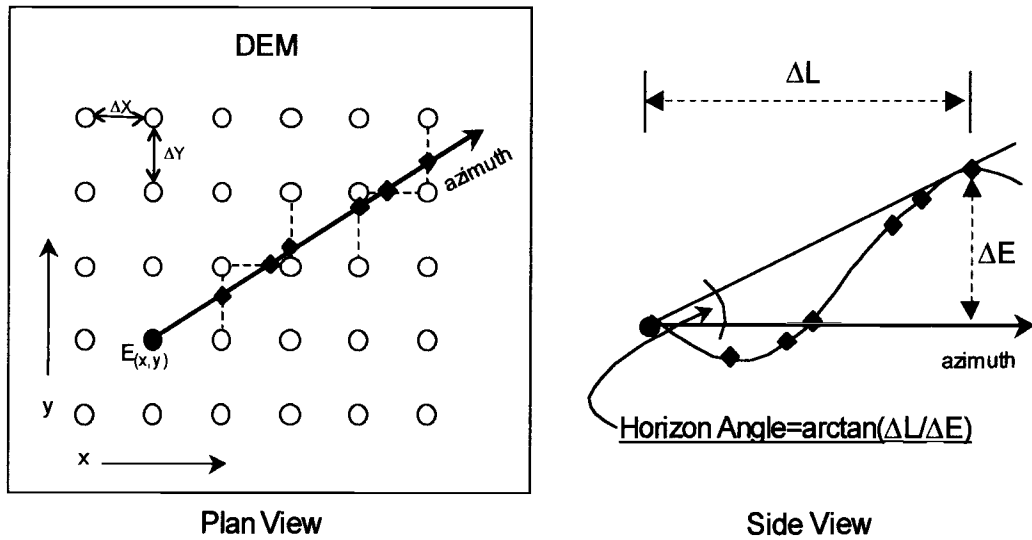


Figure 3.2: Schematic of horizon angle calculation. Open circles represent DEM grid points. The closed circle represents the origin of a single horizon angle search along shown azimuth. Diamonds represent points in the DEM where elevations are interpolated from surrounding grid nodes to determine the maximum angle to the horizon, as shown in the side view.

the selected azimuth. Following Williams et al. (1972), the elevation at each intersection of the azimuth with a row or column is interpolated from the nearest two grid nodes along that row or column (Figure 3.2). If the interpolated elevation is greater than the elevation of the starting grid node, the angle between the two elevations is calculated. The greatest angle along 36 azimuths spaced at 10 degree intervals is stored in an array. At each timestep, the solar elevation angle above the horizon is checked against the horizon angle at each grid node for the azimuth that is closest to the solar azimuth. As long as the solar elevation angle is less than the horizon angle, the grid node is considered to be shaded, and only diffuse and reflected shortwave radiation values are used in energy balance calculations.

To adjust diffuse radiation for the effects of topography a sky view factor ($V_{f(sky)}$) is calculated for each grid cell to determine the portion of sky that is unobstructed by surrounding terrain. The view factor is calculated in the model by the following equation (Oke, 1987), which represents the sky view factor of an isotropic basin:

$$V_{f(sky)} = \cos^2(\bar{\beta}) \quad (3.13)$$

The formula calculates $V_{f(sky)}$ as a dimensionless number between 0 and 1. $\bar{\beta}$ is the mean horizon angle for the grid node. A horizontal surface with no obstructions has a sky view factor of 1. The equation for a basin generally best represents cirque morphology, and is commonly used in alpine energy balance studies (Dozier and Outcalt, 1979; Marks and Dozier, 1979; Olyphant, 1986). If the model is to be used on an ice cap, an equation that represents a simple slope would be more appropriate, but the formula could be easily adjusted to reflect the change in morphology.

The horizon angle array calculated by the model, along with the mean horizon angle for each grid cell, are written to two external files. Thus the time consuming process of calculating these angles is only undergone for the first model run on each glacier. For subsequent model runs, the program simply reads in the external files and stores them in internal arrays that are then passed to the energy balance subroutine for reference in adjusting radiation receipts. The slope, aspect, and solar calculations

do not significantly increase the program run time, so these values are recalculated and stored in internal memory for each run in order to save disk storage space.

Net Balance Subroutine

The net balance of each grid node on the glacier surface is calculated within the net balance subroutine. The elevation, slope, aspect, and view factor for each grid node are passed from the main program to the subroutine. Before the start of the energy balance calculations the atmospheric pressure (P) at the grid elevation is calculated using the hypsometric equation with a scale height of 7 km (Wallace and Hobbs, 1977):

$$P = P_0 \exp(-E_{(x,y)} / 7000) \quad (3.14)$$

where P_0 is the standard atmospheric pressure at sea level (101,325 Pa).

On the first day of the model run at each grid node the existing snowpack must be initialized, and unless the run is starting at the end of the ablation season the snow depth is added to the total accumulation. A simple linear equation is used to calculate the snow depth (m.w.e.) at the beginning of the model run following Arnold et al. (1996):

$$d = \text{spack1} + (E_{(x,y)} * \text{spack2}) \quad (3.15)$$

where d is snow depth, and spack1 and spack2 are user defined parameters (Table 3.1). The snow depth at the elevation the climate data are extracted for may be determined by looking at the average precipitation in the climate file. The spack^* variables are calculated before the start of the model run by examining regression relationships between altitude and accumulation at the glacier. The snow depth calculated in equation 3.15 is then used to calculate the initial albedo of the grid cell. After initialization, both snow depth and albedo are computed by the model.

At the beginning of each timestep the model reads in the climate data from an external file. Air temperature is then adjusted for elevation using a lapse rate of 0.0065 degrees $^{\circ}\text{C m}^{-1}$. If the air temperature is less than 1°C any precipitation falling at that timestep is assumed to fall as snow, and the amount is added to the total accumulation. The model does not currently treat the contribution of rainfall to the surface energy balance, or the erosive effects of rain on the snowpack, so if the temperature is above 1°C the precipitation is ignored.

Shortwave radiation

After checking for precipitation, the model calculates and/or adjusts the components of the main energy balance equation (equation 3.3). The radiation value given in the input file is a total global shortwave radiation value received at a

horizontal surface with no terrain obstructions. This value is split into direct and diffuse components, and the direct component must be adjusted for the slope and aspect of the glacier surface at each grid node. The atmospheric component of diffuse radiation is assumed to be 20% of the global radiation (Arnold et al., 1996).

If a grid node at any timestep is determined to be shaded by the horizon then only diffuse radiation is applied to the energy balance equation. If the node is in the sun, the amount of direct radiation (DirSW) received is corrected for surface slope and aspect following Robinson (1966) and Oke (1987):

$$\text{DirSW} = 0.8 G \left[\sin(\hat{b}) \cos(S) + \sin(S) \cos(\hat{b}) \cos(\hat{A} - A) \right] / \sin(\hat{b}) \quad (3.16)$$

Diffuse radiation is received at the surface through scattering of shortwave radiation by the atmosphere, and by reflection of shortwave radiation from surrounding terrain. Total diffuse radiation (DifSW) received is calculated as:

$$\text{DifSW} = 0.2 G V_{f(\text{sky})} + \alpha_{\text{basin}} (0.8 G V_{f(\text{terrain})}) \quad (3.17)$$

where the atmospheric component is specified as 20% of the global radiation (G), and the reflected component is calculated by assuming a mean basin albedo (α_{basin}). The terrain view factor ($V_{f(\text{terrain})}$) represents the amount of surrounding terrain that is visible from the grid node, and is simply the reciprocal of the sky view factor. The adjusted direct and diffuse radiation values are added to obtain the total incoming shortwave radiation value used in equation 3.3.

Special treatment of the shortwave radiation is required when the program is set to run on a daily timestep because the solar angle and day length vary considerably throughout the year. In order to adjust a total daily radiation receipt for slope, aspect, shading, and reflection, the model divides the daily value into hourly components by calculating a theoretical value for clear sky direct and diffuse radiation (I) using standard equations from Robinson (1966) and Oke (1987) at all hourly timesteps where the sun is above the horizon. At each timestep I is adjusted for the solar angle using equations 3.16 and 3.17. The ratio of the daily sums of adjusted and unadjusted theoretical radiation is then multiplied by the actual daily global radiation value that was input to the model to obtain an adjusted radiation value. The validity of this method was confirmed by comparing daily radiation totals returned by an hourly dataset adjusted using equations 3.16 and 3.17 with the daily averages of the same dataset that were adjusted using the above method. The correlation between the two methods was $r^2 = 0.996$ at the 99% confidence level, showing that the two methods return essentially the same results.

Longwave Radiation

The net longwave radiation value used in equation 3.3 is the sum of incoming and outgoing longwave radiation. The glacier surface is treated as a blackbody for outgoing longwave radiation, and as the surface in the model is assumed to be at the melting point at all times, the outgoing longwave radiation flux at each grid cell is 316 Wm^{-2} (Oerlemans, 1992; Olyphant, 1986; Arnold et al., 1996).

Incoming longwave radiation received at the surface is a combination of atmospheric radiation and radiation emitted from surrounding terrain. Longwave radiation is proportional to the fourth power of the emitting surface temperature (Brunt, 1932; Brutsaert, 1975), so the LW_{in} value of atmospheric radiation at the base elevation given in the climate file is adjusted for the atmospheric temperature lapse between the base elevation and the elevation of each grid node. This is accomplished at each timestep by calculating the difference between theoretical longwave radiation values at the grid node elevation and the base climate elevation. The difference between the two theoretical values is then subtracted from the input longwave radiation value. The atmospheric portion of incoming atmospheric longwave radiation is also adjusted to account for the portion of sky obscured by surrounding terrain. Incoming longwave radiation is calculated as:

$$LW_{in} = (LW_{in} - LW_{lapse})V_{f(sky)} + \epsilon\sigma T_a^4 V_{f(terrain)} \quad (3.18)$$

The first part of the right-hand-side of the equation adjusts the input atmospheric radiation (LW_{in}) for the elevation of the grid cell (LW_{lapse}) and the sky view factor. The second part of the equation approximates terrestrial radiation from the obstructed portion of the sky hemisphere. The emissivity of the surrounding terrain (ϵ) is assumed to be 0.95 (Olyphant, 1986), σ is the Stefan Boltzman constant ($5.7 \times 10^{-8} \text{ Wm}^{-2}\text{K}^{-4}$) and the surface temperature of the surrounding terrain is assumed to be equal to the mean air temperature (T_a) (Marks and Dozier, 1979; Olyphant, 1986).

Turbulent Heat Fluxes

The turbulent heat fluxes of latent and sensible heat are calculated following Paterson (1994). Sensible heat flux (H_s) is calculated as:

$$H_s = \rho_a c_p (P / P_0) K_h u (T_a - T_s) \quad (3.19)$$

where ρ_a is the density of dry air (1.29 kg m^{-3}), c_p is the specific heat of air ($1010 \text{ J kg}^{-1} \text{ K}^{-1}$), P is the atmospheric pressure at the elevation of the grid cell in pascals, P_0 is the atmospheric pressure at sea level (101325 Pa), K_h is a dimensionless transfer coefficient, u is wind speed (m s^{-1}), T_a is air temperature at the grid elevation (degrees K, adjusted from the base climate elevation using the standard lapse rate of $-0.00065 \text{ deg m}^{-1}$), and T_s is the surface temperature (273.15 K).

The latent heat (H_l) is calculated as:

$$H_l = L_v (0.622) (\rho_a / P_0) K_h u (e_a - e_s) \quad (3.20)$$

where e_a is the atmospheric vapor pressure (Pa), and e_s is the saturation vapor pressure at the surface, which is 611 Pa for a melting snow or ice surface (Oke, 1987). Following Braithwaite et al. (1998) and Gruell and Konzelmann (1994) the latent heat of vaporization (L_v) varies according to whether sublimation or evaporation is occurring. When e_a is greater than e_s condensation occurs and $L_v = 2.514 \times 10^6 \text{ J kg}^{-1}$. When e_a is less than e_s sublimation occurs, and $L_v = 2.849 \times 10^6 \text{ J kg}^{-1}$. The model uses

transfer coefficient (K_h) values of 0.0015 for snow covered surfaces, and 0.002 for surfaces of bare ice (Paterson, 1994).

Albedo

The treatment of surface albedo is critical in energy balance studies, because the range of albedo can reduce incoming shortwave radiation receipts at a snow covered surface by over 90%. Spatial and temporal variations of albedo are very complicated to model, because the albedo of snow varies for different wavelengths of light at different angles of incidence, and thus leads to diurnal albedo variations that are related to the solar angle of incidence (Hubley, 1955; Carroll and Fitch, 1981; Dirmhirn and Eaton, 1975). The metamorphosis of snow crystals as the snow ages also causes variations of albedo (Dirmhirn and Eaton, 1975; Oke, 1987), as do seasonal changes in the presence of darker surficial debris. Most energy balance studies follow simplified approaches for estimating albedo that rely on prescribed values for different surface types, such as snow, firn, ice, etc. (Williams 1974; Munro and Young, 1982; Zuo and Oerlemans, 1996), or that attempt to model the temporal change in albedo by explicit parameterizations of snow aging and melting (Oerlemans, 1992; Arnold et al., 1996; Zuo and Oerlemans, 1996; Oerlemans and Knap, 1998).

My model uses a combination of the time-variant methods presented in Zuo and Oerlemans (1996) and Oerlemans and Knap (1998). Each grid cell is assigned a base albedo at the beginning of the model run. This base albedo represents the 'background' surface of ice or firn that is present at the end of an ablation season.

The base albedo is calculated as a function of elevation relative to the ELA, based on the assumption that the ice albedo in the ablation zone will be reduced relative to higher elevations by debris that is brought to the surface (Oerlemans, 1992). The base albedo (α_b) at each grid node is calculated as:

$$\alpha_i = a1 * \arctan\left(\frac{E_{(x,y)} - ELA + a2}{a3}\right) + a4 \quad (3.21)$$

where a1-a4 are parameters that are chosen so that the base albedo for each glacier ranges from ~ 0.2 at the toe to ~ 0.5 at the highest elevation. The range of base albedo from 0.2 to 0.5 was chosen to represent a transition from dirty ice at the glacier toe to firn in the accumulation zone, using published values (Mountain, 1990; Koelemeijer et al., 1993; Paterson, 1994).

The albedo of snow (α_s) is assumed to be age dependent, and is constrained between a maximum value for new snow (α_{ns}), and a minimum value for old snow or firn (α_{os}) (Oerlemans and Knap, 1998):

$$\alpha_s = \alpha_{os} + (\alpha_{ns} - \alpha_{os}) \exp\left(\frac{t_l - t_c}{a5}\right) \quad (3.22)$$

The last part of the equation determines how quickly the albedo of new snow approaches that of old snow, where t_l is the last day when snow fell, t_c is the current day number, and a5 is the aging factor. The value for new snow used in the model is 0.75, and the value for firn is 0.55 (Arnold et al., 1996; Oerlemans and Knap, 1998).

Snow depth (snowd) is also accounted for in the albedo parameterization, so the amount that the underlying ice or firn contributes to the albedo is considered. This effects a smooth transition to the base albedo as the snow melts (Oerlemans and Knap, 1998). Following Zuo and Oerlemans (1996) an additional weathering factor is added to account for accumulation of surface debris during the ablation season, so that the final albedo (α) is calculated as:

$$\alpha = \alpha_s + (\alpha_{os} - \alpha_s) \exp(-1 * \text{snowd}/a6) - (a7 * M_s) \quad (3.23)$$

where M_s is the cumulative ablation over the course of the current melt season. The parameter $a6$ controls how much of the base surface is ‘seen’ through the existing snow depth, while $a7$ controls how quickly weathering of the surface reduces the final albedo value. The weathering factor allows the albedo to decrease below the base albedo. The final albedo is not allowed to decrease more than 20% below the base albedo, and a minimum value of 0.12 is used for the lower portions of the ablation zone (Arnold et al., 1996; Zuo and Oerlemans, 1996; Paterson, 1994).

APPLICATION OF MODEL TO A MODERN GLACIER

Before using the model on a paleoclimate application, the ability of the model to simulate mass balance was verified using modern field data. Although there have been many energy and mass balance studies on alpine glaciers (March, 1998; Oerlemans and Knap, 1998; Arnold et al., 1996; Hogg et al., 1982; Wendler and

Weller, 1982; La Chapelle, 1961) there remains a lack of consistent, detailed climate, topographic, and ablation data that would allow testing of the model over a complete annual cycle. I was able to obtain a dataset for Haut Glacier d'Arolla, Valais, Switzerland, from the 1990 ablation season. The main equations in the model are used to calculate ablation, so even though I was not able to determine how well the net specific balance over a full water year is reproduced by the model, the test of the model against measured ablation data should justify use of the model for paleoclimate sensitivity tests.

Haut Glacier d'Arolla is a valley glacier located in southeast Switzerland at 45.96° N, 7.52° E. The glacier is about 4 km long with a surface area close to 5 km^2 . It ranges in elevation from approximately 2550 to 3640 meters (Figure 3.3). Elevation and climate data for the glacier were collected in 1989 and 1990 (Arnold et al., 1996), and were provided by Sharp (pers. comm., 1998) and Arnold (pers. comm., 1999). The climate dataset included hourly values of incoming shortwave radiation, relative humidity, air temperature, wind speed, and precipitation from May 31, 1990 to August 25, 1990. To obtain the data for model input, atmospheric vapor pressure was calculated from the relative humidity and air temperature, and incoming longwave radiation was calculated using the equations given in Arnold et al. (1996). Daily averages of air temperature, wind speed, and atmospheric pressure, and daily sums of radiation and precipitation were calculated from the hourly data. The parameters used as model input for Haut Glacier d'Arolla are given in Table 3.2. Most of the independent variables used in the albedo equations (equations 3.21-3.23) were

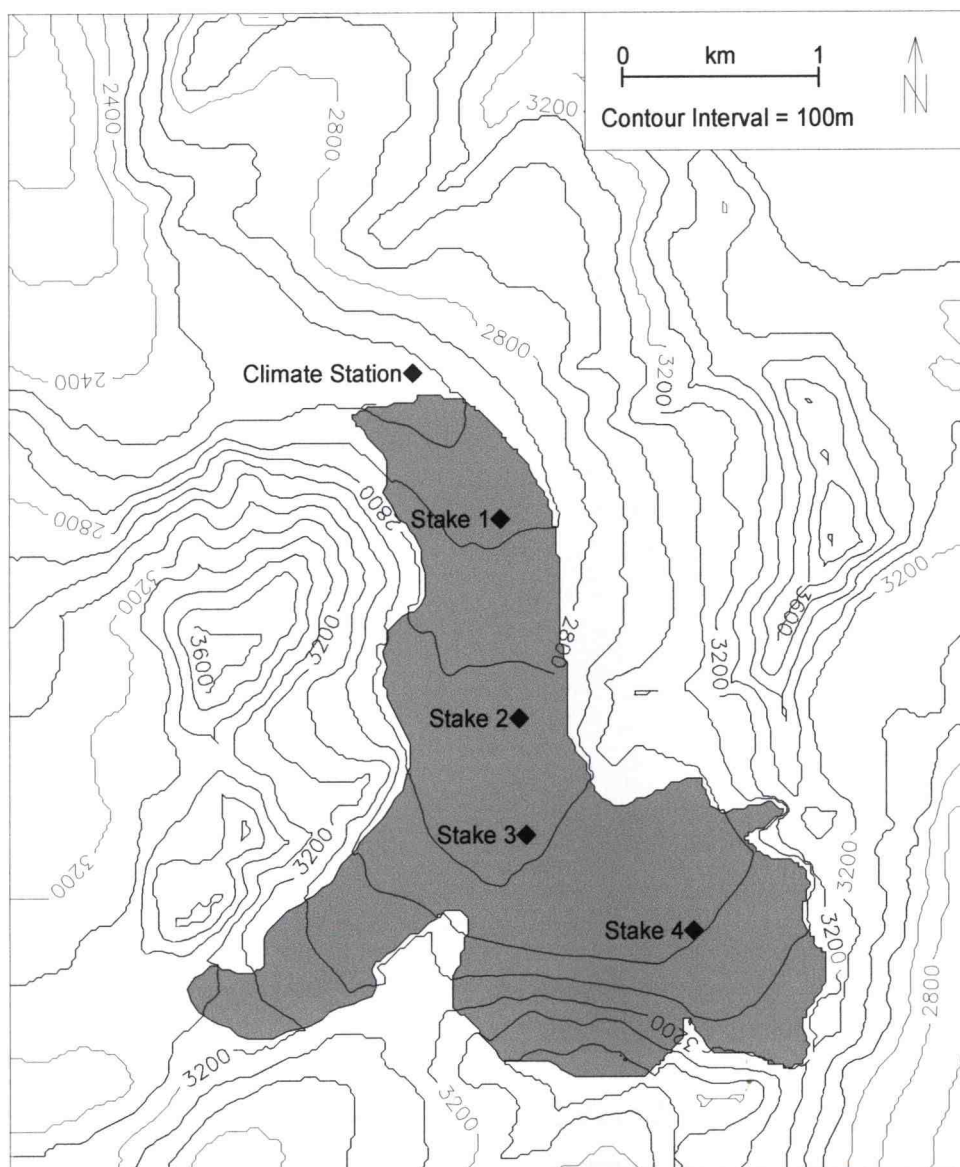


Figure 3.3: Contour map of glacier and terrain DEM for Haut Glacier d'Arolla. Shaded area indicates the surface of the glacier as represented in the model. Elevation is accurate to within 1 meter for the glacier surface, and to within 10 meters for the surrounding terrain (Sharp, pers. comm., 1998).

Table 3.2: Parameters used in model run on Haut Glacier d'Arolla.

Variable	Value	Source
belev	2547m	Arnold et al., 1996
zone	1	
lat	45.96°	Hoelzle and Haeberli, 1999
lon	7.52°	Hoelzle and Haeberli, 1999
ELA	3000m	Arnold et al., 1996
a1	0.137	Arnold et al., 1996
a2	0.3	Fitted by model
a3	300	Arnold et al., 1996
a4	200	Arnold et al., 1996
a5		Fitted by model
a6		Fitted by model
a7		Fitted by model
spack1	0.0019	Arnold et al., 1996
spack2	4.75	Arnold et al., 1996
tmstp	1 day	

Model Results

As the model run was limited to the ablation season for Haut Glacier d'Arolla, the model used the snow depth initialized at the beginning of the run as a proxy for accumulation during the 1990 water year in calculating net specific balance for the glacier. The model returned a net specific balance for the glacier of -1.81 m.w.e., and a computed ELA of ~ 3426 meters. Figure 3.4 is a map of the net mass balance at each grid node over the glacier surface at the end of the ablation season. The relationship of glacier slope, aspect and shading from surrounding terrain to the

spatial distribution of mass balance can be seen in Figure 3.4 as the mass balance at any given elevation is more negative for areas that have lower slopes and are more exposed to incoming shortwave radiation.

The high ELA and negative net balance computed by the model indicates that Haut Glacier d'Arolla was out of balance for the 1990 water year. I do not have any figures for the measured net balance of the 1990 water year, but measurements from the 1993 water year indicate a mean lowering of the glacier surface of 0.8 m.w.e., with maximum lowering of 4 m.w.e. in areas of high ablation (Willis, et al., 1998). This indicates that the computed net loss of 1.81 m.w.e. for the 1990 water year is not entirely out of range of recently measured values. The observed ELA as measured by the snow line elevation during the 1990 ablation season was 3000 meters (Arnold et al., 1996). The higher ELA generated by the model is most likely a combination of underestimation of initial snowpack and overestimation of ablation.

The individual components of the mean calculated energy balance for all the grid cells on the glacier over the ablation season are shown in Table 3.3. The adjusted incoming shortwave radiation is the largest positive contributor to the energy balance. If the net longwave radiation is broken into its respective components (Table 3.4) we see that the incoming longwave radiation actually contributes more than twice the melt energy of incoming shortwave radiation. Thus the calculation of incoming longwave radiation and the calculation of albedo provide two of the largest uncertainties in the calculation of the overall energy balance.

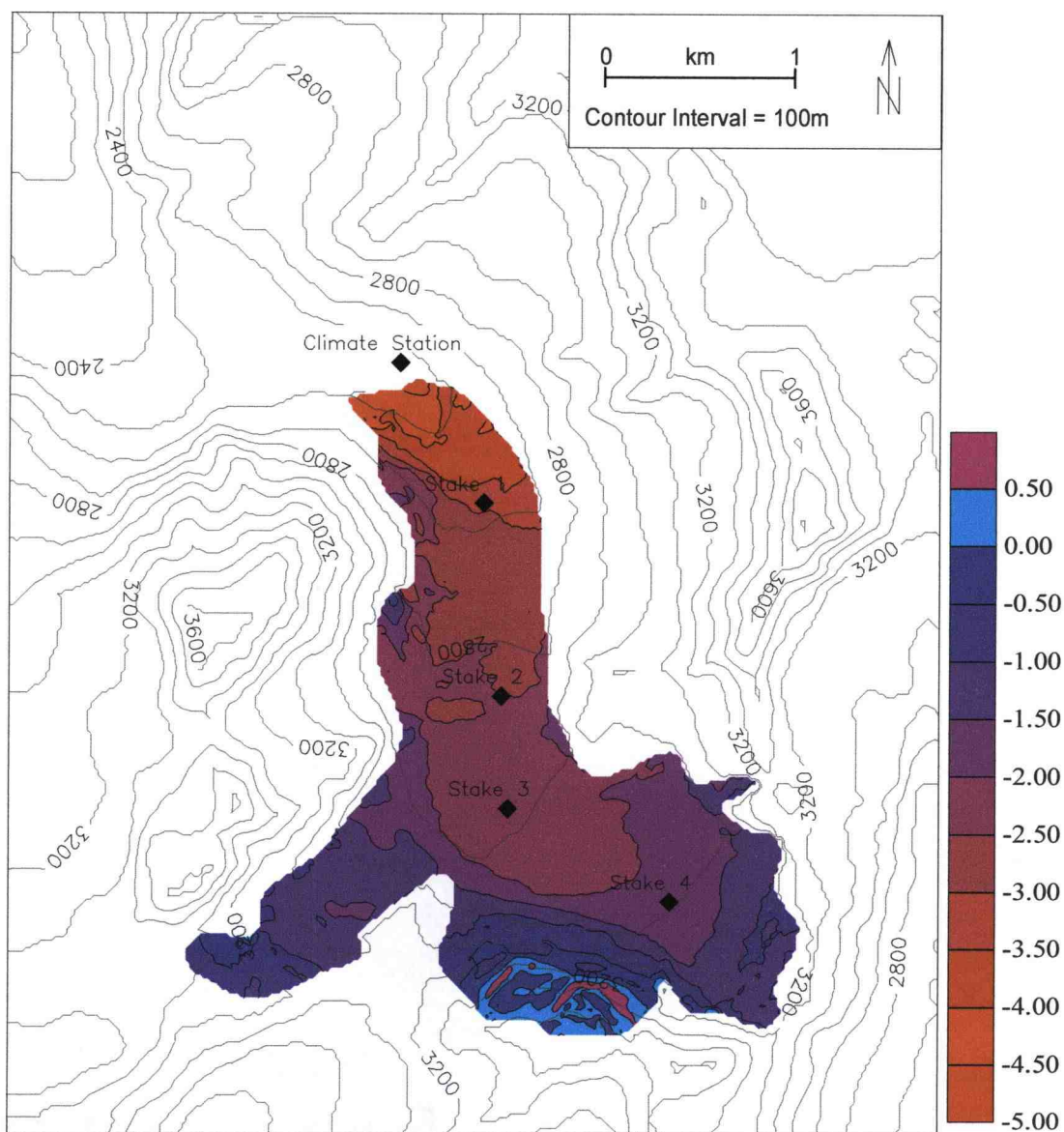


Figure 3.4: Net specific balance of Haut Glacier d'Arolla for 1990 ablation season. Elevation contours are shown in gray. Net balance values are in meters water equivalent.

Table 3.3: Average daily values of energy balance equation components for Haut Glacier d'Arolla.

Energy balance Component	(m.w.e. day ⁻¹)
$(1-\alpha)G$	0.0285
LW_n	-0.0103
H_s	0.0047
H_l	0.0020
Energy Balance	0.0249

Table 3.4: Individual model calculated components of longwave radiation for Haut Glacier d'Arolla.

Longwave Radiation Components	(m.w.e. day ⁻¹)
LW_{in}	0.0637
$LW_{terrain}$	0.0077
LW_{out}	-0.0817
LW_{net}	-0.0103

Model Accuracy

To test the accuracy of the model I compared the calculated cumulative ablation over the melt season with field data. Observed daily ablation values for four measurement stakes in the ablation zone (Figure 3.3) were obtained by digitizing Figure 8 from Arnold et al. (1996). Data for the corresponding coordinates on the glacier DEM were output from the model for comparison. Figure 3.5 shows the modeled and observed cumulative ablation for the four stake locations shown in Figure 3.3. The model replicates the cumulative ablation at the end of the melt season

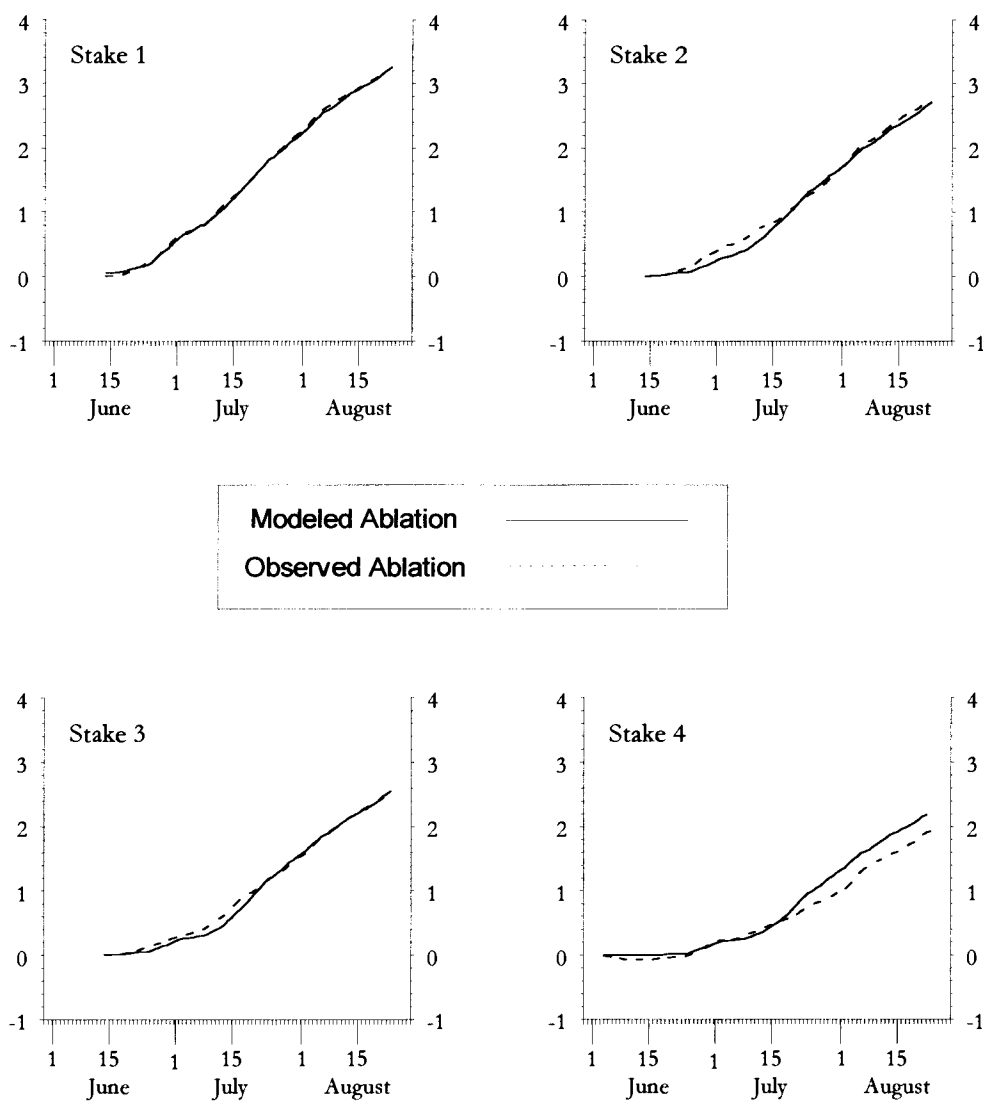


Figure 3.5: Observed versus modeled cumulative ablation for Haut Glacier d'Arolla. Cumulative ablation shown in meters water equivalent.

exactly for Stakes 1 and 2, is 0.06 m.w.e. higher than observed for Stake 3, and 0.25 m.w.e. higher for Stake 4. A comparison of daily ablation values (Figure 3.6) shows that while the model does not perfectly replicate the measured daily ablation values, it does capture the general trends quite well. The largest divergence of the model from the observed values occurs on the upper two stake locations between July 15-20 (Figure 3.6), where the modeled ablation curve increases and the observed ablation decreases.

Figure 3.7 shows the relationship between modeled and observed ablation values at each stake location. I was curious to see whether the lower stake locations were more accurate than the upper locations, as they are closer to the elevation where climate data was collected and the climate data at these points had not been extrapolated as much as at the higher locations. The correlation coefficient between modeled and observed data for Stake 3 is equal to that of Stake 1 ($r=0.781$). The correlation at Stake 4 is slightly higher than the other stakes ($r=0.8$), while Stake 2 returned the lowest correlation value ($r=0.73$) (Figure 3.7). When the data for the period of July 15-20 is removed the correlation between modeled and observed ablation at the upper two stakes increases significantly (Figure 3.8), and the overall correlation for all the data increases from an r value of 0.797 (Figure 3.9a) to 0.822 (Figure 3.9b). There is no indication from the scatter diagrams or correlation coefficients that the accuracy of the model decreases with increasing elevation. The spike in the modeled ablation between July 15-20 at the upper stakes (Figure 3.6) may simply reflect an inability of the model to replicate microclimate variations over the glacier surface.

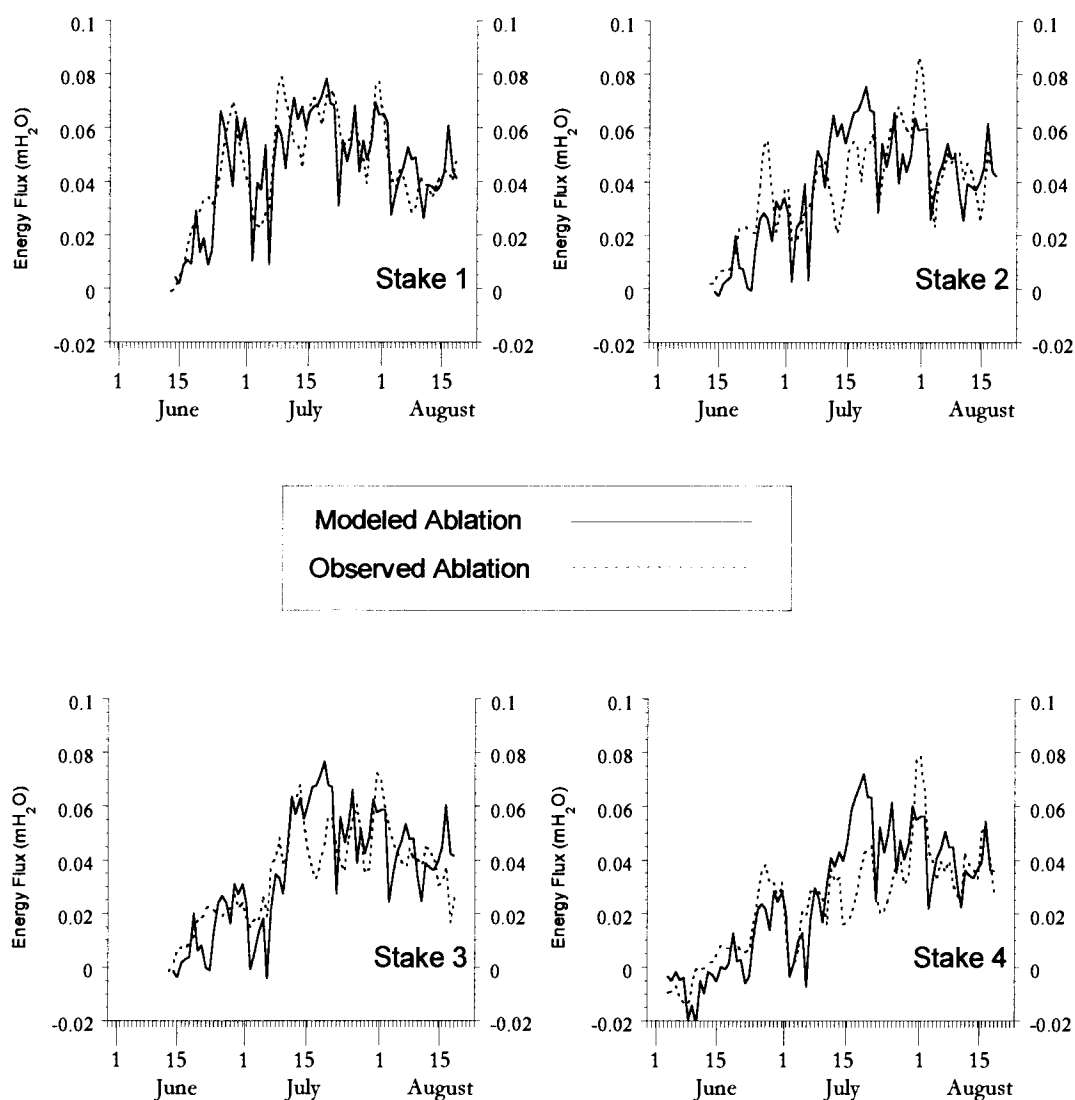


Figure 3.6: Daily modeled and observed ablation values for Haut Glacier d'Arolla. Ablation values are in meters water equivalent.

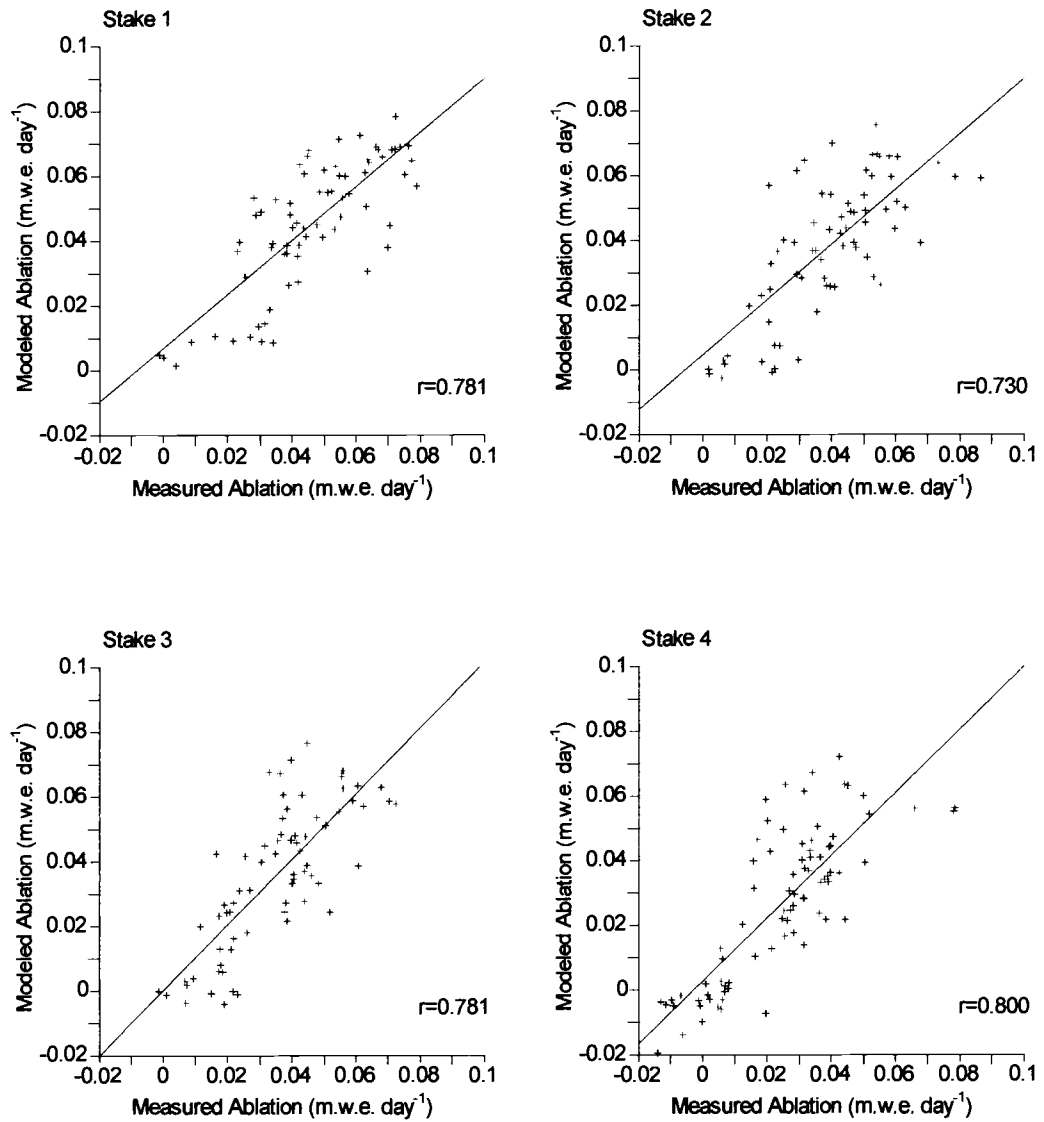


Figure 3.7: Scatter plots of measured versus modeled ablation for stake locations shown in Figure 3.3.

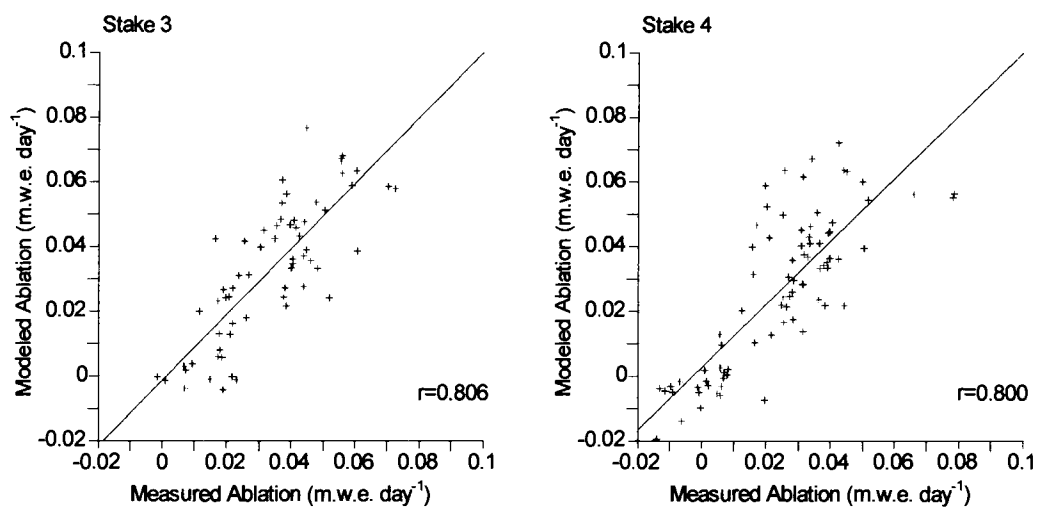


Figure 3.8: Scatter plots of measured versus modeled ablation for stake locations 3 and 4 with the data from July 15-20 removed.

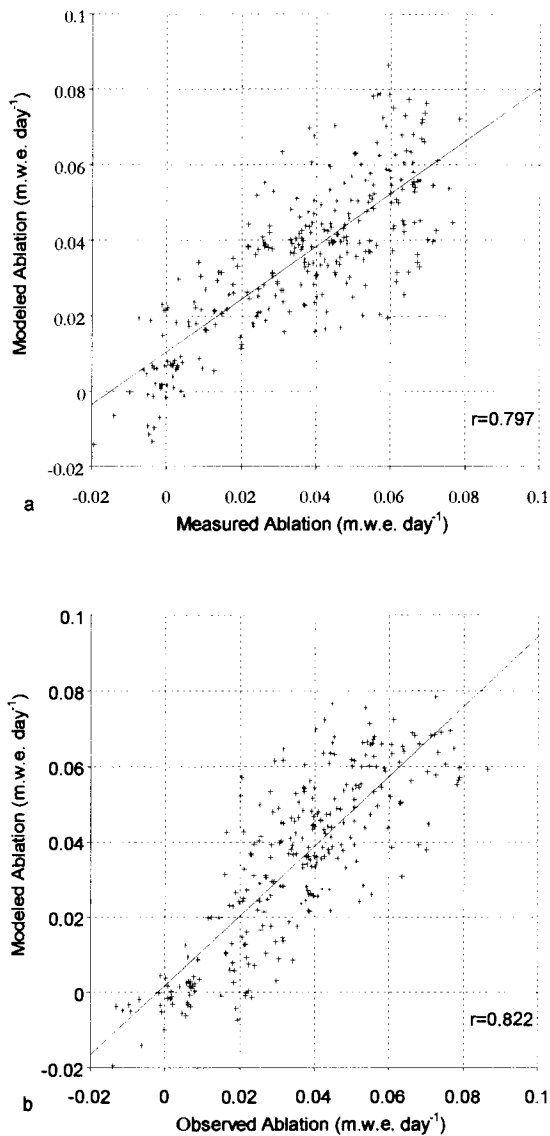


Figure 3.9:

a: Scatter plot of measured versus modeled ablation data combined from all stake locations.

b: Scatter plot of measured versus modeled ablation values for all stake locations excluding the data from July 15-20 at stake locations 3 and 4.

APPLICATION OF MODEL TO FORMER GLACIERS

The validated model was applied to reconstructed glacier surfaces on San Francisco Mountain, Arizona, using climate data output from a regional climate model (RCM). San Francisco Mountain, commonly referred to as the San Francisco Peaks, is a composite volcanic cone located near the southern boundary of the Colorado Plateau at 35° 20'N and 111° 40'W. There has been no numerical age dating of the moraines on the mountain, but relative dating studies suggest that there were three separate glacial sequences in the late Pleistocene, with the youngest glaciation representing the LGM, the second oldest representing Oxygen Isotope Stage 4, and the oldest representing Stage 6 (Sharp, 1942; Pewe and Updike, 1976). As a part of this study I mapped the elevation of the moraine crests on the mountain and conducted a semi-quantitative relative dating survey of the moraines (Poellot, in prep.). It was assumed from the results of the relative dating survey that the most recent glaciation on the mountain represents the last glacial maximum (LGM), but given the rapid rate of weathering that is apparent on the volcanic rock, it is also possible that the youngest moraines are from a younger cooling event, and the middle moraine set represents the LGM.

Model Inputs

The mapped moraine crests were used to reconstruct ice-surface DEMs in four separate valleys for the youngest glaciation (Figure 3.10), and in one valley for the second oldest glaciation (Figure 3.11). ELAs for the reconstructed glaciers were

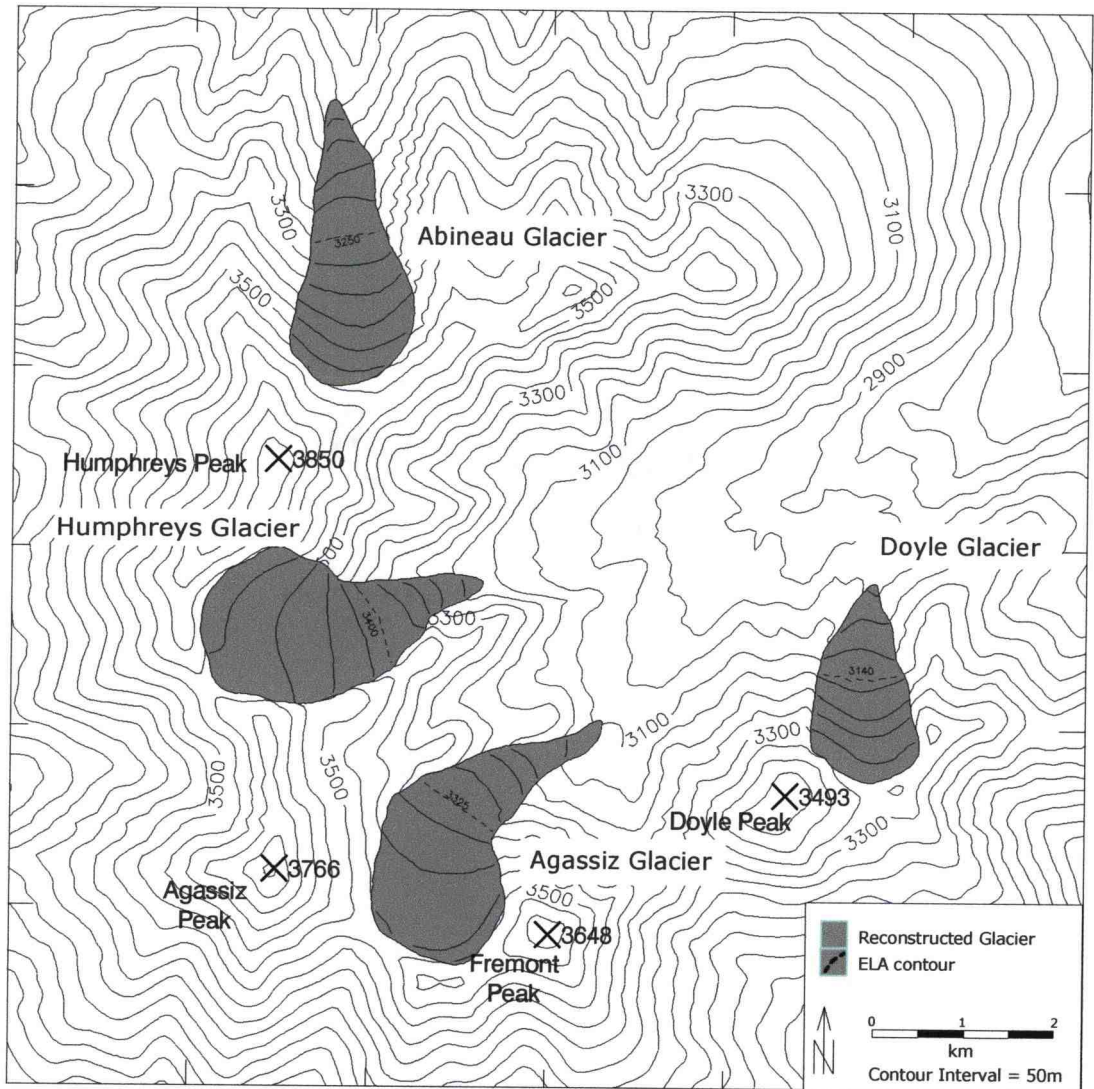


Figure 3.10: Reconstructed glaciers on San Francisco Mountain, Arizona from the youngest moraine set on the mountain.

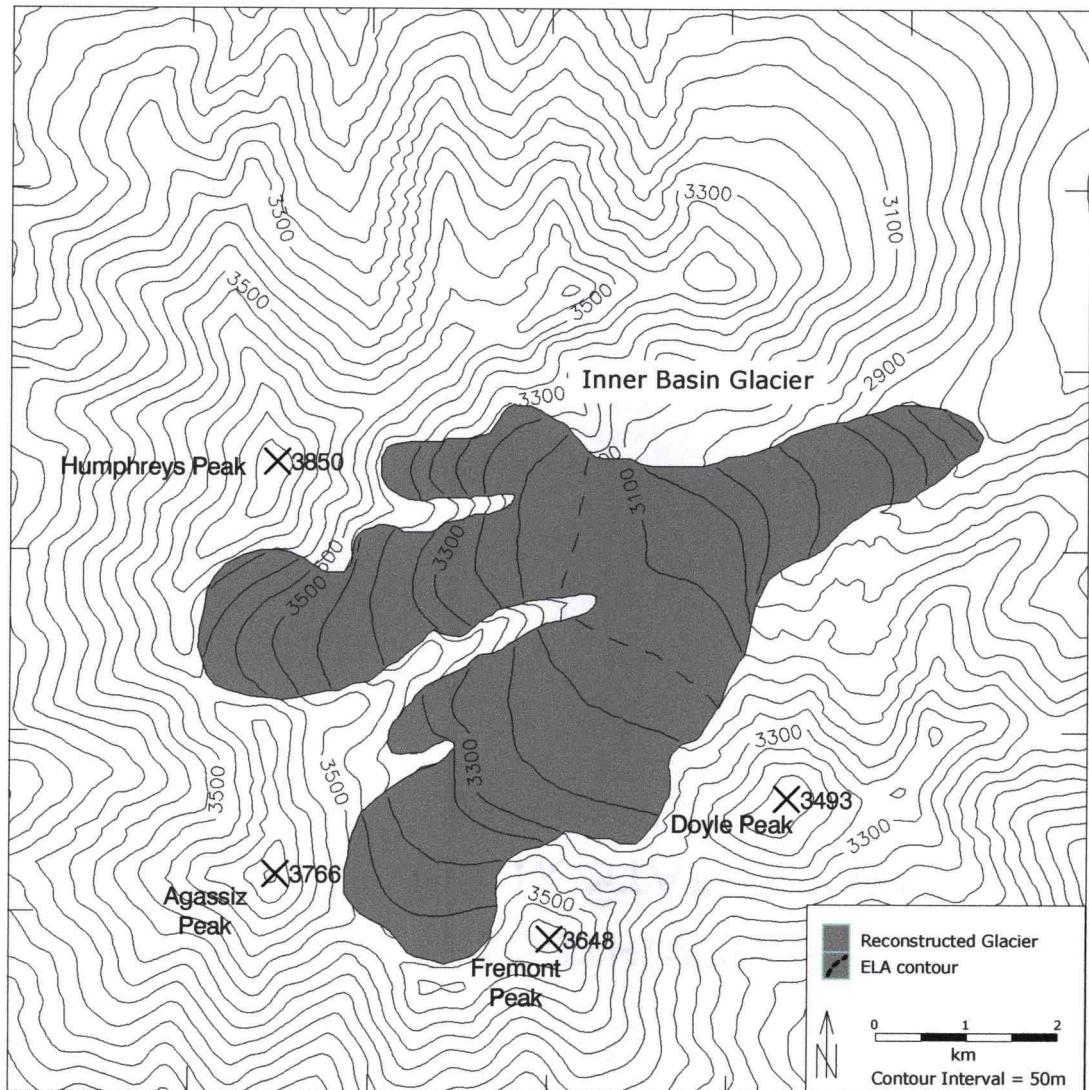


Figure 3.11: Reconstructed glacier for the second oldest moraine set on San Francisco Mountain, Arizona.

determined by the AAR method, using an accumulation area ratio of 0.65 (Meierding, 1982). Climate data for the model runs were provided by Steve Hostetler (1999) from the nearest point in the regional climate model centered at 35° 14'N, 111°63'W, and 1620m. Two datasets were provided: a control (modern) set and a set from a LGM run. Both datasets are for 4-year periods starting January 1. The climate variables output from the RCM were daily averages of air temperature, atmospheric vapor pressure, wind speed, precipitation, and shortwave radiation. The longwave radiation values provided were calculated from the air temperature and atmospheric vapor pressure generated by the model (Hostetler, 1999). The input parameters for each glacier are listed in Table 3.5. The values used for variables a5-a7 were the same as for the model run on Haut Glacier d'Arolla. The use of these variables carries some uncertainty in that they were specifically fitted to produce optimal results on a modern glacier in a completely different geographic location than the reconstructed glaciers. However, generalized variables that are known to produce accurate results in multiple locations will not be possible until more testing of the model is possible with modern data. The initial snowpack at the base elevation was calculated by finding the average accumulation during the four year period of the climate data, and using modern precipitation lapse rates to generate the spack* variables.

Table 3.5: Input parameters for San Francisco Mountain reconstructed glaciers.

Variable	Abineau Glacier	Agassiz Glacier	Humphreys Glacier	Doyle Glacier	Inner Basin Glacier
belev	1620 m	1620 m	1620 m	1620 m	1620 m
zone	-7	-7	-7	-7	-7
lat	35.33	35.33	35.33	35.33	35.33
lon	-111.67	-111.67	-111.67	-111.67	-111.67
ELA	3250 m	3325 m	3450 m	3140 m	3150 m
a1	0.180	0.150	0.234	0.200	0.290
a2	250.0	245.0	300.0	150.0	250.0
a3	200.0	180.0	200.0	150.0	300.0
a4	0.270	.0300	0.230	0.270	0.175
a5	0.064	0.064	0.064	0.064	0.064
a6	8.000	8.000	8.000	8.000	8.000
a7	0.350	0.350	0.350	0.350	0.350
spack1	0.0002	0.0002	0.0002	0.0002	0.0002
spack2	-0.2673	-0.2673	-0.2673	-0.2673	-0.2673
tmstp	1 day	1 day	1 day	1 day	1 day

Model Results

As no glaciers exist on the mountain at present, the model runs with the control data should show all the glaciers to be out of balance with very negative net balances and no ELAs. Assuming that the RCM data accurately represents the LGM climate, and that glacier reconstructions are accurate, the results of the LGM runs should show which of the two hypotheses regarding the extent of glaciers on SFP at the LGM are accurate. If the youngest glacier set is from the LGM, I would expect the smaller glaciers should show net balances close to zero, and the larger, older glacier to show a negative net balance. In contrast, if the older of the two glaciations

was from the LGM, and the younger set is from a more recent cooling period, the Inner Basin Glacier will show a net balance close to zero, and the younger glaciers will show highly positive net balances.

Table 3.6 shows the ELA and net balance values returned by the control and LGM runs for each glacier. Minimum and maximum elevations for each glacier along with the initial ELA are shown for comparison with the model-generated ELAs. As expected, none of the model runs returned an ELA for the modern climate data, with all of the glaciers showing highly negative net balances. All of the calculated net balances for the LGM run were positive, and the Inner Basin glacier (from the second oldest glaciation) is clearly the closest to being in balance.

Table 3.6: Results of model runs on the San Francisco Mountain former glaciers.

	Abineau Glacier	Agassiz Glacier	Flagstaff Glacier	Dacite Glacier	Inner Basin Glacier
Minimum Elevation (m)	3001	3100	3170	2989	2731
Maximum Elevation (m)	3356	3509	3643	3347	1.21
Initial ELA (m)	3250	3325	3450	3140	3150
Control ELA (m)	N/A	N/A	N/A	N/A	N/A
LGM ELA (m)	3065	3136	3178	3095	3120
Control B_n (m.w.e.)	-7.27	-7.06	-4.62	-9.28	-10.10
LGM B_n (m.w.e.)	2.65	2.97	3.68	1.53	1.21

Figures 3.12 and 3.13 show the modeled accumulation and ablation zones on the reconstructed glaciers with the original glacier ELAs shown for reference. The ELA for the Inner Basin glacier (Figure 3.13) is generally less than 30 meters lower than the original ELA. The Abineau, Agassiz, and Flagstaff glaciers (Figure 3.12) are all clearly out of balance, with only miniscule ablation zones and greatly lowered ELAs. The Humphreys glacier had the highest ELA of the glaciers, and occupied a very sheltered east facing cirque, so it is not surprising that the calculated net balance of this glacier is the least negative for the control run and the highest of the LGM run. The calculated net balance and ELA for Doyle glacier are much closer to that of the Inner Basin glacier for both the control and the LGM run. The reason for this may be that even though the Doyle glacier surface was reconstructed from the younger set of moraines, it is much lower in elevation than the other glaciers, with a reconstructed ELA that is just about equal to that of the Inner Basin Glacier. It is also possible considering the lower elevation of the Doyle glacier's ELA, along with the energy balance modeling results, that the Doyle glacier was a satellite glacier of the same age as the Inner Basin Glacier.

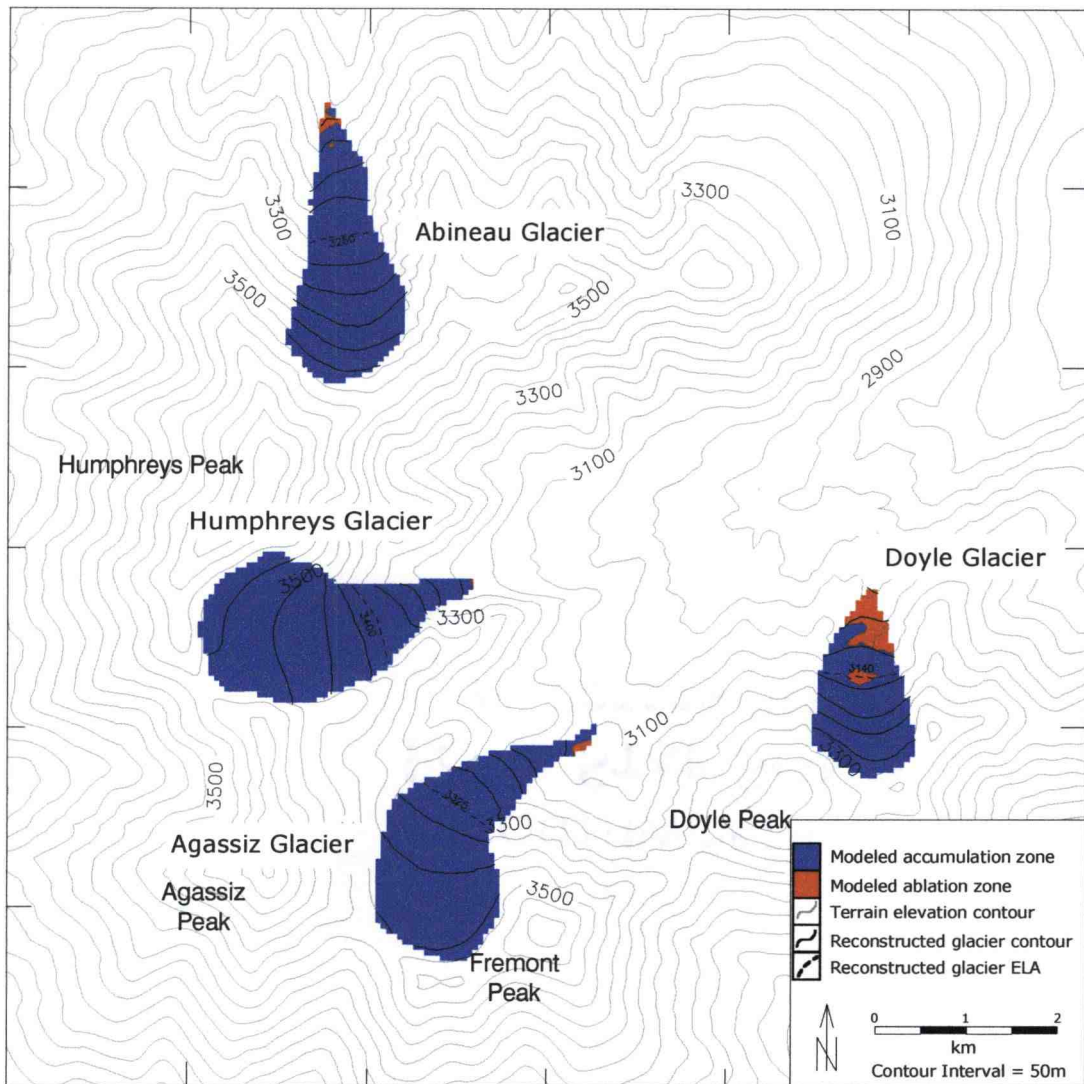


Figure 3.12: Comparison of LGM model run results with original reconstructed elevation contours and ELAs for the youngest reconstructed glaciers on San Francisco Mountain.

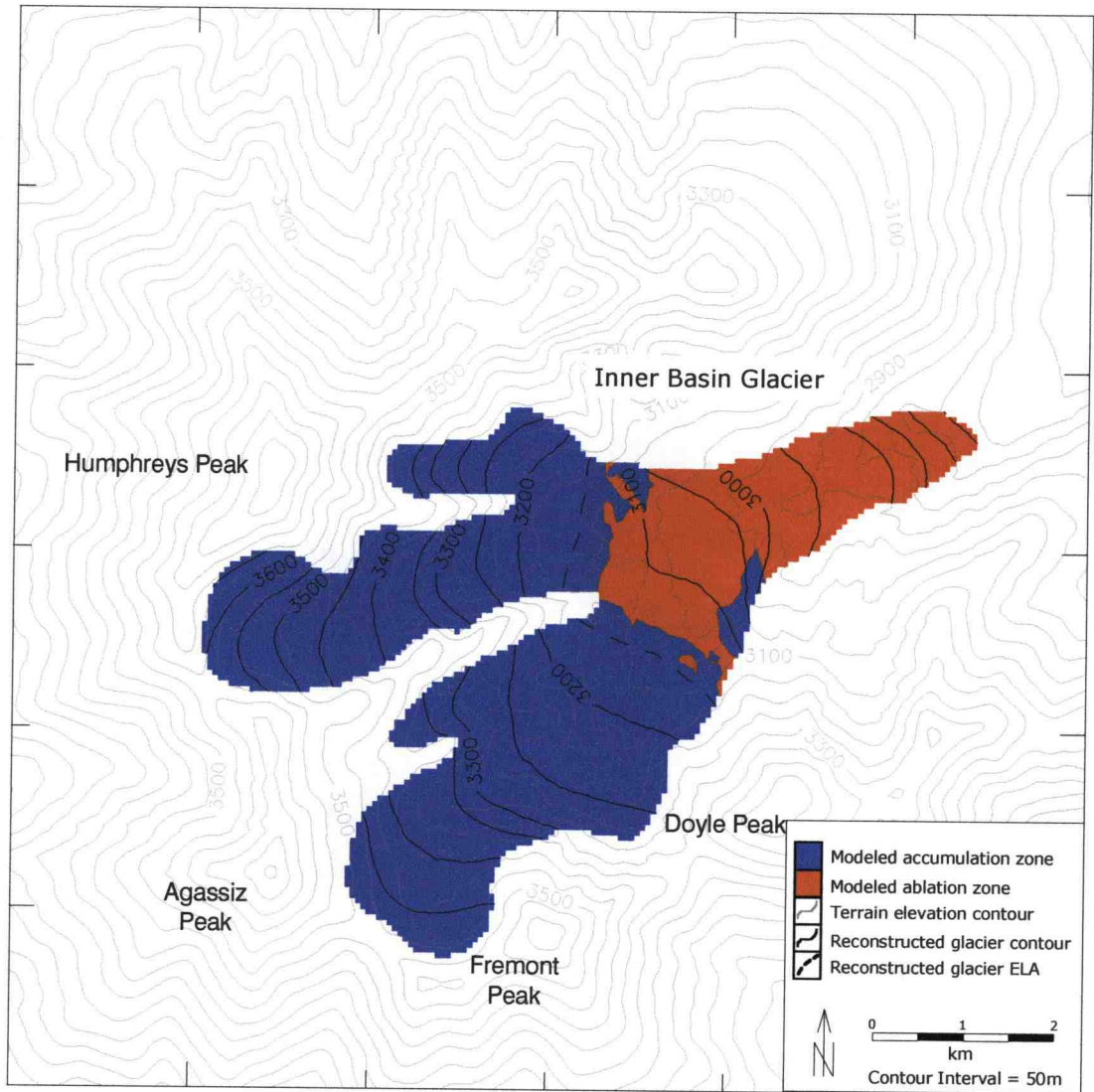


Figure 3.13: Comparison of LGM model run results with original reconstructed elevation contours and ELA for the second youngest reconstructed glacier on San Francisco Mountain.

Given the assumptions inherent in the mass balance model, and the lack of more detailed testing against modern field data, it would be presumptuous to make claims regarding the accuracy of the modeled mass balance of the reconstructed former glaciers, or the ages of the glacial deposits on San Francisco Mountain. It is encouraging, however, to see that the modern climate data provided supports the absence of glaciers on the mountain today, and the paleoclimate data supports the existence of glaciers during the LGM, suggesting that the model should be able to be used with confidence as a tool to test the reaction of former glaciers to changes in temperature, precipitation, or other climate variables provided by the RCM.

CONCLUSIONS

A distributed surface energy balance model was developed and tested for application on alpine glaciers. The model is designed to use output of climate models as input for equations that calculate specific net balance for a given time period. The model was tested against field data from Haut Glacier d'Arolla, Switzerland, and returned excellent results in comparing modeled and observed ablation data for four locations on the glacier. Using output from a high-resolution regional climate model as input and some of the specific variables generated for Haut Glacier d'Arolla, the model was applied to reconstructed DEMs of late-Pleistocene glaciers on San Francisco Mountain, Arizona with promising results. Although further testing of the model with modern field data is needed to generate albedo equation variables that are general enough to use on glaciers in different climatic and geographic regions, the

model in its current state can still be used to test sensitivity of former glaciers to changes in specific climate variables.

REFERENCES

- Andrews, J.T., 1972, Glacier power, mass balances, velocities and erosion potential: *Z. Geomorph, N.F., Suppl. Bd. 13*, pp. 1-17.
- Arnold, N.S., Willis, I.C., Sharp, M.J., Richards, K.S., and Lawson, W.J., 1996, A distributed surface energy-balance model for a small valley glacier. I. Development and testing for Haut Glacier d'Arolla, Valais, Switzerland: *Journal of Glaciology*, v. 42, pp. 77-89.
- Arnold, N.S., 1999, Personal Communication: Department of Geography, University of Cambridge. Downing Place, Cambridge CB2 3EN, England. February, 1999.
- Bevis, K.A., 1995, Reconstruction of late Pleistocene paleoclimatic characteristics in the Great Basin and adjacent areas: Unpublished Doctoral Thesis, Oregon State University, 270 pp.
- Braithwaite, R.J., Konzelmann, T., Christoph, M., and Olesen, O.B., 1998, Reconnaissance study of glacier energy balance in North Greenland, 1993-94: *Journal of Glaciology* v. 44, pp. 239-247.
- Brunt, D., 1932, Notes on radiation in the atmosphere: *Quarterly Journal of the Royal Meteorological Society*, v. 58, pp. 389-420.
- Brutsaert, W., 1975, On a derivable formula for longwave radiation from clear skies: *Water Resources Research*, v. 11, pp. 724-744.
- Carlson, A., 1995, Equation of Time: URL: <http://www.jpp.mpg.de/~awc/sundial.html>
- Carroll, J.J., and Fitch, B.W., 1981, Effects of solar elevation and cloudiness on snow albedo at the South Pole: *Journal of Geophysical Research*, v. 86, pp. 5271-5276.
- Clark, P.U., and Bartlein, P.J., 1995, Correlation of late Pleistocene glaciation in the western United States with North Atlantic Heinrich events: *Geology*, v. 23, pp. 483-486.

- Cygnus Solutions, 1999, Cygwin B20.1 Development Tools; URL:
<http://www.sourceforge.cygwin.com>
- Dirmhirn, I., and Eaton, F.D., 1975, Some characteristics of the albedo of snow:
Journal of Applied Meteorology, v. 11, pp. 375-379.
- Dozier, J., and Outcalt, S.I., 1979, An approach toward energy balance simulation
 over rugged terrain: *Geographical Analysis*, v. 11, pp. 65-85.
- Gregory, J.M., and Oerlemans, J., 1998, Simulated future sea-level rise due to glacier
 melt based on regionally and seasonally resolved temperature changes:
Nature, v. 391, pp. 474-476.
- Greuell, W., and Konzelmann, T., 1994, Numerical modelling of the energy balance
 and the englacial temperature of the Greenland ice sheet. Calculations for the
 ETH-Camp location (West Greenland, 1155 m a.s.l.): *Global and Planetary
 Change*, v. 9, pp. 91-114.
- Grobneck, C., 1999, SunAngle: Sustainable Design web page:
<http://www.susdesign.com/sunangle/index.html>
- Hogg, I.G.G., Paren, J.G., and Timmis, R.J., 1982, Summer heat and ice balances on
 Hodges Glacier, South Georgia, Falkland Islands Dependencies: *Journal of
 Glaciology*, v. 28, pp. 221-238.
- Hostetler, S.W., and Clark, P.U., 1997, Climatic controls of western U.S. glaciers at the
 last glacial maximum: *Quaternary Science Reviews*, v. 16, pp. 505-511.
- Hostetler, S.W., 1999, Personal Communication: United States Geological Society,
 200 SW 35th Street, Corvallis, OR 97333, U.S.A.. April, 1999.
- Hubley, R.C., 1955, Measurements of diurnal variations in snow albedo on Lemon
 Creek Glacier, Alaska: *Journal of Glaciology*, v. 2, pp. 560-563.
- Khan, M., 1999, EGCS Development Toolchain For x-86-Win32 Targets: URL:
<http://www.xraylith.wisc.edu/~khan/software/gnu-win32/egcs.html>
- Koelemeijer, R., Oerlemans, J., and Tjemkes, S., 1993, Surface reflectance of
 Hintereisferner, Austria, from Landsat 5 TM imagery: *Annals of Glaciology*,
 v. 17, pp. 17-22.
- La Chapelle, E., 1961, Energy exchange measurements on the Blue Glacier,
 Washington: *IAHS*, v. 54, pp. 302-310.

- Leonard, E.M., 1984, Late Pleistocene equilibrium-line altitudes and modern snow accumulation patterns, San Juan Mountains, Colorado, United States.: *Arctic and Alpine Research*, v. 16, pp. 65-76.
- Leonard, E.M., 1989, Climatic change in the Colorado Rocky Mountains: Estimates based on modern climate at late Pleistocene equilibrium lines, *Arctic and Alpine Research*, v. 21, pp. 245-255.
- Locke, W.W., 1990, Late Pleistocene glaciers and climate of western Montana, U.S.A., *Arctic and Alpine Research*, v. 22, pp. 1-13.
- March, R.S., 1998, Mass balance, meteorological, ice motion, surface altitude, and runoff data at Gulkana Glacier, Alaska, 1994 balance year: U.S. Geological Survey Water-Resources Investigations Report 97-4251, 31 pp.
- Marks, D., and Dozier, J., 1979, A clear-sky longwave radiation model for remote alpine areas: *Archiv Für Meteorologie Geophysik Und Bioklimatologie, Series B*, v. 27, pp. 159-187.
- Mathews, W.H., 1967, Profiles of late Pleistocene glaciers in New Zealand: *New Zealand Journal of Geology and Geophysics*, v. 10, pp. 146-163.
- McClung, D.M., and Armstrong, R.L., 1993, Temperate glacier time response from field data: *Journal of Glaciology*, v. 39, pp. 323-326.
- McCoy, W.D., and Williams, L.D., 1985, Application of an energy-balance model to the late Pleistocene Little Cottonwood Canyon glacier with implications regarding the paleohydrology of Lake Bonneville: *in* Kay, P.A., and Diaz, H.F., eds., *Problems of and prospects for predicting Great Salt Lake levels*: Center for Public Affairs and Administration, University of Utah, pp.40-53.
- Meeus, J., 1998, *Astronomical Algorithms: Second Edition*: Willman Bell, Inc., Richmond, VA, 477 pp.
- Meier, M.F., 1965, *Glaciers and climate, the Quaternary of the United States*: edited by H.E. Wright, Jr., and D.G. Frey, pp. 795-805.
- Meierding, T.C., 1982, Late Pleistocene glacial equilibrium-line altitudes in the Colorado Front Range: A comparison of methods: *Quaternary Research*, v. 18, pp. 289-310.
- Mountain, K.R., 1990, A clear sky net radiation model fro the high-elevation glacial environment: Unpublished Doctoral Thesis, Ohio State University, 290 pp.
- Munro, D.S., and Young, G.J., 1982, An operational net shortwave radiation model for glacier basins: *Water Resources Research*, v. 18, pp. 220-230.

- Oerlemans, J., 1992, Climate sensitivity of glaciers in southern Norway: Application of an energy-balance model to Nigardsbreen, Hellstugubreen and Alftobreen: *Journal of Glaciology*, v. 38, pp. 223-231.
- Oerlemans, J., and Knap, W.H., 1998, A 1 year record of global radiation and albedo in the ablation zone of Morteratschgletscher, Switzerland: *Journal of Glaciology*, v. 44, pp. 231-238.
- Oke, T.R., 1987, *Boundary Layer Climates*, 2nd Edition: Methuen, London and New York.
- Olyphant, G.A., 1986, Longwave radiation in mountainous areas and its influence on the energy balance of alpine snowfields: *Water Resources Research*, v. 22, pp. 62-66.
- Paterson, W.S.B., 1994, *The Physics of Glaciers*: Third Edition: Pergamon Press, New York, 250 pp.
- Péwé, Troy L., and Updike, Randall C., 1976, *San Francisco Peaks, A guidebook to the geology*, Second Edition: Museum of Northern Arizona, Flagstaff, Arizona, 80 pp.
- Phillips, F.M., Zreda, M.G., Elmore, D., and Sharma, P., 1993, Evidence for a connection between dynamic behavior of the Laurentide Ice Sheet and mountain glaciation in western North America: *EOS (Transactions, American Geophysical Union)*, v. 74, p. 360.
- Poellot, C.D.P., in prep., *Glacial deposits of San Francisco Mountain, Arizona*: Masters Thesis, Oregon State University.
- Porter, S.C., 1964, Composite Pleistocene snow line of Olympic Mountains and Cascade Range, Washington: *Geological Society of America Bulletin*, v. 75, pp. 477-481.
- Porter, S.C., Pierce, K.L., and Hamilton, T.D., 1983, Late Wisconsin mountain glaciation in the western United States: *in* Porter, S.C., ed., *Late Quaternary environments of the United States, Volume 1, The late Pleistocene*: Minneapolis, University of Minnesota Press, pp. 71-114.
- Robinson, N., 1966, *Solar Radiation*: Elsevier Publishing Company, NY, 347 pp.
- Sharp, M.J., 1998, Personal Communication: Department of Geography, University of Alberta, Edmonton, Alberta T6G 2H4, Canada. May, 1998.

- Sharp, R.P., 1942, Multiple Pleistocene glaciation on San Francisco Mountain, Arizona: *Journal of Geology*, 42, 481-503.
- Wallace, J.M., and Hobbs, P.V., 1977, *Atmospheric Science: An Introductory Survey*: Academic Press, New York, 467 pp.
- Walters, R.A., and Meier, M.F., 1989, Variability of glacier mass balances in Western North America: American Geophysical Union, *Geophysical Monograph* 55, pp. 365-374.
- Walraven, R., 1978, Calculating the position of the Sun: *Solar Energy*, v. 20, pp. 393-397.
- Wendler, G., and Weller, G., 1982, A heat-balance study on McCall Glacier, Brooks Range, Alaska: A contribution to the international hydrological decade: *Journal of Glaciology*, v. 13, pp. 13-26.
- Williams, L.D., Barry, R.G., and Andrews, J.T., 1972, Application of computed global radiation for areas of high relief: *Journal of Applied Meteorology*, v.11, pp. 526-533.
- Williams, L.D., 1974, Computer simulation of glacier mass balance throughout an ablation season: *Proceedings of the Western Snow Conference, Annual Meeting*, pp. 23-28.
- Willis, I., Arnold, N., Sharp, M., Bonvin, J.M., and Hubbard, B., 1998, Mass balance and flow variations of the Haut Glacier d'Arolla, Switzerland calculated using digital terrain modelling techniques: In Lane, S.N., Chandler, J.H., and Richards, K.S. (Eds.), *Landform Monitoring, Modelling and Analysis*. Wiley. Chichester.
- Zielinski, G.A., and McCoy, W.D., 1987, Paleoclimatic implications of the relationship between modern snowpack and late Pleistocene equilibrium-line altitudes in the mountains of the Great Basin, western U.S.A., *Arctic and Alpine Research*, v.19, pp. 127-134.
- Zuo, Z., and Oerlemans, J., 1996, Modelling albedo and specific balance of the Greenland ice sheet: Calculations for the Søndre Strømfjord transect: *Journal of Glaciology*, v. 42., pp. 305-317.

CHAPTER 4

SUMMARY

Glacial moraines were mapped on San Francisco Mountain, Arizona, and semi-quantitative relative dating data were collected from ten moraines in order to separate glacial events within individual drainages, and to correlate events between drainages. The results of the weathering data corroborate earlier studies that suggest a threefold sequence of glaciation on the mountain. The youngest moraines were most likely deposited around the last glacial maximum. The other two drift units may reflect the presence of glaciers during oxygen-isotope stages 4 and 6, respectively. Glaciers from the two most recent glacial events were reconstructed to show possible ice extents for the last glacial maximum. Paleo-ELAs ranging from 3100 to 3400 meters agree with regional reconstructions.

A distributed surface energy balance model was developed and tested for application on alpine glaciers. The model is designed to use output of climate models as input for equations that calculate specific net balance for a given time period. The model was tested against field data from Haut Glacier d'Arolla, Switzerland, and returned excellent results in comparing modeled and observed ablation data for four locations on the glacier. Using output from a high-resolution regional climate model as input and some of the specific variables generated for Haut Glacier d'Arolla, the model was applied to reconstructed DEMs of late-Pleistocene glaciers on San

Francisco Mountain, Arizona with promising results. Although further testing of the model with modern field data is needed to generate albedo equation variables that are general enough to use on glaciers in different climatic and geographic regions, the model in its current state can still be used to test sensitivity of former glaciers to changes in specific climate variables.

BIBLIOGRAPHY

- Andrews, J.T., 1972, Glacier power, mass balances, velocities and erosion potential: *Z. Geomorph, N.F., Suppl. Bd. 13*, pp. 1-17.
- Arnold, N.S., Willis, I.C., Sharp, M.J., Richards, K.S., and Lawson, W.J., 1996, A distributed surface energy-balance model for a small valley glacier. I. Development and testing for Haut Glacier d'Arolla, Valais, Switzerland: *Journal of Glaciology*, v. 42, pp. 77-89.
- Arnold, N.S., 1999, Personal Communication: Department of Geography, University of Cambridge. Downing Place, Cambridge CB2 3EN, England. February, 1999.
- Atwood, W.W., 1905, Glaciation of San Francisco Mountain, Arizona: *Journal of Geology*, 8, 276-279.
- Bevis, K.A., 1995, Reconstruction of late Pleistocene paleoclimatic characteristics in the Great Basin and adjacent areas: Unpublished Doctoral Thesis, Oregon State University, 270 pp.
- Braithwaite, R.J., Konzelmann, T., Christoph, M., and Olesen, O.B., 1998, Reconnaissance study of glacier energy balance in North Greenland, 1993-94: *Journal of Glaciology* v. 44, pp. 239-247.
- Brunt, D., 1932, Notes on radiation in the atmosphere: *Quarterly Journal of the Royal Meteorological Society*, v. 58, pp. 389-420.
- Brutsaert, W., 1975, On a derivable formula for longwave radiation from clear skies: *Water Resources Research*, v. 11, pp. 724-744.
- Burke, R.M., and Birkeland, P.W., 1979, Reevaluation of multiparameter relative dating techniques and their application to the glacial sequence along the eastern escarpment of the Sierra Nevada, California: *Quaternary Research*, v. 11, pp. 21-51.
- Carlson, A., 1995, Equation of Time: URL: <http://www.jpp.mpg.de/~awc/sundial.html>
- Carroll, J.J., and Fitch, B.W., 1981, Effects of solar elevation and cloudiness on snow albedo at the South Pole: *Journal of Geophysical Research*, v. 86, pp. 5271-5276.

- Clark, P.U., and Bartlein, P.J., 1995, Correlation of late Pleistocene glaciation in the western United States with North Atlantic Heinrich events: *Geology*, v. 23, pp. 483-486.
- Colman, S.M., and Pierce, K.L., 1986, Glacial sequence near McCall, Idaho: Weathering rinds, soil development, morphology, and other relative-age criteria: *Quaternary Research*, 25, 25-42.
- Cygnus Solutions, 1999, Cygwin B20.1 Development Tools; URL: <http://www.sourceware.cygnus.com>
- Dirmhirn, I., and Eaton, F.D., 1975, Some characteristics of the albedo of snow: *Journal of Applied Meteorology*, v. 11, pp. 375-379.
- Dozier, J., and Outcalt, S.I., 1979, An approach toward energy balance simulation over rugged terrain: *Geographical Analysis*, v. 11, pp. 65-85.
- Gibbons, A.B., Megeath, J.D., and Pierce, K.L., 1984, Possibility of moraine survival in a succession of glacial advances: *Geology*, v. 12, pp. 327-330.
- Golden Software, 1995, Surfer v. 6.01 Surface Mapping System: Golden Software Inc., Golden, Colorado.
- Gregory, J.M., and Oerlemans, J., 1998, Simulated future sea-level rise due to glacier melt based on regionally and seasonally resolved temperature changes: *Nature*, v. 391, pp. 474-476.
- Greuell, W., and Konzelmann, T., 1994, Numerical modelling of the energy balance and the englacial temperature of the Greenland ice sheet. Calculations for the ETH-Camp location (West Greenland, 1155 m a.s.l.): *Global and Planetary Change*, v. 9, pp. 91-114.
- Grobneck, C., 1999, SunAngle: Sustainable Design web page: <http://www.susdesign.com/sunangle/index.html>
- Hogg, I.G.G., Paren, J.G., and Timmis, R.J., 1982, Summer heat and ice balances on Hodges Glacier, South Georgia, Falkland Islands Dependencies: *Journal of Glaciology*, v. 28, pp. 221-238.
- Hostetler, S.W., and Clark, P.U., 1997, Climatic controls of western U.S. glaciers at the last glacial maximum: *Quaternary Science Reviews*, v. 16, pp. 505-511.
- Hostetler, S.W., 1999, Personal Communication: United States Geological Society, 200 SW 35th Street, Corvallis, OR 97333, U.S.A.. April, 1999.

- Hubley, R.C., 1955, Measurements of diurnal variations in snow albedo on Lemon Creek Glacier, Alaska: *Journal of Glaciology*, v. 2, pp. 560-563.
- Khan, M., 1999, EGCS Development Toolchain For x-86-Win32 Targets: URL: <http://www.xraylith.wisc.edu/~khan/software/gnu-win32/egcs.html>
- Koelemeijer, R., Oerlemans, J., and Tjemkes, S., 1993, Surface reflectance of Hintereisferner, Austria, from Landsat 5 TM imagery: *Annals of Glaciology*, v. 17, pp. 17-22.
- La Chapelle, E., 1961, Energy exchange measurements on the Blue Glacier, Washington: *IAHS*, v. 54, pp. 302-310.
- Leonard, E.M., 1984, Late Pleistocene equilibrium-line altitudes and modern snow accumulation patterns, San Juan Mountains, Colorado, United States.: *Arctic and Alpine Research*, v. 16, pp. 65-76.
- Leonard, E.M., 1989, Climatic change in the Colorado Rocky Mountains: Estimates based on modern climate at late Pleistocene equilibrium lines, *Arctic and Alpine Research*, v. 21, pp. 245-255.
- Locke, W.W., 1990, Late Pleistocene glaciers and climate of western Montana, U.S.A., *Arctic and Alpine Research*, v. 22, pp. 1-13.
- March, R.S., 1998, Mass balance, meteorological, ice motion, surface altitude, and runoff data at Gulkana Glacier, Alaska, 1994 balance year: *U.S. Geological Survey Water-Resources Investigations Report 97-4251*, 31pp.
- Marks, D., and Dozier, J., 1979, A clear-sky longwave radiation model for remote alpine areas: *Archiv Für Meteorologie Geophysik Und Bioklimatologie, Series B*, v. 27. pp. 159-187.
- Mathews, W.H., 1967, Profiles of late Pleistocene glaciers in New Zealand: *New Zealand Journal of Geology and Geophysics*, v. 10, pp. 146-163.
- McClung, D.M., and Armstrong, R.L., 1993, Temperate glacier time response from field data: *Journal of Glaciology*, v. 39, pp. 323-326.
- McCoy, W.D., and Williams, L.D., 1985, Application of an energy-balance model to the late Pleistocene Little Cottonwood Canyon glacier with implications regarding the paleohydrology of Lake Bonneville: *in* Kay, P.A., and Diaz, H.F., eds., *Problems of and prospects for predicting Great Salt Lake levels*: Center for Public Affairs and Administration, University of Utah, pp.40-53.
- Meeus, J., 1998, *Astronomical Algorithms: Second Edition*: Willman Bell, Inc., Richmond, VA, 477 pp.

- Meier, M.F., 1965, *Glaciers and climate, the Quaternary of the United States*: edited by H.E. Wright, Jr., and D.G. Frey, pp. 795-805.
- Meierding, T.C., 1982, Late Pleistocene glacial equilibrium-line altitudes in the Colorado Front Range: A comparison of methods: *Quaternary Research*, v. 18, pp. 289-310.
- Merrill, R.E., and Péwé, T.L., 1972, Late Quaternary glacial chronology of the White Mountains, east-central Arizona: *Journal of Geology*, v. 80, pp. 493-501.
- Mitchell, V.L., 1976, The regionalization of climate in the western United States: *Journal of Applied Meteorology*, v. 15, pp. 920-927.
- Monteith, J.L., 1962, Attenuation of solar radiation: A climatological study: *Quarterly Journal of the Royal Meteorological Society*, v. 88, pp. 508-521.
- Mountain, K.R., 1990, A clear sky net radiation model fro the high-elevation glacial environment: Unpublished Doctoral Thesis, Ohio State University, 290 pp.
- Munro, D.S., and Young, G.J., 1982, An operational net shortwave radiation model for glacier basins: *Water Resources Research*, v. 18, pp. 220-230.
- Nye, J.F., 1952, A comparison between the theoretical and the measured long profile of the Unteraar glacier: *Journal of Glaciology*, v. 2, pp. 103-107.
- Oerlemans, J., 1992, Climate sensitivity of glaciers in southern Norway: Application of an energy-balance model to Nigardsbreen, Hellstugubreen and Alftobreen: *Journal of Glaciology*, v. 38, pp. 223-231.
- Oerlemans, J., and Knap, W.H., 1998, A 1 year record of global radiation and albedo in the ablation zone of Morteratschgletscher, Switzerland: *Journal of Glaciology*, v. 44, pp. 231-238.
- Oke, T.R., 1987, *Boundary Layer Climates*, 2nd Edition: Methuen, London and New York.
- Olyphant, G.A., 1986, Longwave radiation in mountainous areas and its influence on the energy balance of alpine snowfields: *Water Resources Research*, v. 22, pp. 62-66.
- Paterson, W.S.B., 1994, *The Physics of Glaciers*: Third Edition: Pergamon Press, New York, 250 pp.
- Pearson, G.A., 1931, Forest types in the southwest as determined by climate and soil: U.S. Department of Agriculture Technical Bulletin, v. 247, p. 144.

- Péwé, Troy L., and Updike, Randall C., 1976, San Francisco Peaks, A guidebook to the geology, Second Edition: Museum of Northern Arizona, Flagstaff, Arizona, 80 pp.
- Phillips, F.M., Zreda, M.G., Elmore, D., and Sharma, P., 1993, Evidence for a connection between dynamic behavior of the Laurentide Ice Sheet and mountain glaciation in western North America: EOS (Transactions, American Geophysical Union), v. 74, p. 360.
- Poellot, C.D.P., in prep., Glacial deposits of San Francisco Mountain, Arizona: Masters Thesis, Oregon State University.
- Porter, S.C., 1964, Composite Pleistocene snow line of Olympic Mountains and Cascade Range, Washington: Geological Society of America Bulletin, v. 75, pp. 477-481.
- Porter, S.C., Pierce, K.L., and Hamilton, T.D., 1983, Late Wisconsin mountain glaciation in the western United States: *in* Porter, S.C., ed., Late Quaternary environments of the United States, Volume 1, The late Pleistocene: Minneapolis, University of Minnesota Press, pp. 71-114.
- Richmond, G.M., 1987, Stratigraphy and correlation of glacial deposits of the Rocky Mountains, the Colorado Plateau, and the ranges of the Great Basin: Quaternary Science Reviews, v. 5, pp. 99-127.
- Robinson, N., 1966, Solar Radiation: Elsevier Publishing Company, NY, 347 pp.
- Sharp, M.J., 1998, Personal Communication: Department of Geography, University of Alberta, Edmonton, Alberta T6G 2H4, Canada. May, 1998.
- Sharp, R.P., 1942, Multiple Pleistocene glaciation on San Francisco Mountain, Arizona: Journal of Geology, 42, 481-503.
- Sheridan, M.G., and Updike, R.G., 1975, Sugarloaf Mountain tephra - Pleistocene rhyolitic deposit of base-surge origin in northern Arizona: Geological Society of America Bulletin, v. 86, pp. 571-581.
- Wallace, J.M., and Hobbs, P.V., 1977, Atmospheric Science: An Introductory Survey: Academic Press, New York, 467 pp.
- Walters, R.A., and Meier, M.F., 1989, Variability of glacier mass balances in Western North America: American Geophysical Union, Geophysical Monograph 55, pp. 365-374.

- Walraven, R., 1978, Calculating the position of the Sun: *Solar Energy*, v. 20, pp. 393-397.
- Wendler, G., and Weller, G., A heat-balance study on McCall Glacier, Brooks Range, Alaska: A contribution to the international hydrological decade: *Journal of Glaciology*, v. 13, pp. 13-26.
- Williams, L.D., Barry, R.G., and Andrews, J.T., 1972, Application of computed global radiation for areas of high relief: *Journal of Applied Meteorology*, v.11, pp. 526-533.
- Williams, L.D., 1974, Computer simulation of glacier mass balance throughout an ablation season: *Proceedings of the Western Snow Conference, Annual Meeting*, pp. 23-28.
- Willis, I., Arnold, N., Sharp, M., Bonvin, J.M., and Hubbard, B., 1998, Mass balance and flow variations of the Haut Glacier d'Arolla, Switzerland calculated using digital terrain modelling techniques: In Lane, S.N., Chandler, J.H., and Richards, K.S. (Eds.), *Landform Monitoring, Modelling and Analysis*. Wiley. Chichester.
- Zielinski, G.A., and McCoy, W.D., 1987, Paleoclimatic implications of the relationship between modern snowpack and late Pleistocene equilibrium-line altitudes in the mountains of the Great Basin, western U.S.A., *Arctic and Alpine Research*, v. 19, pp. 127-134.
- Zuo, Z., and Oerlemans, J., 1996, Modelling albedo and specific balance of the Greenland ice sheet: Calculations for the Søndre Strømfjord transect: *Journal of Glaciology*, v. 42., pp. 305-317.

APPENDIX

NET BALANCE PROGRAM CODE

The model is implemented in a stand-alone computer program that was coded in FORTRAN 77. The following code was developed and tested on IBM compatible PCs using the GNU Project Cygwin development tools for Windows 95® (Cygnus Solutions, 1999). Executables were compiled using the FSF-g77 version 0.5.24 FORTRAN compiler under the EGCS development toolchain version egcs-2.91.66 (Khan, 1999).

MAIN PROGRAM BLOCK

```

      program PCebal !Time-stamp: <1999-05-03 17:30:03 Poellot>
      implicit none
      *****
c The main program block ("PCebal") shuffles and organizes inputs
c and outputs - major calculations are performed in five
c subroutines.
c
c Subroutines:
c PARAMETERS: this is an input subroutine that reads a parameters
c file containing glacier and climate specific data.
c
c SOLAR: for the input latitude and longitude, this sub
c calculates hourly values of solar elevation and azimuth to be
c used to adjust radiation values in the energy balance
c calculations.
c
c TERRAIN: calculates slope and aspect of each grid cell to be
c used in adjusting direct radiation - angles returned in radians
c - slope b/t 0. and pi/2; aspect b/t -pi and pi w/ west
c positive.
c
c HORIZON: calculates 36 maximum horizon angles for each cell of
c the glacier DEM using the base DEM of the basin. This sub is
c only used on initial runs of a glacier, as the results are
c stored in an external file 'horizon.txt'. On subsequent runs,
c the 'horizon.txt' file is read into an internal array. This
c sub also calculates the mean horizon angle at each grid node to
c be used in the view factor equation (stored in external file
c 'meanHangle.txt'.
c
c EBALANCE: this sub calculates mass balance for each grid cell
c over the span of the climate record. it is currently designed

```

```

c   to make calculations on GCM/RCM climate data.
c
c Input files:
c   The program reads in elevation data from an ASCII grid file:
c   - "glacier.grd".
c   - "base.grd" is read into an internal array when status =
'new'.
c   Climate data is read in the following format:
c   - "met" has wind speed, atmos. vapor pres., net longwave rad.,
c     incoming shortwave rad., and precip
c   Geographic and equation variables are input from a parameters
c   file:
c   - "param2d"
c
c Output files:
c   The program writes data to three ASCII SURFER grid files:
c
c   - "Mbal.dat" contains mass balance data for each grid cell
c     (mmH2O).
c   - "Aspect.dat" contains aspect data for each grid cell
c     (degrees).
c   - "Slope.dat" contains slope data for each grid cell
c     (degrees).
c
c   The program also returns the following tab-delimited ASCII text
c   files for data evaluation:
c
c   - "Stake##.txt": in the "param2d" input file the user may
c     enter the coordinates of specific grid cells. Data from
c     the EBALANCE subroutine is written to these files.
c   - "Mbal.txt" contains elevation averages of mass balance over
c     the entire glacier to be used in constructing a mass
c     balance profile, also contains background albedo for the
c     elevations.
c   - "Solardump.txt" contains any discrepancies between the "met"
c     input file and the internally calculated solar elevations.
c   - "Snowelev.txt" contains the day and elevation of the first
c     day that snow depth = 0 for each user specified grid cell.
c   - "Solel.txt" contains daily solar elevations.
c   - "Solaz.txt" contains daily solar azimuths (both solar files
c     contain hourly values in degrees).
c   - "Horizon.txt" contains 36 azimuthal horizon angles for each
c     grid cell of 'glacier.grd' for use in determining shading
c     of grid cells.
c
c   Notes on output files:
c   - "Slope.dat", "Aspect.dat", "Solel.txt", "Solaz.txt", and
c     "Solardump.txt" are only written if the user sets a
c     conditional statement in the "param2d" input file.
c   - In order to grid the SURFER *.dat files, open the files in a
c     SURFER worksheet, and save as space delimited, no quotes
c     around text strings DAT file with a ".grd" extension.
c
c *****
c *   DECLARATIONS   *
c *****
c     INTEGER i,j,k,z,count,total,sum,first,last,firstday,lastday

```

```

        LOGICAL sorted,same
c
c DEM parameters: number of rows and columns, min/max x,y,z coords,
c base and grid node elevation, mass balance, max/min massbal,
c sorting
c holds, glacier and grid node area, net balance, ELA id variables,
c DEM header.
        INTEGER nrows,ncols,xmin,xmax,ymin,ymax,zmin,zmax,x,y
        INTEGER nrowssb,ncolssb,xminb,xmaxb,yminb,ymaxb,zminb,zmaxb
        INTEGER DR,DC,GR,HC,SR,SC,NR,NC,cellnum,nd
        REAL Gelev,Belev,massbal,Mmax,Mmin,hold1,hold2,hold3
        REAL size,glarea,gnarea,netbal,ELAmin,ELAmass,blank
        REAL rzmin,rzmax,rzminb,rzmaxb
        CHARACTER*4 header
c
c Array row/column parameters
        PARAMETER
            $      (DR=500,          ! max number of rows in DEMs
            $      DC=500,          ! max number of columns in DEMs
            $      GR=25000,        ! max number of glacier grid nodes
            $      SR=2000,         ! max number of days in climate
record
            $      NR=20)          ! max number of grid cell output
locations
c
c slope and aspect parameters
        REAL slope,aspect,Smax,Smin,Amax,Amin,north,south,east,west
c
c solar angle and elevation parameters, horizon angle params
        INTEGER zone
        REAL lat,lon,day,rad
        REAL Horiz,TotHoriz,skyview
c
c DEM arrays, Mass balance, Slope and Aspect arrays, sorting arrays
        REAL Gdem(DR,DC),Bdem(DR,DC),M(DR,DC),S(DR,DC),A(DR,DC)
        REAL mbaldata(GR,3),mbaldata2(GR,3),Hangle(GR,36)
        REAL solaz(SR,24),solel(SR,24),MeanHangle(GR)
c
c Parameters input from file (see parameters subroutine for
c description
c   of variables)
        INTEGER dasvtm,stkloc(NR,2),numstk,tmstp
        REAL
Khs,Khi,a1,a2,a3,a4,a5,a6,a7,Tdep,ELA,balb,spack1,spack2,
        $      snowdns,snowd,pre_laps
c
c Character variables for internal write statements used in
c variable
c   format descriptors, and status indicator (new or old)
        CHARACTER*3 status
        CHARACTER*2 c2
        CHARACTER*15 filename,efluxfile
        CHARACTER*30 fmat1,fmat2
c
c Variables used for calculation of Inlwrad.
        REAL Trange,cloud(SR),temp(24),Tmax,Tmin
c

```

```

c Glacier averages of Eflux components
  REAL AveG,Aveinlwrad,AveLnet,AveHs,AveHl,AveEflux,netG,
  $      netinlwrad,netLnet,netHs,netHl,netEflux,Avetlwrad,
  $      nettlwrad
c
c Variables to write system time stamp to file
  INTEGER stime
  INTEGER time
  CHARACTER*30 tmstamp
c
c fixed parameters
  PARAMETER (rad=0.01745329251994,
  $          blank=1.70141e38)
c
*****
*   Initialize variables & arrays   *
*****
  data ELAmin,Smax,Amay,Mmax/4*-1.0e20/
  data ELAmax,Smin,Amin,Mmin/4*1.0e20/
  do i=1,DR
    do j=1,DC
      Gdem(i,j)=0.
      M(i,j)=0.
      S(i,j)=0.
      A(i,j)=0.
    enddo
  enddo
  do i=1,GR
    MeanHangle(i)=0.
    do j=1,3
      mbaldata(i,j)=0.
      mbaldata2(i,j)=0.
    enddo
    do k=1,36
      Hangle(i,j)=0.
    enddo
  enddo
  do i=1,SR
    cloud(i)=0.
    do j=1,24
      solaz(i,j)=0.
      solel(i,j)=0.
    enddo
  enddo
  do i=1,NR
    do j=1,2
      stkloc(i,j)=0
    enddo
  enddo
  HC=36      !max number of columns in horizon array
  NC=2       !max number of columns in stkloc array
  SC=24      !frequency of solar elev./azim. measurements per
day
  firstday=0
  lastday=0
  count=0
  nd=0

```

```

        cellnum=0
        Horiz=0.
C
*****
*   Open data.txt, get parameters *
*****
        open (unit=20,file="data.txt",status="new")
        stime=time()
        call Ctime(tmstmp,stime)
        write(20,*)tmstmp
        call
parameters(model,Belev,Khs,Khi,Tdep,a1,a2,a3,a4,a5,a6,a7,
$
ELA,zone,lat,lon,dasvtm,status,spack1,spack2,numstk,NR,NC,
$      stkloc,tmstp,snowdns,pre_laps)
C
*****
*   Open input files *
*****
        open (unit=11,file="met",status="old")
        open (unit=12,file="glacier.grd",status="old")
C
*****
*   Open output files that are always written *
*****
        open (unit=19,file="Snowelev.txt",status="new")
        open (unit=21,file="Mbal.dat",status="new")
        open (unit=22,file="Mbal.txt",status="new")
        do i=1,numstk ! opens grid data point files (stake01.txt,...)
            write(c2,"(i2.2)") i !create a string with leading zeros.
            filename="Stake"//c2//".txt"
            efluxfile="Eflux"//c2//".txt"
            open (unit=29+i,file=filename,status="new")
            open (unit=59+i,file=efluxfile,status='new')
        enddo
C
*****
*   Write headers to "output" files *
*****
C
C Snowelev.txt
        write (19,fmt=500)
        $      "Day",char(9),
        $      "Elevation (m)"
C
C Stake##.txt
        do i=1,numstk
            write (unit=29+i,fmt=510)
            $      "day",char(9),
            $      "airtemp (K)",char(9),
            $      "wind (m/s)",char(9),
            $      "avp (kPa)",char(9),
            $      "svp (kPa)",char(9),
            $      "totswrad (mH2O)",char(9),
            $      "netswrad (mH2O)",char(9),
            $      "inlwrad (mH2O)",char(9),
            $      "tlwrad (mH2O)",char(9),

```

```

$      "netlwrad (mH2O)",char(9),
$      "Hs (mH2O)",char(9),
$      "H1 (mH2O)",char(9),
$      "Eflux (mH2O)",char(9),
$      "albedo (%)",char(9),
$      "ablation (mH2O)",char(9),
$      "snowd (mH2O)",char(9),
$      "precip (mH2O)",char(9),
$      "snowfall (mH2O)",char(9),
$      "totaccum (mH2O)",char(9),
$      "totabltm (mH2O)",char(9),
$      "rsum abl (mH2O)"
C
C Eflux##.txt
      write (unit=59+i,fmt=515)
$      'day',char(9),
$      'hour',char(9),
$      'direct rad',char(9),
$      'diffuse rad',char(9),
$      'inlwrad',char(9),
$      'tlwrad',char(9),
$      'Hs',char(9),
$      'H1',char(9),
$      'Eflux'
      enddo
500  format (a3,a1,a15)
510  format
(a3,a1,a12,a1,a11,a1,2(a10,a1),2(a16,a1),a15,a1,a14,a1,
$      a16,a1,2(a10,a1),a13,a1,a11,a1,a16,a1,a13,a1,a15,a1,
$      3(a16,a1),a16)
515  format (a3,a1,a4,a1,a10,a1,a11,a1,a6,a1,a7,a1,2(a2,a1),a5)
C
*****
*   Input elevation data from dem, echo to standard output   *
*****
      read(12,*)header
      if(header.ne."DSAA") stop "DEM in wrong format"
      read(12,*)ncols,nrows
      read(12,*)xmin,xmax
      read(12,*)ymin,ymax
      read(12,*)rzmin,rzmax
      zmin=int(rzmin)
      zmax=int(rzmax)
      do i=1,nrows
         read(12,*) (Gdem(i,j),j=1,ncols)
      enddo
C
      write(20,*)
      write(20,*) "DEM DATA:"
      write(20,*)"local latitude in degrees (north +) = ",lat
      write(20,*)"local longitude in degrees (east +) = ",lon
      write(20,520)nrows,ncols
      write(20,530)xmin,ymin
      write(20,540)xmax,ymax
      write(20,550)zmin
      write(20,560)zmax
520  format(1x,"This DEM has ",i3," rows, and ",i3," columns.")

```

```

530 format(1x,"The lower left corner of the DEM is: ",i6," ",i7)
540 format(1x,"The upper right corner of the DEM is: ",i6,"
",i7)
550 format(1x,"Minimum elevation of the DEM is: ",i4," meters.")
560 format(1x,"Maximum elevation of the DEM is: ",i4," meters.")
c
*****
* If status='old' then open dependant input files, read in      *
* Hangle and MeanHangle arrays                                  *
*****
      if(status.eq.'old') then
        open (unit=18,file="Horizon.TXT",status="old")
        open (unit=17,file="MeanHangle.TXT",status="old")
c
c read in data from 'Horizon.txt' file to Hangle array, and from
c 'MeanHangle.txt' to MeanHangle array
      read(17,*)cellnum !get number of cells in glacier array
      do i=1,cellnum
        read(17,*)MeanHangle(i)
        read(18,*)(Hangle(i,j),j=1,HC)
      enddo
c
c Convert Hangle array to radians
      do i=1,cellnum
        do j=1,HC
          Hangle(i,j)=Hangle(i,j)*rad
        enddo
      enddo
      cellnum=0
    endif
c
*****
* If status='new' then open dependant input/output files *
* and write headers to files                               *
*****
      if(status.eq."new")then
        open (unit=13,file="base.grd",status="old")
        open (unit=16,file="Stake_hangles.txt",status="new")
        open (unit=18,file="Horizon.TXT",status="new")
        open (unit=17,file="MeanHangle.TXT",status="new")
        open (unit=23,file="Slope.dat",status="new")
        open (unit=24,file="Aspect.dat",status="new")
        open (unit=25,file="Solel.txt",status="new")
        open (unit=26,file="Solaz.txt",status="new")
c
c read in Bdem array, check to see if Bdem and Gdem cover the same
c coords.
      read(13,*)header
      if(header.ne."DSAA") stop "DEM in wrong format"
      read(13,*)ncolsb,nrowsb
      if (ncols.ne.ncolsb.or.nrows.ne.nrowsb)
$        stop "Grids are not the same size"
      read(13,*)xminb,xmaxb
      read(13,*)yminb,ymaxb
      if (xmin.ne.xminb.or.xmax.ne.xmaxb.or.ymin.ne.yminb.or.
$        ymax.ne.ymaxb)
$        stop "Grids do not have the same geographic coords"

```



```

        read(13,*)rzminb,rzmaxb
        zminb=int(rzminb)
        zmaxb=int(rzmaxb)
        do i=1,nrowsb
            read(13,*)(Bdem(i,j),j=1,ncolsb)
        enddo
    endif
C
*****
*   Blank first and last row and column of glacier grid *
*****
        do i=1,ncols
            Gdem(1,i)=blank
            Gdem(nrows,i)=blank
        enddo
        do i=1,nrows
            Gdem(i,1)=blank
            Gdem(i,ncols)=blank
        enddo
C
*****
*   Count unblanked cells in DEM, calculate glacier area. *
*****
        do i=1,nrows
            do j=1,ncols
                if(Gdem(i,j).lt.1.0e6)count=count+1
            enddo
            total=total+count
            count=0
        enddo
        size=(xmax-xmin)/(ncols-1)
        gnarea=size*size
        glarea=total*gnarea
        write(20,*)"This glacier has",total," grid nodes"
        write(20,*)"The area for each grid node = ",gnarea," m^2"
        write(20,*)"The glacier has a total area of ",glarea," m^2"
        write(20,*)
C
*****
*   Determine first and last day of climate record, find *
*   Daily Temperature range if tmstp > 1 *
*****
        rewind (11)
10    count=count+1
        if (tmstp.gt.1) then
            Tmax=-1.0e20
            Tmin=1.0e20
            do i=1,24
                read(11,*,end=20)day,temp(i)
                if(temp(i).gt.Tmax)Tmax=temp(i)
                if(temp(i).lt.Tmin)Tmin=temp(i)
            enddo
            Trange=Tmax-Tmin
            cloud(count)=-0.098*Trange+1.285
            if (cloud(count).gt.1.)cloud(count)=1.
            if (cloud(count).lt.0.)cloud(count)=0.
            if(count.eq.1)firstday=int(day)

```

```

        lastday=int(day)
    else
        read(11,*,end=20)day
        if(count.eq.1)firstday=int(day)
        lastday=int(day)
    endif
    goto 10
20  nd=lastday-firstday+1
    count=0
    write(fmat1,570)nd
    write(fmat2,580)nd
570  format("(a4,a1","i4.4","(i4,a1),i4)")
580  format("(i2,a1","i4.4","(f9.2,a1),f9.2)")
c
*****
* Call SOLAR subroutine to compute lookup tables for *
* solar elevation and azimuth *
*****
        call solar(solaz,solel,firstday,lastday,SR,SC,zone,lat,lon,
$          dasvtm)
c
c Blank first and last rows and columns of slope and aspect arrays
    do i=1,ncols
        S(1,i)=blank
        A(1,i)=blank
        S(nrows,i)=blank
        A(nrows,i)=blank
    enddo
    do i=1,nrows
        S(i,1)=blank
        A(i,1)=blank
        S(i,ncols)=blank
        A(i,ncols)=blank
    enddo
c
*****
* Call TERRAIN subroutine to calculate slope and aspect *
* of glacier grid nodes *
*****
    do i=2,nrows-1
        do j=2,ncols-1
            Gelev=Gdem(i,j)
            if(Gelev.lt.blank) then
                north=Gdem(i+1,j)
                south=Gdem(i-1,j)
                east=Gdem(i,j+1)
                west=Gdem(i,j-1)
                call terrain(Gelev,north,south,east,west,size,slope,
+                  aspect)
                S(i,j)=slope/rad
                A(i,j)=aspect/rad
            else
                S(i,j)=Gelev
                A(i,j)=Gelev
            endif
        enddo
    enddo
enddo

```

```

C
*****
* If status = "new" then call HORIZON subroutine to compute *
* lookup tables for horizon angles, also write slope and *
* aspect data to output files. *
*****
      if(status.eq.'new') then
C
C Call HORIZON subroutine for all glacier grid nodes
      do i=1,nrows
        do j=1,ncols
          if(gdem(i,j).lt.blank)then
            cellnum=cellnum+1
            x=j
            y=i
            gelev=Gdem(i,j)
            call horizon(x,y,Bdem,nrows,ncols,DR,DC,gelev,
$              size,cellnum,Hangle,GR,HC)
            do k=1,numstk
              if(x.eq.stkloc(k,1).and.y.eq.stkloc(k,2)) then
                write(16,585) (90-Hangle(cellnum,z)/rad,
$                  char(9),z=1,35),
$                  90-Hangle(cellnum,36)/rad
              endif
            enddo
          endif
        enddo
      enddo
      enddo

C
C Compute mean Horizon angle for each grid cell for
C calculating the skyview factor
      do i=1,cellnum
        TotHoriz=0.
        do j=1,HC
          Horiz=Hangle(i,j)
          TotHoriz=TotHoriz+Horiz
        enddo
        MeanHangle(i)=TotHoriz/float(HC)
      enddo

C
C Write output to 'Horizon.txt' and 'MeanHangle.txt' files
      write(17,*)cellnum !write number of cells in glacier array
      do i=1,cellnum
        write(17,*)MeanHangle(i)
        write(18,fmt=585) (Hangle(i,j)/rad,char(9),
$          j=1,HC-1),Hangle(i,HC)/rad
      enddo
585      format(1x,35(f4.1,a1),f4.1)
      cellnum=0

C
C write header info for ASCII grid files
      write(23,*)"DSAA"
      write(23,*)ncols,nrows ! The ncols and nrows for the slope
      write(23,*)xmin,xmax ! and aspect grid files will be the
      write(23,*)ymin,ymax ! same as the nrows and ncols for
      write(24,*)"DSAA" ! the "glacier.grd" input file.
      write(24,*)ncols,nrows

```

```

write(24,*)xmin,xmax
write(24,*)ymin,ymax
do i=1,nrows          ! Calculate Smin,Smax,Amin,Amax
  do j=1,ncols
    if(S(i,j).le.Smin) Smin=S(i,j)
    if(S(i,j).ge.Smax.and.S(i,j).lt.1.0e6) Smax=S(i,j)
    if(A(i,j).le.Amin) Amin=A(i,j)
    if(A(i,j).ge.Amax.and.A(i,j).lt.1.0e6) Amax=A(i,j)
  enddo
enddo
write(23,*)Smin,Smax
write(24,*)Amin,Amax

C
C DEM data output
  do i=1,nrows
    write(23,*) (S(i,j),j=1,ncols) !Slope.dat
    write(23,*)
    write(24,*) (A(i,j),j=1,ncols) !Aspect.dat
    write(24,*)
  enddo

C
C Solar Elevation and Azimuth data files
  write (25,fmat1)"hour",char(9),(i,char(9),i=firstday,
$      lastday-1),lastday
  write (26,fmat1)"hour",char(9),(i,char(9),i=firstday,
$      lastday-1),lastday
C      format(a4,a1,92(i4,a1),i4)
C
  do i=1,24
    write(25,fmat2)i,char(9),
$      (solel(j,i)/rad,char(9),j=1,nd-1),solel(nd,i)/rad
    write(26,fmat2)i,char(9),
$      (solaz(j,i)/rad,char(9),j=1,nd-1),solaz(nd,i)/rad
  enddo
  close (17)
  close (18)
  close (23)
  close (24)
  close (25)
  close (26)
endif

C
*****
* Calculate mass balance for each unblanked grid node *
* using EBALANCE subroutine *
*****
  do i=1,nrows
    do j=1,ncols
      x=j
      y=i
      Gelev=Gdem(i,j)
      if(Gelev.lt.blank) then
        cellnum=cellnum+1
        slope=S(i,j)*rad
        aspect=A(i,j)*rad
        skyview=cos(MeanHangle(cellnum))**2
        call ebalance(model,Gelev,Belev,Khs,Khi,Tdep,a1,a2,

```

```

$          ELA,slope,aspect,solel,solaz,SR,SC,
$          balb,a3,a4,a5,a6,a7,spack1,spack2,x,y,
$          NR,NC,numstk,stkloc,tmstp,size,
$          snowdns,status,cloud,cellnum,Hangle,skyview,GR,
$          HC,snowd,massbal,AveG,Aveinlwrad,Avetlwrad,
$          AveLnet, AveHs,AveHl,AveEflux,pre_laps)
      M(i,j) = massbal
      mbaldata(cellnum,1)=int(Gelev)
      mbaldata(cellnum,2)=massbal
      mbaldata(cellnum,3)=balb
      netbal=netbal+gnarea*massbal
      netG=netG+AveG
      netinlwrad=netinlwrad+Aveinlwrad
      nettlwrad=nettlwrad+Avetlwrad
      netLnet=netLnet+AveLnet
      netHs=netHs+AveHs
      netHl=netHl+AveHl
      netEflux=netEflux+AveEflux
    else
      M(i,j) = Gelev
    endif
    Gelev=0
    massbal=0
  enddo
enddo
netbal=netbal/glarea
netG=netG/float(cellnum)
netinlwrad=netinlwrad/float(cellnum)
nettlwrad=nettlwrad/float(cellnum)
netLnet=netLnet/float(cellnum)
netHs=netHs/float(cellnum)
netHl=netHl/float(cellnum)
netEflux=netEflux/float(cellnum)
C
*****
* Sort elevation and massbal data in "data" array for output*
*****
      sorted=.false.
      first=1
      last=cellnum-1
30    if(.not.sorted)then
      sorted=.true.
      do i=first,last
        if(mbaldata(i,1).gt.mbaldata(i+1,1)) then
          hold1=mbaldata(i,1)
          hold2=mbaldata(i,2)
          hold3=mbaldata(i,3)
          mbaldata(i,1)=mbaldata(i+1,1)
          mbaldata(i,2)=mbaldata(i+1,2)
          mbaldata(i,3)=mbaldata(i+1,3)
          mbaldata(i+1,1)=hold1
          mbaldata(i+1,2)=hold2
          mbaldata(i+1,3)=hold3
          sorted=.false.
        endif
      enddo
      last=last-1

```

```

        goto 30
    endif
C
*****
* Calculate internally generated ELA for glacier*
*****
    do i=1,cellnum-1
        if(mbaldata(i,2).le.0.and.mbaldata(i+1,2).gt.0) then
            ELAmin=mbaldata(i,1)
            ELAmax=mbaldata(i+1,1)
        endif
    enddo
    if(ELAmin.gt.-1.0e20) then
        ELA=(ELAmin+ELAmax)/2.
        write(20,*)"Grid elevation below ELA = ",ELAmin
        write(20,*)"Grid elevation above ELA = ",ELAmax
        write(20,*)"New ELA = ",ELA
    else
        write(20,*)"Glacier not in balance (no new ela)"
    endif
    write(20,*)"Net balance of glacier =      ",netbal
    write(20,*)
    write(20,*)"Net incoming shortwave rad = ",netG
    write(20,*)
    write(20,*)"Net incoming longwave rad =  ",netinlwrad
    write(20,*)
    write(20,*)"Net terrain longwave rad =   ",nettlwrad
    write(20,*)
    write(20,*)"Net total longwave rad =     ",netLnet
    write(20,*)
    write(20,*)"Net sensible heat flux =     ",netHs
    write(20,*)
    write(20,*)"Net latent heat flux =       ",netHl
    write(20,*)
    write(20,*)"Net energy flux at surface=  ",netEflux
C
*****
* Check for identical elevations in the 'data' array.  compute *
* average Mass balances and albedos for "identical" elevations*
*****
    sum=0
    hold1=0
    hold2=0
    j=0
    same=.false.
    do 40 i=1,cellnum-1
        if(mbaldata(i,1).eq.mbaldata(i+1,1)) same=.true.
        if(.not.same.and.sum.gt.0) then
            mbaldata2(j,1)=mbaldata(i,1)
            mbaldata2(j,2)=(hold1+mbaldata(i,2))/(sum+1)
            mbaldata2(j,3)=(hold2+mbaldata(i,3))/(sum+1)
            sum=0
            hold1=0
            hold2=0
            goto 40
        else if (.not.same.and.sum.eq.0) then
            j=j+1

```

```

        mbaldata2(j,1)=mbaldata(i,1)
        mbaldata2(j,2)=mbaldata(i,2)
        mbaldata2(j,3)=mbaldata(i,3)
        goto 40
    else
        if(sum.eq.0) j=j+1
        hold1=hold1+mbaldata(i,2)
        hold2=hold2+mbaldata(i,3)
        sum=sum+1
        same=.false.
    endif
40  continue
    do i=1,j-1
        if(mbaldata2(i,2).le.0.and.mbaldata2(i+1,2).gt.0) then
            ELAmin=mbaldata2(i,1)
            ELAmax=mbaldata2(i+1,1)
        endif
    enddo
    if(ELAmin.gt.-1.0e20) then
        ELA=(ELAmin+ELAmax)/2.
        write(20,*)"Grid elevation below ELA = ",ELAmin
        write(20,*)"Grid elevation above ELA = ",ELAmax
        write(20,*)"New ELA = ",ELA
    else
        write(20,*)"Glacier not in balance (no new ela)"
    endif

C
*****
* Write data to Mbal.txt and Mbal.dat files *
*****
C
c Mbal.txt output
    write(22,fmt=600)"Elevation",char(9),"MassBal",
    $      char(9),"Albedo"
    do i=1,j-1
        write(22,fmt=610) mbaldata2(i,1),char(9),mbaldata2(i,2),
    $      char(9),mbaldata2(i,3)
    enddo
600  format(a9,a1,a7,a1,a7)
610  format(f8.0,a1,f7.4,a1,f6.4)
C
c header info for DEMs
    write(21,*)"DSAA"
    write(21,*)ncols,nrows
    write(21,*)xmin,xmax
    write(21,*)ymin,ymax
    do i=1,nrows
        do j=1,ncols
            if(M(i,j).le.Mmin) Mmin=M(i,j)
            if(M(i,j).ge.Mmax.and.M(i,j).lt.1.0e10) Mmax=M(i,j)
        enddo
    enddo
    write(21,*)Mmin,Mmax
C
c DEM data output
    do i=1,nrows
        write(21,*)(M(i,j),j=1,ncols) !Mbal.dat
    enddo

```

```

        write(21,*)
    enddo
C
*****
*   close up stuff & end for now   *
*****
        close(11)
        close(12)
        stime=time()
        call Ctime(tmstmp,stime)
        write(20,*)tmstmp
        close(20)
        close(21)
        close(22)
        close(19)
        do i=1,numstk
            close(29+i)
        enddo
    end

```

PARAMETERS SUBROUTINE

```

*****
C
    subroutine parameters(model,belev,Khs,Khi,Tdep,a1,a2,a3,
$      a4,a5,a6,a7,ELA,zone,lat,lon,dasvtm,status,spack1,
$      spack2,numstk,NR,NC,stkloc,tmstp,snowdns,pre_laps)
    implicit none
C
*****
* Abstract:  collects various geographic and climatic variables
* needed for specific runs from "parameters" file.
*
* Input: Data is returned to the main program in the following
* order: *
*
*      model  number used to choose which set of ebalance
*              equations to use:
*              1=Oerlemans(1992),
*              2=Paterson(1994),
*              3=Arnold, et. al.(1996).
*      belev  base elevation for grid (meters).
*      Khs    turbulent heat bulk transfer coefficient (for snow
*              if using Paterson's equations, for snow and ice if
*              using Oerleman's).
*      Khi    turbulent heat bulk transfer coefficient for ice
*              (Paterson).
*      Tdep   temperature depression (degrees).
*      a1-a6  albedo parameterizations.
*      ELA    initial E.L.A. of reconstructed glacier (meters).
*      zone   time zone based on GUT (Pacific St. Time = zone 8).
*      lat    local latitude of Gdem in degrees north (e.g.

```



```

*          35.783). *
*      lon      local longitude of Gdem in degrees west of
*              Greenwich. *
*      dasvtm toggle for daylight savings time (1=on, 0=off).
*      status "old" or "new": tells program if a run has been
*              made for this particular glacier and timespan
*              before. if "old" then the model skips the solar
*              and terrain subroutines to save time.
*      spack* variables to compute snowpack at start of model
*              run. *
*      stkloc integer array to contain grid points at which
*              energy balance data will be recorded.
*      numstk number of stake locations (data files).
*      tmstp number of time steps per day to calculate energy
*              balance variables.
*      snowdns snow density for use in spack equation! added
*              1-29-99*
*      pre_laps variable for precipitation lapse rate calc.
*              4-9-99
*****
C
C Declarations
      INTEGER model,zone,dasvtm,numstk,NR,NC,stkloc(NR,NC),i,tmstp
      REAL
Belev,Khs,Khi,Tdep,a1,a2,a3,a4,ELA,lat,lon,spack1,spack2,
      $      a5,a6,a7,snowdns,pre_laps
      CHARACTER*3 status
C
C Open parameters file for model variables
      open (unit=10, file="param2d", status="old")
      rewind (10)
C
C Determine which model type is being run
      read (10,*) model
      if (model.eq.2) then
          write(20,*)"This model calculates turbulent heat
fluxes",
          1          " using equations"
          write(20,*)"from Paterson (1994)"
      else if (model.eq.1) then
          write(20,*)"This model calculates turbulent heat fluxes",
          1          " using equations"
          write(20,*)"from Oerlemans (1992)"
      else
          write(20,*)"This model calculates turbulent heat fluxes",
          $          " using equations"
      write(20,*)"from Arnold et. al. (1996)"
      endif
C
C Read the rest of the parameter variables: echo to std. output
      read(10,*) Belev
      write(20,*)"Base elevation = ",Belev
      read(10,*) Khs
      if (model.eq.2) then
          write(20,*)"Bulk exchange coefficient for snow =",Khs
      else if (model.eq.1) then
          write(20,*)"Bulk exchange coefficient = ",Khs

```

```

endif
read(10,*) Khi
if (model.eq.2) write(20,*) "Bulk exchange coefficient for ",
+ "ice = ", Khi
read(10,*) Tdep
write(20,*) "Temperature Depression = ",Tdep
read(10,*) a1
write(20,*) "Albedo parameter 1 = ",a1
read(10,*) a2
write(20,*) "Albedo parameter 2 = ",a2
read(10,*) a3
write(20,*) "Albedo parameter 3 = ",a3
read(10,*) a4
write(20,*) "Albedo parameter 4 = ",a4
read(10,*) a5
write(20,*) "Albedo parameter 5 = ",a5
read(10,*) a6
write(20,*) "Albedo parameter 6 = ",a6
read(10,*) a7
write(20,*) "Albedo parameter 7 = ",a7
read(10,*) ELA
write(20,*) "Initial Equilibrium Line Altitude = ",ELA
read(10,*) zone
write(20,*) "local time zone (GUT) = ",zone
write(20,*)
read(10,*) lat
read(10,*) lon
read(10,*) dasvtm
if (dasvtm.eq.1) write (20,*) "Daylight savings time on."
read(10,*) status
read(10,*) spack1
read(10,*) spack2
read(10,*) numstk
write(20,*) 'Stake grid coordinates'
do i=1,numstk
    read(10,*) stkloc(i,1),stkloc(i,2)
    write(20,*)stkloc(i,1),stkloc(i,2)
enddo
read(10,*) tmstp
write(20,*) "The number of timesteps per day for calculating"
write(20,*) " energy balance =",tmstp
read(10,*) snowdns
write(20,*) "Mean density of snowpack =",snowdns
read(10,*) pre_laps

c
c close data file and return to main program
close (10)
return
end

```

SOLAR SUBROUTINE

```

*****
      Subroutine Solar(solaz,solel,firstday,lastday,SR,SC,zone,lat,
      $      lon,dasvtm)
      implicit none
*****
* This subroutine calculates the solar angle and elevation at one
* hour intervals for a specified number of days. Data are
* written to an array of (x,24) dimensions, where x is the number
* of days of climate data. Calculations are based on the
* following references:*
*
* Walraven, R., 1978, Calculating the position of the Sun: Solar
* Energy, 20, 393-397.
*
* Grobneck, Christopher, 1998, SunAngle: http://solstice.crest.org/
* staff/ceg/sunangle/index.html
* Inputs :
*   solaz: array containing solar azimuth data
*   solel: array containing solar elevation data
*   firstday: first day of climate record
*   lastday: last day of climate record
*   SR/SC: dimensioned size of the arrays
*   Zone: Time zone based on GUT (East is +, West is - )
*         (e.g. P.S.T. = zone -8)
*   Lat: local latitude in degrees (north is positive)
*   Lon: local longitude in degrees (east = positive)
*         (west = negative)
*   dasvtm: daylight savings time toggle (1=on, 0=off)
*
* Outputs:
*   Sazim: solar azimuth in radians
*   Selev: solar elevation in radians (positive for daylight)
*
* Local variables
*   day: day of the year, starting w/ 1
*   hour: hour of the day (1-24)
*   twopi: pi times 2
*   rad: conversion to radians from degrees
*   gamma: day angle
*   Decl: declination of the sun
*   H: hour angle of the sun
*   phi: local latitude in radians
*   LSTM: Local Standard Time Meridian
*   LST: Local Time (hours)
*   LSoT: Local Solar Time (hours)
*   EOT: Equation of Time (minutes)
*****
C
C declarations
      INTEGER day,zone,firstday,lastday,SR,SC,i,j,
      $      yearno,hour,count,dasvtm
      REAL Sazim,Selev,Decl,H,phi
      REAL solaz(SR,SC),solel(SR,SC),rad,lat,lon,LSTM,LST,
      $      EOT,B,LSoT

```

```

c
    PARAMETER (rad=0.01745329251994)
    yearno=0
    count=0
    LSTM=zone*15.

c
    do i=firstday,lastday
        if(mod(i,365).eq.0) yearno=yearno+1
        day=i-(yearno*365)
        count=count+1

c
        do j=0,23

c
c Calculate Equation of Time and Local Solar Time
c
            hour=j
            LST=hour*60.-dasvtm*60.
            B=(360.*(day-81)/365.)*rad
            EOT=9.87*sin(2*B)-7.53*cos(B)-1.5*sin(B)
            LSoT=(LST+4*(lon-LSTM)+EOT)/60.

c
c Calculate Solar Declination
c
            Decl=(23.45*rad)*sin(rad*(360./365.*(284+day)))

c
c Calculate Hour Angle
c
            H=((LSoT-12.)*-15.)*rad

c
c Calculate Solar Elevation and Azimuth
c
            phi=Lat*rad
            Selev=asin(sin(phi)*sin(decl)+cos(phi)*cos(decl)*cos(H))
            Sazim=acos((sin(Selev)*sin(phi)-sin(decl))/
$              (cos(Selev)*cos(phi)))
c              if(sin(Selev).ge.sin(decl)/sin(phi)) goto 10
c              if(Sazim.lt.0.) Sazim=Sazim+twopi
c              Sazim=pi-Sazim
            if(H.lt.0..and.Sazim.gt.0.) Sazim=Sazim*-1.
            if(H.gt.0..and.Sazim.lt.0.) Sazim=Sazim*-1.
10          solaz(count,j+1)=Sazim
            solel(count,j+1)=Selev
        enddo
    enddo

c
    return
end

c

```

TERRAIN SUBROUTINE

```

*****
      subroutine terrain(Gelev,north,south,east,west,size,slope,
+   aspect)
      implicit none
*****
*   This subroutine calculates slope and aspect for a given grid
*   node of a "blanked" SURFER ASCII grid file.
*   If the node surrounded by 1 or more blanked cells, then the
*   the program interpolates the elevation of the blanked cell by
*   looking at the opposite elevation and the grid node. If the
*   opposite cell is also blanked (i.e. north and south) then the
*   slope and aspect are calculated from the existing values.
*
*   Inputs:
*       Gelev:  grid node elevation (meters)           R4
*       north:  X(i,j+1) where X is the elevation array R4
*       south:  X(i,j-1)                               R4
*       east :  X(i+1,j)                               R4
*       west :  X(i-1,j)                               R4
*       size :  length of grid cell (meters)           R4
*   Outputs:
*       slope :  (positive value b/t 0. and 1.57)       R4
*       aspect:  3.14159 to -3.14159 (0=south, +is west) R4
*****
C
C   Declarations
      REAL Gelev,north,south,east,west,slope,aspect,blank,size
      blank=1.0e20
C
C   determine if any bordering cells are blanked
      if(north.gt.blank.or.south.gt.blank.or.east.gt.blank.or.
+       west.gt.blank) goto 100
C
C   calculate slope
10  slope=sqrt(((north-south)/(size*2))*((north-south)/(size*2))+
+       ((east-west)/(size*2))*((east-west)/(size*2)))
      slope=atan(slope)
C
C   if north=south then assign value to aspect to avoid division/0
      if(north.eq.south) then
          if(east.eq.west) aspect=0.
          if(east.gt.west) aspect=1.570795
          if(west.gt.east) aspect=-1.570795
          return
      else
          continue
      endif
C
C   if east=west then assign value to aspect according to N-S slope
      if(east.eq.west) then
          if(north.eq.south) aspect=0.
          if(north.lt.south) aspect=3.14159
          if(north.gt.south) aspect=0.
          return

```

```

        else
            continue
        endif
c
c calculate aspect
    aspect=((west-east)/(size*2))/((south-north)/(size*2))
    aspect=atan(aspect)
    if(south.gt.north.and.east.gt.west) aspect=aspect+3.14159
    if(south.gt.north.and.west.gt.east) aspect=aspect-3.14159
    return
c
c if cells are blanked estimate blanked values
100  if(north.gt.blank.and.south.lt.blank) then
        if(south.gt.Gelev) then
            north=Gelev-(south-Gelev)
        else
            north=Gelev+(Gelev-south)
        endif
    endif
    if(north.gt.blank.and.south.gt.blank) then
        north=Gelev
        south=Gelev
    endif
    if(south.gt.blank.and.north.lt.blank) then
        if(north.gt.Gelev) then
            south=Gelev-(north-Gelev)
        else
            south=Gelev+(Gelev-north)
        endif
    endif
    if(east.gt.blank.and.west.lt.blank) then
        if(west.gt.Gelev) then
            east=Gelev-(west-Gelev)
        else
            east=Gelev+(Gelev-west)
        endif
    endif
    if(east.lt.blank.and.west.gt.blank) then
        if(east.gt.Gelev) then
            west=Gelev-(east-Gelev)
        else
            west=Gelev+(Gelev-east)
        endif
    endif
    if(east.gt.blank.and.west.gt.blank) then
        east=Gelev
        west=Gelev
    endif
    goto 10
end

```

c

HORIZON SUBROUTINE

```

*****
      subroutine horizon(x,y,Bdem,nrows,ncols,DR,DC,Gelev,
$         size,cellnum,Hangle,GR,HC)
      implicit none
C
*****
* Abstract: This subroutine calculates the maximum angle to the
* horizon for the input grid cell along 36 ten degree azimuthal
* increments. Azimuths follow the same pattern as in the SOLAR
* subroutine, where 0 to 180 are east of south, and 0 to -180
* are west of south, with 0 being due south.
*
* The subroutine is input the coordinates and elevation of a
* point on the glacier. For each azimuth, the program 'walks'
* away from the glacier cell along the azimuth using basic trig.
* functions to determine whether the azimuth will first cross a
* row or a column. Whenever the azimuth crosses a row or column,
* the elevation at that point is interpolated from the two
* nearest elevations on the row or column (following Williams et.
* al., 1972)*
*
* The angle from horizontal between the original cell and the
* new elevation is then calculated (if the new elevation is
* greater than the original elevation), and if this angle is
* greater than the previous max angle, it is recorded.
*
* References for equations/ideas/validation of ideas...
* Williams, L.D., Barry, R.G., and Andrews, J.T., 1972,
* Application of computed global radiation for areas of high
* relief: Journal of Applied Meteorology, v.11, pp.526-533.
* (specifically eqns. 5 (p.528) and 6 (p.529))
*
* Dozier, J., and Outcalt, S.I., 1979, An approach toward energy
* balance simulation over rugged terrain: Geographical
* Analysis, v.11, pp.65-85.
*
* Inputs:
*
*      x: column number of input cell          I4
*      y: row number of input cell             I4
*      Bdem: DEM of elevations (from 'base.grd') R4 array
*      nrows: number of rows in Bdem           I4
*      ncols: number of columns in Bdem        I4
*      Gelev: elevation of input cell          R4
*      size: length of grid cell (m)          R4
*      cellnum: number of input cell           I4
*      GR: original number of rows in Hangle array I4
*      HC: original number of columns in Hangle array I4
*      DR: original number of rows in Bdem array I4
*      DC: original number of columns in Bdem array I4
*
* Outputs:
*
*      Hangle: array of 36 azimuthal horizon angles R4 array
*
* Local Variables:
*
*      i,j: counters for elevation grid cells    I4

```

```

*      a-f:  variables for elevation interpolation      I4
*      counti-j:  counters for advancing row or column      I4
*      azim:  counter for do-loop      I4
*      var1-2:  variables for elevation interpolation      R4
*      elevI-J:  Interpolated row & column elevations      R4
*      Li-j:  Distance b/t Bdem(i,j) and Gelev      R4
*      maxhoriz:  maximum horizon angle along azimuth      R4
*      Horiz:  Horizon angle      R4
*      Hazim:  actual azimuth angle      R4
*      elevdif:  elev. difference b/t Bdem(i,j) and Gelev      R4
*      rad:  degree to radian converter      R4
*****
C
C Declare variables
      INTEGER nrows,ncols,DR,DC,GR,HC,x,y,cellnum
      INTEGER azim,i,j,a,b,c,d,e,f,counti,countj
      REAL Li,Lj,rad,var1,var2,elevI,elevJ,size,maxhoriz
      REAL bdem(DR,DC),Hangle(GR,HC),Gelev,elevdif,Horiz,Hazim
      PARAMETER (rad=0.01745329251994)

C
C Begin loop to calculate horizon angles
      do azim=1,36

C
C calculate azimuth where 0=south, 180=north, positive is east of
south
      Hazim=(180.-azim*10.)*rad

C
C initialize counters and maxhoriz
      maxhoriz=0.
      counti=1
      countj=1

C
C Check to see if row or column counters are beyond the array
boundaries.
      10      if(x-counti.lt.1.or.x+counti.gt.ncols) goto 1000
             if(y-countj.lt.1.or.y+countj.gt.nrows) goto 1000

C
C Calculate maxhoriz in NE quadrant (170-100 degrees).
      if(azim.lt.9) then
         i=x+counti !advance column and row counter
         j=y+countj
         c=(j-y)      !compute variables that will determine
                     which
C                     two cells to interpolate elevation
                     between
         f=(i-x)      !
         var1=abs(float(c)*tan(Hazim))
         var2=abs(float(f)*(1./tan(Hazim)))
         a=int(var1)
         b=a+1
         d=int(var2)
         e=d+1
         if(a.lt.d)then ! advance to next row, compute maxhoriz
            elevJ=((var1-a)*bdem(j,x+b))+((b-var1)*bdem(j,x+a))
            countj=countj+1
            elevdif=elevJ-gelev
            if(elevdif.gt.0.)then
               Lj=abs(1./cos(Hazim))*float(c)*size

```



```

        Horiz=atan(elevdif/Lj)
        if(Horiz.gt.maxhoriz) maxhoriz=Horiz
    endif
else ! else advance to next column, compute maxhoriz
    elevI=((var2-d)*bdem(y+e,i))+((e-var2)*bdem(y+d,i))
    counti=counti+1
    elevdif=elevI-gelev
    if(elevdif.gt.0.)then
        Li=abs(1./sin(Hazim))*float(f)*size
        Horiz=atan(elevdif/Li)
        if(Horiz.gt.maxhoriz) maxhoriz=Horiz
    endif
endif
endif
goto 10

c
c Calculate maxhoriz at due east (90 degrees).
    else if (azim.eq.9) then
        i=x+counti
        elevI=bdem(y,i)
        counti=counti+1
        elevdif=elevI-gelev
        if(elevdif.gt.0.)then
            Li=float(i-x)*size
            Horiz=atan(elevdif/Li)
            if(Horiz.gt.maxhoriz) maxhoriz=Horiz
        endif
    endif
    goto 10

c
c Calculate maxhoriz in SE quadrant (80-10 degrees).
    else if(azim.gt.9.and.azim.lt.18) then
        i=x+counti
        j=y-countj
        c=(y-j)
        f=(i-x)
        var1=float(c)*tan(Hazim)
        var2=float(f)*(1./tan(Hazim))
        a=int(var1)
        b=a+1
        d=int(var2)
        e=d+1
        if(a.lt.d)then
            elevJ=((var1-a)*bdem(j,x+b))+((b-var1)*bdem(j,x+a))
            countj=countj+1
            elevdif=elevJ-gelev
            if(elevdif.gt.0.)then
                Lj=abs(1./cos(Hazim))*float(c)*size
                Horiz=atan(elevdif/Lj)
                if(Horiz.gt.maxhoriz) maxhoriz=Horiz
            endif
        else
            elevI=((var2-d)*bdem(y-e,i))+((e-var2)*bdem(y-d,i))
            counti=counti+1
            elevdif=elevI-gelev
            if(elevdif.gt.0.)then
                Li=abs(1./sin(Hazim))*float(f)*size
                Horiz=atan(elevdif/Li)
                if(Horiz.gt.maxhoriz) maxhoriz=Horiz
            endif
        endif
    endif
endif

```

```

        endif
    endif
    goto 10
c
c Calculate maxhoriz for due south (0 degrees).
    else if (azim.eq.18) then
        j=y-countj
        elevJ=bdem(j,x)
        countj=countj+1
        elevdif=elevJ-gelev
        if(elevdif.gt.0.) then
            Lj=float(y-j)*size
            Horiz=atan(elevdif/Lj)
            if(Horiz.gt.maxhoriz) maxhoriz=Horiz
        endif
    endif
    goto 10
c
c Calculate maxhoriz for SW quadrant (-10 to -70 degrees).
    else if(azim.gt.18.and.azim.lt.27) then
        i=x-counti
        j=y-countj
        c=(y-j)
        f=(x-i)
        var1=abs(float(c)*tan(Hazim))
        var2=abs(float(f)*(1./tan(Hazim)))
        a=int(var1)
        b=a+1
        d=int(var2)
        e=d+1
        if(a.lt.d) then
            elevJ=((var1-a)*bdem(j,x-b))+((b-var1)*bdem(j,x-a))
            countj=countj+1
            elevdif=elevJ-gelev
            if(elevdif.gt.0.) then
                Lj=abs(1./cos(Hazim))*float(c)*size
                Horiz=atan(elevdif/Lj)
                if(Horiz.gt.maxhoriz) maxhoriz=Horiz
            endif
        else
            elevI=((var2-d)*bdem(y-e,i))+((e-var2)*bdem(y-d,i))
            counti=counti+1
            elevdif=elevI-gelev
            if(elevdif.gt.0.) then
                Li=abs(1./sin(Hazim))*float(f)*size
                Horiz=atan(elevdif/Li)
                if(Horiz.gt.maxhoriz) maxhoriz=Horiz
            endif
        endif
    endif
    goto 10
c
c Calculate maxhoriz for due west (-90 degrees).
    else if (azim.eq.27) then
        i=x-counti
        elevI=bdem(y,i)
        counti=counti+1
        elevdif=elevI-gelev
        if(elevdif.gt.0.) then

```

```

        Li=float(x-i)*size
        Horiz=atan(elevdif/Li)
        if(Horiz.gt.maxhoriz) maxhoriz=Horiz
    endif
    goto 10
c
c Calculate maxhoriz for NW quadrant (-100 to -170 degrees).
    else if(azim.gt.27.and.azim.lt.36) then
        i=x-counti
        j=y+countj
        c=(j-y)
        f=(x-i)
        var1=float(c)*tan(Hazim)
        var2=float(f)*(1./tan(Hazim))
        a=int(var1)
        b=a+1
        d=int(var2)
        e=d+1
        if(a.lt.d)then
            elevJ=((var1-a)*bdem(j,x-b))+((b-var1)*bdem(j,x-a))
            countj=countj+1
            elevdif=elevJ-gelev
            if(elevdif.gt.0.)then
                Lj=abs(1./cos(Hazim))*float(c)*size
                Horiz=atan(elevdif/Lj)
                if(Horiz.gt.maxhoriz) maxhoriz=Horiz
            endif
        else
            elevI=((var2-d)*bdem(y+e,i))+((e-var2)*bdem(y+d,i))
            counti=counti+1
            elevdif=elevI-gelev
            if(elevdif.gt.0.)then
                Li=abs(1./sin(Hazim))*float(f)*size
                Horiz=atan(elevdif/Li)
                if(Horiz.gt.maxhoriz) maxhoriz=Horiz
            endif
        endif
    endif
    goto 10
c
c Calculate maxhoriz for due north (180 or -180 degrees).
    else if (azim.eq.36) then
        j=y+countj
        elevJ=bdem(j,x)
        countj=countj+1
        elevdif=elevJ-gelev
        if(elevdif.gt.0.) then
            Lj=float(j-y)*size
            Horiz=atan(elevdif/Lj)
            if(Horiz.gt.maxhoriz) maxhoriz=Horiz
        endif
        goto 10
    endif
1000    Hangle(cellnum,azim)=maxhoriz
enddo
return
end

```

ENERGY BALANCE SUBROUTINE

```

*****
      subroutine ebalance(model,Gelev,Belev,Khs,Khi,Tdep,a1,a2,ELA,
      $ slope,aspect,solel,solaz,SR,SC,balb,a3,a4,a5,a6,a7,spack1,
      $ spack2,x,y,NR,NC,numstk,stkloc,tmstp,size,snowdns,status,
      $ cloud,cellnum,Hangle,skyview,GR,HC,snowd,massbal,AveG,
      $ Aveinlwrad,Avetlwrad,AveLnet,AveHs,AveHl,AveEflux,pre_laps)
      implicit none
*****
*
* Abstract:  This subroutine calculates energy balance for each
*            grid elevation in the DEM on a daily timestep.
*
* Input:    The main program sends parameter data.  Climate data is
*            read into the subroutine from the 'met' file.
*            Local variables are described below.
*
* Output:   Returned variables are "massbal" and "balb"
*****
C
*****
* Declarations *
*****
C
c Input parameters and counters
      INTEGER model,yearno,i,j,SR,SC,NR,NC,modelday,numstk,GR,HC
      INTEGER stkloc(NR,NC),x,y,age,tmstp,snowflag,dayvar,cellnum
      INTEGER snowday
      REAL day,CalDay !day=simulation day, CalDay=calendar day
      REAL Gelev,Belev,Khs,Khi,ELA,Tdep,spack1,spack2,size,snowdns
      CHARACTER*3 status
C
c Horizon angle arrays and variables
      REAL Hangle(GR,HC),skyview,decimal
      INTEGER azim,int_saz
C
c Albedo equation variables
      REAL alb,a1,a2,a3,a4,a5,a6,a7,balb
C
c Air Temperature, Wind Speed, vapor pressures
      REAL Atemp,wind,AVP,SVP,light,P
C
c Incoming Shortwave, Net Longwave, Sensible, Latent heat fluxes
      REAL G,Lin,Lnet,Hs(24),Hl(24),cloud(SR),clsky,emiss,
      $      inlwrad(24),tlwrad(24)
C
c Calculated energy flux, ablation, mass balance,rsum ablation
      (mH2O)
      REAL Eflux(24),Abl,massbal,r_abl
C
c Precipitation, Snowfall, Rainfall
      REAL Pre,Snow,Rain,Snowd,newsnow,holdsnowd,pre_laps
C
c Solar insolation variables

```

```

      REAL solel(SR,SC), solaz(SR,SC), Sel, Saz,m, Ins, DirS(24)
      REAL AveDir, DirRatio, DifS(24)
      REAL Rvec, TotS, TotIns, Dir, Dif, slope, aspect, TotG
c
c Daily average/sum variables
      REAL
dailyatemp, dailywind, dailyavp, dailysvp, dailyTotG, dailyG,
$      dailyLnet, dailyHs, dailyHl, dailyEflux, dailyabl, dailypre,
$      dailyAccum, dailyalb, dailyRain, dailyinlwrad, seasonabl,
$      dailytlwrad, Avetlwrad
c
c Total averages/sums for entire run
      REAL
TotAccum, TotRain, TotAbl, AveG, AveInlwrad, AveLnet, AveHs, AveHl,
$      AveEflux, adjG
c
c Physical constant parameters:
      REAL Stemp, Lf, Cp, RHowat, laps, pi, S, rad, stef_bolz, r_h
      PARAMETER
$      (Stemp=273.15,          ! Surface temp (deg K)
$      Lf=334000.,           ! Latent heat of fusion of water
(J/kg)
$      Cp=2106.,             ! Specific heat of ice: (J/deg/kg)
$      RHowat=1000.,         ! Density of water: kg/m^3
$      laps=0.0065,         ! Dry adiabatic lapse rate: deg/m
$      pi=3.14159265359,    ! Pi
$      S=1368.,             ! solar constant: W/m^2,
c                          adj. 3-1-99
$      rad=0.01745329251994, ! degrees to radians conversion
$      stef_bolz=5.7e-8,    ! stefan-bolzmann constant
$      r_h=0.79714679)      ! ratio of earth radius to
c                          atmospheric height
c
c
*****
* Initialize variables, rewind data files *
*****
      totaccum=0.
      totabl=0.
      tottrain=0.
      day=0.
      Atemp=0.
      AVP=0.
      wind=0.
      Lnet=0.
      Lin=0.
      G=0.
      Pre=0.
      Snowd=0.
      balb=0.
      alb=0.
      yearno=0
      modelday=0
      snowday=-2
      age=tmstp*3
      newsnow=0.
      holdsnowd=0.
      snowflag=0

```

```

AveG=0.
AveInlwrad=0.
AveTlwrad=0.
AveLnet=0.
AveHs=0.
AveHl=0.
AveEflux=0.
adjG=0.
seasonabl=0.

c
c calculate P based on hypsometric eq. w/ scale height of 7km
c (Wallace and Hobbs, 1977: p.56, eq.2.26)
c (U.S. Standard atmospheric pressure at sea level of 1013.25mb
c taken from Wallace and Hobbs, 1977: p.61, below eq. 2.35)
c
      P=101325.*exp(-Gelev/7000.)  !Units=Pa
c
      rewind (11)
c
c Initialize internally calculated daily variables
10  SVP=0.
c    Hs=0.
c    Hl=0.
c    Eflux=0.
Abl=0.
Snow=0.
Rain=0.
light=0.
TotS=0.
TotIns=0.
Rvec=0.
Ins=0.
dailyatemp=0.
dailywind=0.
dailyavp=0.
dailysvp=0.
dailyTotG=0.
dailyG=0.
dailyLnet=0.
dailyHs=0.
dailyHl=0.
dailyEflux=0.
dailyabl=0.
dailypre=0.
dailyAccum=0.
dailyalb=0.
dailyRain=0.
dailyinlwrad=0.
dailytlwrad=0.
do i=1,24
      DirS(i)=0.
      DifS(i)=0.
      Eflux(i)=0.
      Hs(i)=0.
      Hl(i)=0.
      inlwrad(i)=0.
      tlwrad(i)=0.

```

```

        enddo
        AveDir=0.
        DirRatio=0.
c
        do i=1,tmstp !start loop for daily calculations
            snow=0. !reset snowfall to zero at beginning of each
timestep
            abl=0.
            rain=0.
            read(11,*,end=1000,err=1020) day,Atemp,AVP,wind,Lin,G,pre
            dailywind=dailywind+wind
            dailypre=dailypre+pre
            dailyavp=dailyavp+avp
c
c Convert simulation day to calendar day
            if(i.eq.1) then
                CalDay=day-(yearno*365)
                if (mod(Calday,365.).eq.0.) then
                    yearno=yearno+1
                endif
                if (mod(Calday,265.).eq.0.) then
                    seasonAbl=0.
                    snowflag=0.
                endif
                modelday=modelday+1
            endif
c
c
c *****
c * Initialize temperature, snowpack, and albedo *
c *****
c
c adjust Atemp for elevation and temperature depression
c
            Atemp=(Atemp+273.15)-((Gelev-Belev)*laps)-Tdep
            dailyAtemp=dailyAtemp+Atemp
c
c adjust precipitation for elevation
            pre=pre+pre*((Gelev-Belev)*pre_laps)
c
c Calculate snowpack depth on day 1 based on elevation dependant
c provided by M. Sharp.
c
            if (modelday.eq.1.and.i.eq.1)then
                snowd=(spack1*Gelev+spack2)*snowdns
                holdsnowd=snowd
                Totaccum=totaccum+snowd
            endif
c
c calculate background albedo for grid elevation on day 1*
c
            if (modelday.eq.1.and.i.eq.1) then
                balb=a1*atan((gelev-ELA+a2)/a3)+a4
                alb=0.75+(balb-0.75)*exp(-1*snowd/a5)
                if(alb.gt.0.85) alb=0.85
                if(alb.lt.0.12) alb=0.12
            endif

```

```

C
*****
* Accumulation calculations*
*****
C
c Calculation of precipitation type and snow depth
      if(pre.gt.0.) then
        if(Atemp.le.274.15) then
          snow=Pre
          snowday=modelday
        else
          rain=Pre
        endif
      endif
c Sum total accumulation and rainfall
      snowd=snowd+snow
      dailyAccum=dailyAccum+snow
      TotAccum=TotAccum+snow
      TotRain=TotRain+rain

C
*****
c Solar radiation notes:
C
c Because this model is set up to run with varying timesteps, the
c treatment of solar radiation, specifically shortwave radiation,
c needs some special attention. For daily timesteps the model will
c intrinsically underestimate incoming shortwave rad (inswrad)
c based on the assumption that the inswrad value supplied is a
c daily average. Also, a daily average value cannot be adjusted
c for slope and aspect at the glacier surface.
c So, daily timesteps are treated as follows:
C
c The model calculates clear sky direct solar radiation for
c daylight hours at each grid node using solar elevation and
c azimuth data from the "solar" subroutine using the following
c calculations:
c - The optical air mass is calculated from Robinson (1966),
c   (eqn. 3.12) with a correction applied for elevation by
c   multiplying the air mass by the ratio of local pressure to
c   sea-level pressure (Oke, 1987).
c - An air transmissivity of 0.84 was used. (Oke, 1987)
c - Radius vector of the earth's orbit Williams et. al., 1972)
c   (p. 527)
c - Insolation on a horizontal surface from Williams et. al.,
c   1972) (eqn. 1a)
c Note: these equations give only a 1st order approximation of
c solar radiation, but they are used as a max. value and should
c be valid as such.
C
c After each hourly value is calculated for a horizontal surface,
c the value is adjusted for the slope and aspect of the glacier
c surface following Arnold et. al., 1996 (eqn. 7).
C
c The model averages this clear sky approximation for the day, and
c divides this average by the average supplied in the met file
c to obtain a ratio of theoretical to observed solar radiation.
c The ratio is then applied to the hourly values of theoretical

```



```

c    radiation to reduce them proportionately to the observed data,
c    producing a daily total of inswrad to be applied to the Eflux!
c
c    Following Arnold et. al., 1996, the diffuse radiation is assumed
c    to be 20 percent of the direct, and is applied via a view
c    factor relationship to the glacier surface (Oke, 1987).
*****
c
c calculate radius vector of the earth's orbit
      if (CalDay.lt.4) then
        dayvar=CalDay+362
      else
        dayvar=CalDay-3
      endif
      Rvec=.01676*cos(pi-0.0172615*dayvar)+1
c
c if timestep is daily then enter loop to adjust daily average
values
      if (tmstp.eq.1) then
c        Dir=G
        do j=1,24
          Sel=solel(modelday,j)
          if (Sel.gt.0.) then
            Saz=solaz(modelday,j) !determine closest horizon
            int_saz=int(Saz/rad/10.) ! angle azimuth to Saz
            decimal=abs(Saz/rad/10.-int_saz)
            if (decimal.lt.0.5) then
              azim=abs(int_saz-18)
            else if (saz.lt.0.) then
              azim=abs(int_saz-18-1)
            else
              azim=abs(int_saz-18+1)
            endif
c compute optical airmass
            m=(sqrt((r_h*sin(Sel))^2+2*r_h+1)-r_h*sin(Sel))*
              + (P/101300.)
c compute incoming direct rad for horizontal surface
            Ins=(S/Rvec*Rvec)*sin(Sel)*0.84**m
            Ins=Ins*3600.      !(convert w/m^2 to J/hr)
c adjust for slope and aspect and shading
            if (Hangle(cellnum,azim).lt.Sel) then
              DirS(j)=Ins*(sin(Sel)*cos(slope)+sin(slope)*
                + cos(Sel)*cos(Saz-aspect))/sin(Sel)
            else
              DirS(j)=0.
            endif
c calculate diffuse rad.
            Dif=0.2*ins*skyview+0.4*ins*(1-skyview)
            DifS(j)=dif
            TotG=TotG+Ins+dif
            TotS=TotS+DirS(j)+Dif
            light=light+1.      !number of daylight hours
          else
            DirS(j)=0.0
            DifS(j)=0.0
          endif
        enddo
      enddo

```

```

c          G=G*light*3600. !calculate total G from daily average?
c
c calculate ratio of model derived average to observed average.
    DirRatio=TotS/TotG
    G=G*DirRatio
    else ! end section to approximate for daily average value.
c
c adjust inswrad value from met file directly.
c
    Sel=solel(modelday,i)
    Saz=solaz(modelday,i) ! Determine closest Horizon
    int_saz=int(Saz/rad/10.) ! angle azimuth to Saz
    decimal=abs(Saz/rad/10.-int_saz)
    if(decimal.lt.0.5)then
        azim=abs(int_saz-18)
    else if(saz.lt.0.)then
        azim=abs(int_saz-18-1)
    else
        azim=abs(int_saz-18+1)
    endif
    if (Sel.gt.0.) then
c
c if solar elevation is positive, check to see if data from "met"
c file is positive, if it is not, write unadjusted climate values.
        if (G.le.0.) then
            G=0.0
            TotG=0.0
            DirS(i)=0.0
            DifS(i)=0.0
        else
c if both solar elevation and G are positive, continue.
            TotG=G
            Dir=G*0.8
c
c If cell is in sun then adjust direct component for slope and
c aspect.
            if(Hangle(cellnum,azim).lt.Sel) then
                Dir=Dir*(sin(Sel)*cos(slope)+sin(slope)*
$                cos(Sel)*cos(Saz-aspect))/sin(Sel)
            else
                Dir=0. !if cell is in shade - dir=0
            endif
            DirS(i)=Dir
c
c adjust diffuse component via view factor for a basin.
            Dif=0.2*G*skyview+0.4*(0.8*G)*(1-skyview)
            DifS(i)=Dif
            TotG=TotG
            G=Dir+Dif
        endif
    else if (G.gt.0.) then
c
c if solar elevation is 0. or less, but G is positive, adjust
c values for a solar elevation of 0.5 degrees 3-4-99.
        TotG=G
        Dir=G*0.8
        Sel=0.008726646 ! 0.5 deg. in radians

```

```

        if (Hangle(cellnum,azim).lt.Sel) then
            Dir=Dir*(sin(Sel)*cos(slope)+sin(slope)*
$           cos(Sel)*cos(Saz-aspect))/sin(Sel)
        else
            Dir=0.          !if cell is in shade - dir=0
        endif
        DirS(i)=Dir
        Dif=0.2*G*skyview+0.4*(0.8*G)*(1-skyview)
        DifS(i)=Dif
        TotG=TotG
        G=Dir+Dif
    endif
endif
G=G/Lf/RHOWat
dailyTotG=dailyTotG+TotG !unadjusted inswrad
dailyG=dailyG+G          !adjusted inswrad
c
c
*****
* Calculation of incoming longwave radiation *
*****
c
    if (tmstp.gt.1) then !calc. inlwrad
        clsky=8.733e-3*(atemp**0.788)
        emiss=(1+0.26*cloud(modelday))*clsky
        inlwrad(i)=stef_bolz*emiss*(atemp**4)!atmospheric LWR
        tlwrad(i)=stef_bolz*0.95*(atemp**4)!terrain LWR 5-2-99
c adjust for view factor via Dozier and Outcalt, 1979;
c Marks and Dozier, 1979 (eq.8,9)
        inlwrad(i)=inlwrad(i)*skyview*86400./float(tmstp)
        tlwrad(i)=tlwrad(i)*(1-skyview)*86400./float(tmstp)
        Lin=inlwrad(i)+tlwrad(i)
        Lnet=Lin-(316.*(86400./float(tmstp)))
skyview    else if (tmstp.eq.1) then !adjust Lin for lapse rate &
skyview
        inlwrad(i)=Lin-(2764.8*(Gelev-Belev))*skyview
        tlwrad(i)=(stef_bolz*0.95*(atemp**4)*86400.)*(1-
skyview)
        Lnet=inlwrad(i)+tlwrad(i)-2.73024e7
    endif
    Lnet=Lnet/Lf/RHOWat
    dailyLnet=dailyLnet+Lnet
    dailyinlwrad=inlwrad(i)+dailyinlwrad
    dailytlwrad=tlwrad(i)+dailytlwrad
c
*****
* Turbulent Heat Flux Equations *
*****
c
c calculate SVP (Pa)
c
    SVP=611.
    if (atemp.gt.273.15) then !Oerlemans, 1992
        SVP=610.8*exp(19.85*(1-(273.15/Atemp)))
    else
        SVP=610.8*exp(22.47*(1-(273.15/atemp)))
    endif
    dailysvp=dailysvp+svp

```

```

C
C calculation of Turbulent heat fluxes
C equations from Paterson, 1994 (pp.64-65, eqs.19,20);
C and Braithwaite, et. al., 1998 (calculations of Lv and cp)
      if(model.eq.2) then      !Paterson eq.s
        if (snowd.gt.0.) then
          Hs(i)=1.29e-2*Khs*P*wind*(Atemp-Stemp)
          if(AVP.lt.SVP)then !evaporation
            Hl(i)=22.56*Khs*wind*(AVP-SVP)
          else                !condensation
            Hl(i)=19.91*Khs*wind*(AVP-SVP)
          endif
        else
          Hs(i)=1.29e-2*Khi*P*wind*(Atemp-Stemp)
          if(AVP.lt.SVP)then !evaporation
            Hl(i)=22.2*Khi*wind*(AVP-SVP)
          else
            Hl(i)=19.91*Khi*wind*(AVP-SVP)
          endif
        endif
      else if(model.eq.3)then
        if(snowd.gt.0.) then
          Hs(i)=4.42e-6*P*(Atemp-Stemp)*wind
          if(AVP.lt.SVP) then !evaporation
            Hl(i)=7.77e-3*(avp-svp)*wind
          else                !condensation
            Hl(i)=6.86e-3*(avp-svp)*wind
          endif
        else
          Hs(i)=6.34e-6*P*(Atemp-Stemp)*wind
          if(AVP.lt.SVP) then
            Hl(i)=11.14e-3*(avp-svp)*wind
          else
            Hl(i)=9.83e-3*(avp-svp)*wind
          endif
        endif
      else
        Hs(i)=Khs*(Atemp-Stemp) !Oerlemans eq.s
        Hl(i)=Khs*0.622*Lf*(AVP-SVP)/(P*Cp)
      endif
      Hs(i)=Hs(i)*(86400./float(tmstp))/Lf/RHOWat
      Hl(i)=Hl(i)*(86400./float(tmstp))/Lf/RHOWat
      dailyHs=dailyHs+Hs(i)
      dailyHl=dailyHl+Hl(i)
      dailyalb=dailyalb+alb

C
*****
* Calculation of Energy Flux      *
*****

C
      Eflux(i)=(1-Alb)*G+Lnet+Hs(i)+Hl(i)
      dailyEflux=dailyEflux+Eflux(i)
      adjG=(1-alb)*G
      aveG=aveG+adjG

C
*****
* Calculation of Ablation and snowmelt *

```

```

*****
c
    if(Eflux(i).gt.0.) Abl=Eflux(i)
    snowd=snowd-Abl
    if (snowd.lt.0.) snowd=0.
c
    dailyAbl=dailyAbl+Abl
    TotAbl=TotAbl+Abl
    seasonabl=seasonabl+abl
c
*****
c calculation of new albedo based on presence of snow *
*****
c
    alb=0.53+(0.75-0.53)*exp((snowday-modelday)/a6)
    alb=alb+(balb-alb)*exp(-1*snowd/a5)-(a7*seasonabl)
    if (alb.gt.0.85) alb=0.85
    if (alb.lt.0.12) alb=0.12
c
    enddo ! end timestep loop
c
c Calculate daily averages and sums of ebal variables
c
    Atemp=dailyatemp/float(tmstp)
    wind=dailywind/float(tmstp)
    avp=dailyavp/float(tmstp)
    svp=dailysvp/float(tmstp)
    totG=dailytotG/Lf/RHWat
    dailyalb=dailyalb/float(tmstp)
    r_abl=TotAbl-TotAccum
    dailyinlwrad=dailyinlwrad/Lf/RHWat
    dailytlwrad=dailytlwrad/Lf/RHWat
c
c Increment average energy flux components
    Aveinlwrad=dailyinlwrad+aveinlwrad
    Avetlwrad=dailytlwrad+avetlwrad
    AveLnet=dailyLnet+AveLnet
    AveHs=dailyHs+AveHs
    AveHl=dailyHl+AveHl
    AveEflux=dailyEflux+AveEflux
c
c Track snowline elevation changes on stake locations
    if(snowd.le.0..and.holdsnowd.gt.0..and.snowflag.eq.0)then
        do i=1,numstk
            if(x.eq.stkloc(i,1).and.y.eq.stkloc(i,2)) then
                write(19,500)Calday,char(9),gelev
                snowflag=1
                goto 99
            endif
        enddo
    99  endif
    500  format(1x,f6.1,a1,f8.2)
        holdsnowd=snowd
c
c Write output to Stake*.txt files
    do i=1,numstk
        if(x.eq.stkloc(i,1).and.y.eq.stkloc(i,2)) then

```

```

        write(29+i,510)
$         int(day),char(9),
$         atemp,char(9),
$         wind,char(9),
$         avp,char(9),
$         svp,char(9),
$         totG,char(9),
$         dailyG,char(9),
$         dailyinlwrad,char(9),
$         dailytlwrad,char(9),
$         dailylnet,char(9),
$         dailyHs,char(9),
$         dailyHl,char(9),
$         dailyEflux,char(9),
$         dailyalb,char(9),
$         dailyabl,char(9),
$         snowd,char(9),
$         dailypre,char(9),
$         dailyAccum,char(9),
$         TotAccum,char(9),
$         TotAbl,char(9),
$         r_abl
        if(mod(modelday,20).eq.0.)then
            if(tmstp.gt.1)then
                do j=1,tmstp
                    write(59+i,520)
$                     int(day),char(9),
$                     j,char(9),
$                     DirS(j)/Lf/RHOWat,char(9),
$                     DifS(j)/Lf/RHOWat,char(9),
$                     inlwrad(j)/Lf/RHOWat,char(9),
$                     tlwrad(j)/Lf/RHOWat,char(9),
$                     Hs(j),char(9),
$                     Hl(j),char(9),
$                     Eflux(j)
                enddo
            else
                do j=1,24
                    write(59+i,530)
$                     int(day),char(9),
$                     j,char(9),
$                     DirS(j)/Lf/RHOWat,char(9),
$                     DifS(j)/Lf/RHOWat
                enddo
            endif
        endif
    endif
endif
enddo
c
510
format(1x,i4,a1,2(f7.2,a1),10(f9.4,a1),f4.3,a1,6(f9.4,a1),f9.4)
520 format(1x,2(i4,a1),6(f8.4,a1),f8.4)
530 format(1x,2(i4,a1),f8.4,a1,f8.4)
c
c Go to beginning of next day
    goto 10
c

```

```

*****
* At end of file calculate massbal for the elevation *
*****
1000 massbal=TotAccum-TotAbl
    AveG=AveG/float(modelday)
    Aveinlwrad=Aveinlwrad/float(modelday)
    Avetlwrad=Avetlwrad/float(modelday)
    AveLnet=AveLnet/float(modelday)
    AveHs=AveHs/float(modelday)
    AveHl=AveHl/float(modelday)
    AveEflux=AveEflux/float(modelday)
    return
1020 write(*,*)"Problem with meteorological data file"
    return
    end

```